THE KINETICS OF SELF DIFFUSION AND DISLOCATION GLIDE IN MAGNESIUM OXIDE

Jagdish Narayan
(Ph. D. thesis)

November 1971

AEC Contract No. W-7405-eng-48

LBL-406
c.1

DISCLAIMER

THE KINETICS OF SELF DIFFUSION AND DISLOCATION GLIDE IN MAGNESIUM OXIDE

Contents

THE KINETICS OF SELF DIFFUSION AND DISLOCATION GLIDE IN MAGNESIUM OXIDE

Jagdish Narayan

Inorganic Materials Research Division, Lawrence Berkeley Laboratory and Department of Materials Science and Engineering, College of Engineering; University of California, Berkeley, California

ABSTRACT

Annealing mechanisms for damage caused by plastic deformation have been studied. This work involved the development of techniques for examination of the same area of a plastically deformed thin foil in an electron microscope under identical diffraction conditions before and after annealing at high temperatures (> 850°C). Below about 1300°C, self climb was found to be the primary mechanism for coarsening of the dislocation loops that result from breaking of dislocation dipoles. Above about 1300°C bulk diffusion becomes important as most of the close pairs have coalesced to form more isolated single loops. Isolated loops always shrink or grow by bulk diffusion. Prismatic slip along $\frac{1}{2}\langle 101\rangle$ directions occurs whenever sources of interaction (surfaces of the foil, nearby dislocations) are close. Frequently annihilation of a vacancy loop by contact with an interstitial loop after slipping along glide cylinders that are at 90° to each other, has been observed. Sometimes mobile screw dislocations cut dislocation loops and there is rapid annihilation by pipe diffusion to the foil surfaces.

Quantitative measurements were made of self climb and climb of $\frac{1}{2}\langle 101\rangle$ edge dislocation loops. The rate of motion of loops was studied by repeated observation of the same areas of a thin foil during a series of annealing treatments at different temperatures (1080°C to 1250°C).

A value of 60,300 ± 3,500 cal/mole for the activation energy for pipe diffusion and $(7.5 \pm 4.3) \times 10^{-18}$ cm^4/sec for the pre-exponential term $D_o^P a^P$ were obtained.

The rate of shrinkage of dislocation loops, which were near the center of the foil and relatively isolated from other loops, was measured in the range of temperature 1080°C to 1427°C. A value of 110,000 ± 4,200 cal/mole for activation energy for bulk diffusion and $(1.37 \pm 0.26) \times 10^{-2}$ cm^2/sec for D_o were obtained in the temperature range 1080°C to 1427°C for MgO of impurity content A. Other specimen of impurity level B behaved like A-MgO below 1300°C, however above 1300°C the value of activation energy for bulk diffusion reduced to 63,600 ± 1,500 cal/mole. This we have explained in terms of oxygen ion mobility and an impurity controlled diffusion mechanism. Above about 1300°C in B-MgO monovalent cationic impurities (Na^+, Cu^+, K^+, etc.) and/or anionic impurities with more than two valency (N^{3-}, etc.) become active and seem to dominate the concentration of vacancies. Below this temperature either the precipitation of impurities (Na^+, K^+, etc.) and/or the transition $Cu^+ + \frac{1}{2} \square^{--} \rightarrow Cu^{++}$ occurs and only the equilibrium number of vacancies take part in the diffusion mechanism.

Quantitative measurements of slip were made for dislocation loops of various sizes and the Peierls stress was found to decrease with the increase in the size of the loop.

The kinetics of annealing out of loops, cut by the surface of a thin foil was also studied. The loops annealed out much faster than those not cut by a surface, by slip, pipe diffusion and surface diffusion.

I. INTRODUCTION

When magnesium oxide is plastically deformed (bending), most of the damage is introduced in the form of dislocation dipoles. A brief description of the mechanism of dislocation dipole formation follows: moving screw dislocations acquire jogs of both kinds during motion, this results in formation of edge dislocation dipoles trailing behind, many of the dipoles are terminated becoming elongated closed loops by the mechanism described by Washburn.[1] Recently good electron microscope evidence of this mechanism has been obtained by Narayan and Washburn.[2] Evidence for collision and rearrangement mechanisms of dipole formation described by Ogawa[3] have also been observed. As the plastically deformed crystals are heated to successively higher annealing temperatures, the dipoles start breaking up into strings of small circular prismatic dislocation loops. First to break up are the dipoles of smallest spacing. The breaking up into circular loops starts at as low as 850°C, depending upon the separation of the two edge dislocations comprising the dipole.[3,4] As the time and temperature of annealing is increased dipoles of larger spacing start breaking up.[4] As the time and temperature of annealing is increased further, loop coarsening takes place. These big loops then anneal out by bulk diffusion and/or prismatic slip[5] to the foil surfaces.

Up to now the exact mechanisms of annealing out dipoles were not clear because thin foils for transmission electron microscopy were obtained from different bulk samples, annealed at different temperatures for various amounts of time. To investigate the mechanisms of annealing in more detail it is necessary to photograph the same area of a thin foil after various annealing treatments. Since for <u>in situ</u> heating it

was difficult to attain a temperature of 850°C and above, a technique of annealing thin foils outside the electron microscope was developed. The temperature of annealing was controlled better than ±3°C, which is not possible in any hot stage (in-situ) annealing. The same area was photographed after each annealing treatment taking care to reproduce identical diffraction conditions.

Our experiments showed that after the initial stages of breaking of dipoles, many pairs of the resulting coplanar groups of loops started moving closer together by self climb during annealing when the separation was small enough for a strong interaction. Up to about 1300°C, self climb was the primary mechanism of loop coarsening. After most of the loop pairs suitable for self climb have coalesced to form single loops, bulk diffusion becomes the predominant mechanism of coarsening. Prismatic slip and pipe diffusion along dislocations connected to surfaces of the foil and the loops inside the foil were also important. Quantitative measurements have been made in each case to determine the activation energy and to help to confirm the diffusion mechanism. For convenience, the results have been presented in three sections: pipe diffusion, bulk diffusion, and prismatic slip.

A. Pipe Diffusion

Self climb of a coplanar prismatic edge dislocation loop $\frac{1}{2}\langle 101\rangle$ takes place by pipe diffusion along the core of an edge dislocation. Pipe diffusion along a screw dislocation has already been reported.[4] In the latter case a dislocation loop $\frac{1}{2}\langle 101\rangle$ inside the foil, was connected to both surfaces of the foil by a screw dislocation of same b-vector.

Self climb of dislocation loops differs from the usual non-conservative growth or shrinkage in the sense that the total area of the loop projected perpendicular to its Burgers vector remains unchanged and climb occurs by migration of atoms along the easiest path, i.e., the core of the dislocation. This type of climb was first proposed by Johnson[6] in order to explain observations of vacancy loop coarsening on annealing bulk samples of quenched aluminum. Unfortunately in his numerical analysis of pipe diffusion, Johnson neglected the driving force term. At approximately the same time Price[7] during electron microscopy of deformed zinc, observed that the prismatic dislocation loops moved due to interactions with a nearby edge dislocation, while remaining on the same basal plane layer. During this motion the area of the loop perpendicular to its b-vector was unchanged. Theoretical treatment of these observations was given by Kroupa and Price.[8]

In self climb, the driving force for pipe diffusion arises from two sources. The first is due to interaction with neighboring loops[9,10,11] or surfaces of the foil[12] or nearby dislocations.[7] This gives rise to differences in concentration of vacancies around the loop (i.e. energy of formation of a vacancy is affected). Coplanar pairs of dislocation loops have strong interaction only if the separation is small (about one diameter of the bigger loop). This interaction results in a net flow of vacancies around the loop. The second is due to direct loop-vacancy interaction. Vacancies once created at a given loop may, however, interact with the surrounding elastic stress field and accordingly the energy for migration of a vacancy will be affected.

Reliable quantitative measurements of climb rates are largely still lacking because of the following experimental difficulties:

1) It is often hard to avoid concurrent prismatic slip; this is particularly true in metals;

2) It is necessary to carry out annealing treatments outside the microscope because of the inherent inaccuracy of temperature measurement in hot stage experiments.

These difficulties have been avoided in our experiments. Magnesium oxide was found to be an ideal material for observing self climb for the following reasons:

1) Prismatic slip in magnesium oxide is not easy even at temperatures high enough for self climb to occur readily.

2) Many of the prismatic dislocation loops, which are formed from the same dislocation dipole on annealing are coplanar.

3) Annealing of thin foils of magnesium oxide outside the electron microscope is relatively easy.

4) The high fracture strength and high yield strength of MgO made it less difficult than for metals to handle thin foils without making dislocations move during a series of electron microscope observations and annealing treatments.

The combination of sources of interaction (neighboring loops, surfaces of the foil) is possible, but for quantitative analysis it is convenient to study one at a time.

The present report contains a quantitative analysis of self climb of coplanar pairs of loops. Only those loops were selected for measurements which were near the center of the foil to minimize the effects of

foil surfaces. The rate of self climb was measured at more than one temperature for the same set of loops to avoid the uncertainty due to poorly known pre-expontential factors. Self climb due to surfaces of the foil or nearby dislocations has also been observed, but it was not possible to make a quantitative analysis. An improved model of self climb of coplanar loops has been used to calculate the activation energy for pipe diffusion. Several weak points of Turnbull's recent analysis of the same problem in UO_2 are discussed.

B. Bulk Diffusion

Here bulk diffusion means the diffusion of vacancies or interstitials through the lattice. Both cations as well as anions diffuse simultaneously in the climb of dislocation loops. However, the rate is governed by the slowest moving species, in this case the anion. In an ionic crystal like MgO, where the bond between a cation and an anion is very strong, both cation and anion have to tumble together during diffusion.[5b]

Groves and Kelly[6] did transmission electron microscopy on thin foils prepared from bulk samples, annealed at different temperatures and determined the average growth rate of dislocation loops. They obtained a value of 75,900 ± 4,600 cal/mole as the activation energy in the range of temperature (1292-1426°C) for the thermally activated process. A major difficulty of this kind of experiment is the initial inhomogeniety in the plastic deformation. Especially MgO deforms so inhomogeneously that samples for electron microscopy obtained even from the same crystal may contain very different amounts of damage. It is also impossible to separate the contributions due to glide and climb. Due to these difficulties it is difficult to associate a unique process with the activation

energy obtained by them. Reliable data for self diffusion by trace or diffusivity measurements are available for cation diffusion in the range of temperature (1100°C-1750°C)[13] and for anion diffusion in the range (1300°C-1750°C).[14]

In our experiment, the same area was photographed after different annealing treatments in the temperature range (1080-1427°C) under identical diffraction conditions. Stereomicroscopy was done at each step and only those loops which were near the center of the foil and isolated from others were selected for measurements. For this case the mechanism of annealing was well defined (bulk diffusion) and the quantitative analysis was easier.

The rate of change of size of dislocation loops was a strong function of loop to sink distance. The effective sinks were surfaces of the foil and nearby dislocations. This indicates that the annealing rate is controlled by diffusion of vacancies rather than their emission. Quantitative analysis similar to that of Dobson et al.[15] was used to calculate activation energy and the pre-exponential factor for bulk diffusion. The rate of shrinkage of dislocation loops was measured at different temperatures, this avoided errors in the activation energy due to some poorly known pre-exponential terms.

C. Dislocation Glide

Glide of a dislocation is defined as its movement on a surface that contains both the dislocation line and its Burgers vector. During glide motion the dislocation has to pass through hills and troughs of atomic potential. The force which opposes glide is the Peierls-Nabarro force and the corresponding stress is the Peierls-Nabarro stress. In ionic

solids, the Peierls-Nabarro stress arises primarily from ions with the same sign having to move past each other during slip.

In thin foils, the interactions which cause slip or glide of dislocations are surface image forces, nearby dislocation loops and dislocations. We observed glide motions of the following types:

1) Two relatively isolated dislocations loops b-vector $\frac{1}{2}\langle 101\rangle$ slipping on glide cylinders with the separation of axes being equal to the sum of radii of two loops;

2) dislocation loops $b = \frac{1}{2}\langle 101\rangle$ slipping solely due to surface effects;

3) big loops that intersected the surface of the foil gliding out where they were nearly parallel to the surface of the foil;

4) two loops of different b-vectors ($\frac{1}{2}[101]$ and $\frac{1}{2}[10\bar{1}]$) slipping on glide cylinders at 90° to each other.

Quantitative estimates of the Peierls-Nabarro stress have been made from glide motions of type 1). Foreman and Eshelby's formulation[13] for the interaction energy of a pair of widely spaced or infinitesimal dislocation loops was used in the case where two small loops were slipping together. Foreman's improved analysis[13a] has also been used for some cases and results compared. For the case where one of the loops was much smaller than the other, a formulation similar to that of Kroupa and Price[8] for interaction of a loop with an edge dislocation was used to calculate the Peierls stress.

II. EXPERIMENTAL

Large grained polycrystalline MgO was purchased from Muscle Shoals Electro-chemical Corp., Tuscumbia, Alabama. Semi-quantitative spectrographic analysis revealed the following impurities:

A - MgO (impurities in PPM)

Al-200, Si-200, Fe-30

Na and K were undetected up to 2 PPM, Ag undetected up to 1 PPM, all other elements also undetected;

B - MgO (percent impurities)

Al - 0.06, K - 0.05, Fe - 0.03, Ca - 0.03, Mn - 0.002, Cr - 0.002, Cu - 0.001, Na - 0.001, Si - < 0.001.

MgO used by Oishi and Kingery[20] contained the following percent impurities: Si $\sim$ 0.01, K $\leq$ 0.01, Fe $\leq$ 0.01, Ca $\leq$ 0.01, Al $<$ 0.01, Ag $<$ 0.01, Cr $<$ 0.01, Cu $<$ 0.01. In our experiments A-MgO was used unless otherwise specified.

Single crystal specimens in the form of thin sheets ($\sim$ 0.50-0.25 mm thick) were obtained by cleaving along {100} planes. The surface damage introduced during cleaving was removed by chemical polishing in hot orthophosphoric acid (150-160°C) to a thickness of about 0.1 mm. These sheets were then bent backwards and forwards (±5 cm radius) about 20 times until they were full of slip bands. Following the deformation the specimens were thinned further, after applying masking lacquer around the edges. Final thinning to obtain electron microscope foils was done by a jet polishing technique.[14] After cold working the thinning was done primarily from one side because plastic deformation is maximum near the surfaces.

In thin sheets bent along the [010] axis, dislocation dipoles are introduced on (101)[$\bar{1}$01], ($\bar{1}$01)[101] and on (110)[$\bar{1}$10], ($\bar{1}$10)[110] slip

systems. Dipoles on (101)[$\bar{1}$01] and ($\bar{1}$01)[101] are of primary interest as dipoles on (110)[$\bar{1}$10] are seen edge-on along [001] which is perpendicular to the surfaces of the foil.

Annealing Technique: An MgO (98%) crucible with an air tight platinum lid was fired at 1500°C for 48 hours. Then an MgO tube 1/16" internal diameter and 14" long was fitted in the crucible so that the atmosphere inside the crucible could be isolated from the furnace atmosphere and could be controlled from the outside. This was also given a firing treatment similar to that of the crucible before connecting it to the crucible. The thin foil was kept between two pure MgO crystals. One of these crystals had a spherical cavity, made by an ultrasonic drill. The thin foil was placed in the cavity in such a way that the area of interest did not touch the enclosing crystals. A calibrated Pt-10% Rh thermocouple was connected to the crucible to measure the temperature inside the crucible. The temperature could be controlled to better than ±3°C. At temperatures above ∿1400°C, there was some indication of non-stoichiometric composition. This could easily be detected as a change in transmitted intensity inside the electron microscope. The problem of non-stoichiometric composition was overcome by introducing some oxygen in the crucible atmosphere. Care was taken not to turn the foil over during electron microscope observations.

Electron Microscopy: All the foils were examined in a Siemens 100 kV electron microscope. For a particular set the same diffraction conditions were used. Most of the stereomicroscopy was done along the 200 Kikuchi band and around the 001 pole. Objective lens current was measured at each step of the picture making, keeping intermediate and projector lens

currents fixed. The microscope was calibrated in small intervals of objective lens current for the same projector and intermediate lens currents.

All the quantitative measurements were made directly from the electron micrograph plates. Electron micrographs were observed in a Nikan enlarger at 20× to make measurements.

III. THEORY AND METHODS OF CALCULATION

A. Pipe Diffusion

Here a general formulation of the rate of self climb of two isolated and interacting loops is presented. The formulation for pipe diffusion along a screw dislocation, connected to both surfaces of the foil and the loop inside the foil of the same b-vector has already been reported.[4a] It is assumed that motion is due only to pipe diffusion and that the only driving force is the interaction between the two loops. The direct vacancy-loop interactions are not included due to uncertainty in the relaxation around vacancies inside the core of a dislocation in ionic crystals. This is thought to be small, as discussed later. Also, in agreement with experimental observations, it is assumed that the loops remain circular while getting closer.

The shift ΔX in the center of gravity due to formation of one vacancy on a loop of radius r_1 at any point p (see Fig. 1) is approximately

$$\Delta X = \frac{b^2 \cos\theta}{\pi r_1} \tag{1}$$

where θ is the angle between the line joining the loop centers and point p. The change in the energy of formation of a vacancy at any point along the circumference of the loop is then:

$$\Delta\mu_{fv} = \frac{dE_{int}}{dX} \Delta X \tag{2}$$

where dE_{int} is the change in interaction energy.

Following Foreman,[13a] dE_{int} is given by

$$dE_{int} = \frac{Gb^2}{4\pi(1-\nu)} d\ell_1 \cdot d\ell_2 \tag{3}$$

where vectors $d\ell_1$ on loop 1 and $d\ell_2$ on loop 2 represent two small segments of their perimeters with coordinates (x_1, y_1) and (x_2, y_2) respectively and $X^2 = (x_2 - x_1)^2 + (y_2 - y_1)^2$.

The vacancy concentration in the dislocation pipe is therefore

$$C^P = C_o^P \, e^{\frac{-\Delta\mu_{fv}}{kT}} \tag{4}$$

where $C_o^P = e^{-\mu_{fv}^P/kT}$, is the equilibrium concentration within the dislocation pipe in the absence of a climb force.

For $\Delta\mu_{fv}$ small compared to kT

$$C^P = C_o^P \, (1 + \Delta\mu_{fv}/kT) \tag{5}$$

The migration rate of the loops is determined by the flux of vacancies passing from the far half into the near half. Assuming that loops remain circular and the equilibrium vacancy concentration given by Eq. (4) are maintained, the flux is

$$J_1 = D^P a^P \frac{1}{r_1} \left(\frac{dC^P}{d\theta}\right)_{\theta=90^\circ} \tag{6}$$

$$= \frac{2D^P a^P C_o^P}{\pi r_1^2 \, kT} \frac{dE_{int}}{dX} \tag{7}$$

where D^P = self diffusion coefficient at the core of the dislocation, a^P = area of cross-section of the dislocation pipe.

Now

$$\left(\frac{dX}{dt}\right)_{\text{loop 1}} = J_1 \frac{b^2}{2r_1}$$

$$= \frac{D^P a^P b^2 C_o^P}{\pi k T r_1^3} \frac{dE_{int}}{dX} \tag{8}$$

If both loops are migrating, the total rate of change of X, $\frac{dX}{dt}$ is the sum $\left(\frac{dX}{dt}\right)_{\text{loop 1}} + \left(\frac{dX}{dt}\right)_{\text{loop 2}}$.

Therefore

$$\frac{dX}{dt} = \left(\frac{dX}{dt}\right)_{\text{loop 1}} + \left(\frac{dX}{dt}\right)_{\text{loop 2}} = \frac{D_p a_p b^2 C_o^P}{\pi k T} \frac{dE_{int}}{dX} \left[\frac{1}{r_1^3} + \frac{1}{r_2^3}\right] \tag{9}$$

where

$$D_P = D_o^P \exp - \left(\frac{\mu_{mv}^P}{kT}\right) \tag{10}$$

$$C_o^P = N_o^P \exp - \left(\frac{\mu_{fv}^P}{kT}\right) \tag{11}$$

μ_{mv}^P and μ_{fv}^P are activation energies for migration and formation of a vacancy respectively at the core of a dislocation, N_o^p = atomic density at the core of the dislocation.

Substituting for D_p and C_o^p into Eq. (9)

$$\frac{dX}{dt} = \frac{D_o^P a^P N_o^P}{\pi k T} \frac{dE_{int}}{dX} \left[\frac{1}{r_1^3} + \frac{1}{r_2^3}\right] \exp - \frac{\mu_{mv}^P + \mu_{fv}^P}{kT} \tag{12}$$

Defining $\bar{X} = X/r_1$ and rearranging Eq. (12), we have

$$d\bar{X} \cdot \frac{d\bar{X}}{dE_{int}} = K dt$$

where

$$K = \frac{D_o^P a^P N_o^P}{\pi k T r_1^2} \left[\frac{1}{r_1^3} + \frac{1}{r_2^3} \right] \exp - \frac{\mu_{mv}^P + \mu_{fv}^P}{kT}$$

and r_1 is the diameter of bigger loop.

On integration of Eq. (13), we have

$$\int_{\bar{X}_1}^{\bar{X}_2} d\bar{X} \quad \frac{d\bar{X}}{dE_{int}} = \int_{t_1}^{t_2} K dt \tag{14}$$

To evaluate the integral on the left side, $\frac{d\bar{X}}{dE_{int}}$ vs $\bar{X}$ data were calculated for the sets of loops, suitable for self climb rate measurements. For cases $r_1 = r_2$, $r_2 = r_1/2$ and $r_2 = r_1/10$, graphs are given in Figs. 4a, 4c and 4e respectively. The calculated graphs of E_{int} vs $\bar{X}$ from Eq. (3) for these cases are also given in Figs. 4b, 4d and 4f respectively. E_{int} vs $\bar{X}$ for infinitesimal or widely spaced loops from Foreman and Eshelby formulation are also shown in Figs. 4b, 4d and 4f for comparison.

Graphical integrations were performed from $\bar{X}_1$ to $\bar{X}_2$ corresponding to intervals of time Δt to get A_1, A_2 etc. Therefore for an interval of time Δt^1 at temperature T_1

$$A_1 = K_1 \Delta t^1 \tag{15}$$

Similarly for another time interval Δt^2 at temperature T_2

$$A_2 = K_2 \Delta t^2 \tag{16}$$

From Eq. (15) and Eq. (16) we have

$$\frac{A_1}{A_2}\ \frac{\Delta t^2}{\Delta t^1} = \frac{T_2}{T_1} \exp \frac{E_{act}}{RT}\left(\frac{1}{T_2} - \frac{1}{T_1}\right) \tag{17}$$

Therefore

$$E_{act} = \frac{RT_1T_2}{T_1-T_2}\ \ell n\ \frac{A_1\Delta t^2 T_1}{A_1\Delta t^1 T_2} \tag{18}$$

B. Bulk Diffusion

Under diffusion-controlled conditions it is not necessary to make any detailed assumptions about the state of the dislocation core other than that it can maintain the vacancy concentration in the lattice surrounding the loop at its local equilibrium concentration. The rate of climb is then determined by the vacancy flux between the lattice surrounding the loop and surfaces of the foil. The vacancy concentration in the vicinity of the dislocation loop is $C_o \exp [\frac{F_c B^2}{RT}]$, where F_c is the driving force for climb and B^2 is the cross-sectional area of a vacancy and at the surfaces of the foil vacancy concentration is C_o. When the radius of the dislocation loop (r) is small compared with the foil thickness; the loop can be considered as a sphere of radius r and diffusion equation is solved for spherical symmetry, with the boundary conditions that vacancy concentration:
$C = C_o \exp [\frac{F_c b^2}{kT}]$ at $x = r$ and $C = C_o$ at $x = L$. Here x is measured from the center of the dislocation loop, and 2L is the thickness of the foil. The rate of shrinkage, dr/dt (following Dobson et al.[15]) for this case is given by

$$\frac{dr}{dt} = -\frac{2D}{b}\left[\exp\frac{F_c B^2}{kT} - 1\right] \tag{19}$$

where D is the self bulk diffusion coefficient.

For large loop radii ($r > L$), loop can be approximated by a straight line of length $2\pi r$ and the diffusion equation is solved for cylindrical symmetry with the boundary conditions that $C = C_o \exp[F_c B^2/kT]$ at $x=b$ and $C=C_o$ at $x=L$, where x is measured from the dislocation line. The rate of shrinkage dr/dt for this case is given by

$$\frac{dr}{dt} = -2\pi \frac{D}{b} \ln\left(\frac{L}{b}\right) [\exp(F_c B^2/kT)-1] \tag{20}$$

Following Seidman and Balluffi,[16] for small loops the diffusion geometry may be better represented by a toroidal source (radii r and r_o and concentration C_1 on the torus) situated at the center of a sphere of radius L. The concentration on the surface of the sphere is C_o. The shrinkage rate is given by

$$\frac{dr}{dt} \cong \frac{-2\pi D}{b} \frac{(C_1-C_o)}{\ln(8r/r_o)} \tag{21}$$

For large loop radii, the rate equation corresponding to Eq. (20) is

$$\frac{dr}{dt} = \frac{-2\pi D}{b} \frac{(C_1-C_o)}{\ln(\frac{4L}{\pi r_o})} \tag{22}$$

Using the expression given by Bacon and Crocker[17] for the elastic energy of a prismatic dislocation loop, F_c can be written as

$$F_C = \frac{\mu b^2}{4\pi(1-\nu)r}\left[\ln\frac{8r}{r_o} - 2 + \frac{3-2\nu}{4(1-\nu)}\right] \tag{23}$$

where ν is the Poisson's ratio and r_o is the radius of the core of a dislocation.

Substituting for $\nu \simeq 0.3$ in the range of temperature 1080-1450°C and r_o ($r_o \simeq 1.5\ b$), F_c can be rewritten as

$$F_C = \frac{\mu b^2}{2.8\pi r} \ln \frac{1.7r}{b} \tag{24}$$

Since $F_c b^2 << kT$, the Eq. (19) can be rewritten as

$$\frac{dr}{dt} = \frac{-2D}{b} \frac{F_C b^2}{kT} \tag{25}$$

because $B^2 \simeq b^2$ for $\frac{1}{2}\langle 101\rangle$ prismatic edge dislocation loops.

By substituting for F_c in Eq. (25) and simplifying, we have

$$\frac{r\ dr}{\ln \frac{1.7r}{b}} = \frac{-\mu D b^3}{1.4\pi kT}\ dt \tag{26}$$

Similarly Eq. (20) can be written as

$$\frac{rdr}{\ln \frac{1.7r}{b}} = \frac{-\mu D b^3 \ln(L/b)}{1.4\pi kT}\ dt \tag{27}$$

By integrating numerically the left hand side of Eq. (26) and Eq. (27) (see Fig. 5) from r_1 to r_2 corresponding to a given interval of time of annealing at temperature T and recalling that $D = D_o \exp^{-E_{act}/kT}$, we can find activition energy (E_{act}). The same loops were annealed at different temperatures to avoid the errors in activation energy due to the lack of precise knowledge of pre-exponential constants. Using this value of activation energy the pre-exponential term D_o was then determined.

C. Dislocation Glide

Following Foreman and Eshelby,[13] for the case of two infinetisimal or widely spaced loops the force for glide motion is

$$\frac{\partial E_{int}}{\partial Z} = \frac{\mu b_1 b_2 A_1 A_2}{4\pi(1-\nu)} \quad \frac{3\cos\theta}{R^4} (3-30\cos^2\theta + 35\cos^4\theta) \qquad (28)$$

where b_1, b_2 and A_1, A_2 are the Burgers vectors and areas of the two dislocation loops respectively, θ is the angle that R makes with the loop normal. R is the separation of centers of two loops.

We can write

$$\sin\theta = \frac{S_p}{R} \quad , \cos\theta = \frac{Z}{R} \qquad (29)$$

where S_p is the separation between axes of glide cylinders.

Using relations of Eq. (29), one can write Eq. (28) as

$$\frac{\partial E_{int}}{\partial Z} = \frac{\mu b_1 b_2 A_1 A_2}{4\pi(1-\nu)} \quad \frac{3Z}{(S_p^2+Z^2)^{5/2}} \left(3 - \frac{30Z^2}{S_p^2+Z^2} + \frac{35Z^4}{(S_p^2+Z^2)^2}\right) \qquad (30)$$

From this

$$\Delta E_{int} = \frac{3\mu b_1 b_2 A_1 A_2}{4\pi(1-\nu)} \left[-2(S_p^2 + Z^2)^{-3/2} + 8S_p^2(S_p^2+Z^2)^{-5/2} - 5S_p^2(S_p^2+Z^2)^{-7/2}\right]_{Z=Z_1}^{Z=Z_2} \qquad (31)$$

$$\Delta E_{int} = 2\pi r\, \tau_p b(Z_2-Z_1) \qquad (32)$$

where τ_p is the Peierls stress, r is the radius of the gliding loop and b is its burgers vector.

Foreman's analysis is an improvement over Foreman and Eshelby's analysis. This holds for loops of all sizes and separations. Foreman's

analysis reduces to Foreman and Eshelby's analysis for infinitesimal and widely spaced loops.

Let the center of one loop be at the origin of an orthogonal coordinate system (x,y,z) with z axis perpendicular to the plane of the loop and the center of other loops at $(x_1 y_1 z_1)$. If the vectors $d\ell_1$ on one loop and $d\ell_2$ on the other loop represent two small segments of their perimeters with coordinates $(x_1 y_1 z_1)$ and $(x_2 y_2 z_2)$ respectively, the interaction energy dE_{int} between them according to Foreman is:

$$dE_{int} = \frac{\mu b^2}{4\pi(1-\nu)} \left\{ \frac{1}{R} + \frac{(z_1-z)^2}{R^3} \right\} d\ell_1 \cdot d\ell_2 \qquad (33)$$

where

$$R^2 = (x_1-x_2)^2 + (y_1-y_2)^2 + (z_1-z_2)^2.$$

The total loop-loop interaction is obtained by taking the double line integral of Eq. (33) around both loops. This integral may not be evaluated analytically. For calculations of ΔE_{int}, Foreman's results of numerical integration have been used (see Fig. 2).

In the case where a small loop is gliding because of interaction with a very big loop (see Fig. 3), the energy of interaction can be approximated by the interaction energy of a loop with a straight dislocation. Following Kroupa and Price,[8] interaction energy can be written as:

$$E_{int} = \frac{\mu b b_1}{1-\nu} RZ \left\{ 1 - \left\{ (2Y^2+Z^2-1)+2\sqrt{[(1+Y^2+Z^2)^2-4Y^2]} \right\}^{-1/2} \right.$$
$$\left. \cdot [(Y^2+Z^2-Y)((Y-1)^2+Z^2)^{-1/2} + (Y^2+Z^2+Y)((Y+1)^2+Z^2)^{-1/2}] \right\} \qquad (34)$$

where b and b_1 are Burgers vectors of loop and dislocations respectively and, $Y = y_1/r$ and $Z = z_1/r$ (Fig. 3).

We have studied cases where Y = 1, so Eq. (34) looks like

$$E_{int} = \frac{\mu b b_1}{1-\nu} \left\{1-[2Z^2+2Z\sqrt{(Z^2+4)}]^{-1/2} \cdot [Z+(2+Z^2)(4+Z^2)^{-1/2}]\right\} \qquad (35)$$

To calculate the Peierls stress τ_P, we have

$$\Delta E_{int} = \int_{Z_1}^{Z_2} dE_{int} = 2\pi r \tau_P b_o (Z_2 - Z_1) \qquad (36)$$

where Δz is the displacement of smaller loop along the glide cylinder and ΔE_{int} is the change in interaction energy.

IV. RESULTS AND DISCUSSION

A. Pipe Diffusion

Figures 6A and B show the self climb of prismatic edge dislocation loops, $b = \frac{1}{2}[101]$ at 1 and 3. Coplanar pairs of loops, near the center of the foil (confirmed from stereopair) moved together by pipe diffusion to form single loops of approximately conserved area (at 1, Fig. 6). At 2 dislocation loop, $b = \frac{1}{2}[101]$ is connected to the surfaces of the thin foil by a screw dislocation of the same b-vector. The dislocation loop is shrinking due to pipe diffusion along the screw dislocation. It can be seen qualitatively that shrinkage rate due to pipe diffusion is much larger than that due to bulk diffusion by observing the behavior of the loop at 4 in Fig. 6, $b = \frac{1}{2}[101]$ which is also near the center of the foil. It did not shrink appreciably by bulk diffusion in spite of being one of the tiniest in the field of view and therefore having a large driving force for shrinkage. Some of the loops of the same size as 4 (near the dipole in Fig. 6) are shrinking with a little faster rate than 4 because of being close to the dislocation dipole. Effective sinks or sources where the vacancy concentration can be maintained near its equilibrium value are the surfaces of the foil and straight or only slightly curved dislocations.

Figures 7A and B show further examples of self climb of coplanar pairs of dislocation loops, $b = \frac{1}{2}[101]$ at 1 and 2. These loops are also near the center of the foil so that changes in the sizes of the loops due to bulk diffusion are almost negligible. Dislocation dipoles at 3 and 4 (Fig. 7) have opened up into dislocation loops $b = \frac{1}{2}[101]$. The dislocation loop at 5 has slipped out of the foil by prismatic slip due

to image forces caused by the surface of the foil.

The set of pictures in Fig. 8 shows another series, photographed after different annealing treatments, outside the electron microscope. At 1, 2, and 3, there are good examples of self climb of coplanar pairs of loops, $b = \frac{1}{2}[101]$, which are also close to the center of the foil. The dislocation loop at 5, $b = \frac{1}{2}[101]$, which was also near the center of the foil is shrinking purely by bulk diffusion. The change in its size is again not measurable in spite of its being one of the smallest loops in the field of view. The dislocation loops at 6 and 7 which are close to the surface of the foil are shrinking by bulk diffusion with much faster rates than 5 and other loops which are relatively far away from the sinks. The dislocation loop at 8, being very close to the surface, has slipped out of the foil by prismatic slip.

The set of pictures in Figs. 9, 10 and 11 is an example, where the same area was photographed after annealing treatments at three different temperatures. Coplanar groups of loops at 1, 2, 3, 7, a, b, c and d move closer together by self climb and form single loops of approximately conserved area. The changes in the sizes of all dislocation loops from Figs. 9A to 11A are negligible. A few loops which were very near to one of the surfaces of the foil have slipped out by prismatic slip along their glide cylinders (see loop 5 and 9 in Figs. 9, 10 and 11).

Quantitative measurements of self climb have been made from the sets of pictures in Figs. 9 through 15. The values of activation energy for pipe diffusion, obtained by measuring the rate of climb of various sets of loops are given in Tables I through IV. The average value of activation energy is 60,300 ± 3,500 cal/mole. An estimate of the uncertainty due to limits of precision in the measurements of separation,

radius and temperature are given for each value. To maximize the precision of measured separations and radii of loops, pictures were taken with both $\bar{2}00$ and 200 diffraction conditions. The results reported in Tables I, II, III and IV represent the average of measurements from the two diffraction conditions. Stereomicroscopy was also done at each step to locate the loops in the foil. Surface dirt particles were helpful as reference points. Only those loops, which were located near the center of the foil and were relatively isolated from other loops were selected for measurements. Surface effects were not important in the calculations because these are of short range and are negligible for loops situated at a depth more than about two diameters of the loop.[18]

In the theory of self climb one of the assumptions was that loops remain circular due to line tension while moving closer together. The dislocation loops at 3 in Fig. 12D and at 2 in Fig. 13D show that loops do remain circular even up to the time of contact. This should be expected because the loop self energy remains large compared to the interaction energy right up to the point where the loops come into contact. Turnbull[11] has mentioned that his formulation for the rate of self climb explains why both loops remain circular while coming closer together. However, this is not true. His analysis considered the shape of the near halfs of the loops. The net force acting on far halfs is repulsion which, in the absence of loop self energy, would make the loops elongate rather than remain circular.

Depending upon the vacancy saturation around the loops, bulk diffusion can cause slight increases or decreases in the sizes of the loops during annealing. If loop size changes, the pipe diffusion path

length changes during the experiment. These changes have been neglected in the formulation for rate of self climb. However in the temperature range of our experiments these changes were very small for the dislocation loops which were near the center of the foil and relatively isolated from other loops. Also since the pipe diffusion path length enters only as the first power [see Eq. (6)], the errors in the calculated values due to this simplification were negligible.

By making measurements of climb rate for a given loop pair at more than one temperature, errors due to inadequate knowledge of the appropriate pre-exponential terms, particularly D_o^P and a^P, have been avoided. Measurements, at one temperature, require theoretical estimate of D_o^P and a^P to permit calculation of the activation energy. Turnbull's quantitative analysis of self climb in UO_2,[11] the first available in the literature, suffers from this necessity. The activation energy calculated from rate measurements at two temperatures (Figs. 9 to 13) was used to calculate the pre-expontential term $D_o^P\, a^P$ $(7.5 \pm 4.3) \times 10^{-18}$ cm^4/sec. This value of $D_o^P\, a^P$ was then used to calculate the activation energy for measurements done at another temperature. The constant activation energy obtained over the temperature range 1100 to 1250°C for various sizes of loops justifies confidence in the model and analysis. If we take $a_P \sim 10^{-15}$ cm^2, D_o^P is about 5×10^{-3} cm^2/sec. This is in good agreement with previous results on pipe diffusion along screw dislocations.* [4a]

This rather low value of D_o^P may be due to precipitation of impurities along the dislocations, which act as traps for vacancies and/or a

---

* A configuration, in which a dislocation loop, $b = \frac{1}{2}[101]$, was connected to both surfaces of a thin foil by a screw dislocation of the same b-vector.

reduced value of the frequency of atomic vibration inside the core of a dislocation.

In Turnbull's paper arguments are also presented for not taking into account direct loop-point defect interaction. He argues that relaxation around vacancies in ionic crystals is small. In general, this is not true. In MgO, the relaxation around a vacancy is about 0.2 to 0.4 times the molecular volume.[28] However, it is not clear how the relaxation around a vacancy in the core of a dislocation might be estimated from this value for an isolated vacancy. However, this interaction does not seem to be very important because of the consistent results obtained for different loop sizes and for pipe diffusion along screw dislocations ($62,700 \pm 2000$ cal/mole)[4a] to the foil surfaces where direct interaction terms would be small. The slightly higher values of activation energy for pipe diffusion along screw compared to that for self climb (pipe diffusion along edge dislocation may be either due to the different nature of the screw dislocation core or because we have neglected direct vacancy-loop interaction. In the latter case our value for edge dislocation pipe diffusion is an underestimate for the true value.

The value of activation energy $60,300 \pm 3500$ cal/mole for pipe diffusion found in our experiments, is consistent with the upper limit estimate of activation energy for pipe diffusion ($71,400 \pm 4600$ cal/mole) obtained by Groves and Kelly. The self climb experiments were done on both A-type and B-type MgO. The differences in the activation energy were within experimental errors.

By measuring the shrinkage rate of dislocation loops due to bulk diffusion in the temperature range 1080-1427°C, the activation energy for intrinsic bulk diffusion was determined to be 110,000 ± 4,200 cal/mole. This is in agreement with that for intrinsic diffusion of oxygen ions obtained from electrical conductivity measurements.[19] Our value of activation energy for self climb is about 0.55 times that for oxygen ion bulk diffusion. This was expected because of smaller enthalpy for formation of a vacancy at the dislocation and easier migration of vacancies along the dislocation.[19a]

From this it can be concluded that pipe diffusion is controlled by oxygen ion mobility which is reasonable in view of ionic radii of O^{--}(1.32 Å) and Mg^{++} (0.66 Å).

B. Bulk Diffusion

Figure 16 is a set of pictures of the same area after various annealing treatments at four different temperatures (1202°C, 1291°C, 1368°C and 1293°C). The pictures represent the end points of annealing treatments. Dislocation loops $b = \frac{1}{2}[101]$, 1, 2, 3, and 4 remained roughly near the center of foil, as confirmed by stereopairs taken after each annealing treatment. The dirt particle on the upper surface of the foil acted as the reference. The ends of the screw dislocation (at the upper right corner in Fig. 16) running from the top to the bottom of the foil could also be used as a reference. Near such surface reference points the perception of depth in stereo is better. Figure 17 shows other areas at the same four different annealing temperatures.

The set in Fig. 18 is at two different annealing temperatures (1260°C and 1400°C) and another set in Fig. 19 is at two different temperatures (1400°C and 1427°C). The measurements at lower temperatures

(below 1200°C) have been made from Figs. 9 to 12. In all of the above cases A-MgO was used. Plots, r^2 vs t, are given in Figs. 20A,B and C for sets in Figs. 16 through 19.

The strong dependence of rate of shrinkage of dislocation loops on loop to sink distance (see loops 6, 7 in Fig. 8) proved that diffusion is controlled by diffusion of vacancies rather than emission of vacancies. The equations for shrinkage rate of dislocation loops under emission controlled conditions differ from that under diffusion conditions only in the pre-exponential terms.[19b] Since, in our experiments, rate of shrinkage of dislocation loops was measured at more than one temperature, it does not matter which model is used in calculations of activation energy.

An average value of activation energy 110,000 ± 4,200 cal/mole was obtained in the temperature range 1080 to 1427°C. The value for D_o in this temperature range was found to be $(1.37 \pm 0.26) \times 10^{-2}$ cm^2/sec. ℓn D vs 1/T plot is shown in Fig. 23.

The set of pictures in Fig. 21 was from B type samples. r^2 vs t plots are given for dislocation loops 1 and 2 (Fig. 21) in Fig. 22. The value of activation in this case dropped to 63,600 ± 1,500 cal/mole above 1300°C (see Fig. 23).

Oishi and Kingery[20] determined the oxygen self diffusion coefficient by measuring the rate of exchange between a controlled gas phase (oxygen gas at 150 mm pressure) enriched with isotope O^{18} and an MgO crystal in the temperature range 1300-1750°C. Their activation energy for bulk diffusion was 62,400 cal/mole. This is in good agreement with our value for B-MgO above 1300°C. They attributed this to impurity controlled diffusion

mechanism. The impurities which can affect the diffusivity in oxygen sublattice are either monovalent cations, trivalent or higher order anions. MgO used by Oishi and Kingery had enough of K^+, Ag^+ and Cu^+ to cause this effect. B-MgO, used in our experiments also contained enough of potassium and copper to get similar effects. Oishi and Kingery used unannealed MgO powder in their experiment. These particles might have contained high dislocation density. So the apparent activation energy obtained by them might be that for pipe diffusion. This has been found to be true for KCl and NaCl powders as discussed by Barr et al.[20a] Furthermore relatively higher values of diffusion coefficients obtained by Oishi and Kingery support this idea.[19,20a] If this is assumed to be true it is interesting to note that their value is very close to our value for activation energy for pipe diffusion.

From pre-exponential factors in the diffusion equations one can easily show that amount of impurities needed to get this effect in this temperature range is less than 1 PPM. It is to be noted that in A-MgO, there are no such impurities (monovalent cations, trivalent or higher order anions) to produce this kind of effect.

The value of activation energy 63,600 ± 1,500 cal/mole corresponds to the extrinsic range and hence is equal to H_m, the enthalpy of motion of the rate controlling ion. Vacancies are created due to the presence of aliovalent impurities, so the $H_f/2$ term from activation energy drops out (H_f = enthalpy of formation of the complete Schottky defect). The activation energy 110,000 ± 4200 cal/mole corresponds to intrinsic diffusivity (no effect of impurities) therefore this corresponds to $\frac{H_f}{2} + H_m$, where H_m is the enthalpy of motion of the rate controlling ion

(in this case O^{--}). From this H_f is 3.6 ± 0.22 eV and H_m is 2.76 ± 0.11 eV. Harding et al.[21] did measurements of self diffusion of Mg^{++} in single crystals of MgO and determined H_f = 3.4 ± 0.2 eV and the enthalpy of motion for cation vacancy (H_m) = 1.7 ± 0.1 eV. There is good agreement in the values of H_f. Both in anion and cation diffusion H_f corresponds to the enthalpy of formation of complete Schottky defect. In the shrinkage and growth of dislocation loops both cations and anions have to move together during diffusion and the rate of diffusion is controlled by the slowest moving species. Since in MgO, the ionic radii of Mg^{++} and O^{--} are 0.66 Å and 1.32 Å respectively, one would expect the diffusion rate to be controlled by O^{--}. Therefore our value for H_m(2.76 ± 0.11 eV) is for oxygen ion and it is higher than that of Mg^{++} (1.7 ± 0.1 eV)[21] as expected.[23]

The two regions intrinsic 1100-1300°C and extrinsic > 1300°C in B-MgO can be explained if there is vacancy-impurity association or impurity precipitation below 1300°C and above 1300°C these impurities break away from complexes and vacancy concentration is controlled by them. However, if the association were the cause, it would be expected that the diffusion coefficient would be impurity concentration dependent in this region, which does not seem to be the case. Furthermore, the transitions would be gradual rather than being so sharp as those found in our experiments.

Precipitation might set in at a well-defined temperature range and give rise to a relatively sharp change in the values of activation energies in two regions and this indeed is found experimentally.[22,23] Also, the values of D in this case would be independent of purity as observed.

Impurity precipitation around 1300°C has been observed by Wuensch and Vasilos.[24]

This sudden change in activation energy in B-MgO might also be explained on the basis of the following reaction

$$Cu^{++} \rightarrow Cu^{+} + \frac{1}{2}\square^{--} \quad > 1300°C$$

$$\leftarrow \quad < 1300°C.$$

Above 1300°C vacancies created by this reaction, become predominant over the equilibrium concentration and the diffusion is controlled entirely by these vacancies. In other words the H_f term in the activation energy for bulk diffusion drops out. However, below 1300°C since Cu^{++} is doubly charged as is Mg^{++}, there are no extra vacancies due to the presence of Cu^{++} and the diffusion is controlled by the equilibrium concentration of vacancies. Therefore activation energy in this temperature range corresponds to $\frac{H_f}{2} + H_m$.

The ionic radii of Cu^{+} and Na^{+} are the same (0.96 Å). This is greater by 0.26 Å than that of Mg^{++} and by 0.21 Å than that of Cu^{++}. The strain-energy should be overcome by the gain in energy in the above reaction at 1300°C. However below 1300° change in strain energy might be inhibiting the transition. The greater stability of Cu^{+} in the presence of surrounding ions has been discussed by Latimer.[26] Also from the fact that $CuO \rightarrow Cu_2O$ (at 1 atm pressure) at $\sim$ 1200°C, we would expect greater stability of Cu^{+} at higher temperatures. As mentioned earlier, reported annealing experiments are at about 1 atm pressure. The latter is not directly applicable as the stability of Cu^{+} and Cu^{++} depends strongly upon the surrounding lattice.[26]

C. Dislocation Glide

Figures 24 to 28 are a set of pictures of the same area after annealing treatments at four different temperatures from 1200-1250°C. Configurations suitable for quantitative measurements of prismatic slip are at 1 (Figs. 24B-C) at 2 (Figs. 24-26) and at 1 (Figs. 30-31). For 1 (Fig. 24B-C) Foreman and Eshelby's formulation of the interaction between dislocation loops of infinitesimal size or wide spacing as well as the improved analysis of Foreman for close loops (see Fig. 4) was used to calculate the Peierls stress in MgO. The values of Peierls stress from two formulations were 1.1×10^{10} dynes/cm^2 and 7.25×10^{8} dynes/cm^2 respectively. The Kroupa and Price formulation for the interaction between a dislocation loop and a straight edge dislocation was used for configuration at 2 (Figs. 24-26). For details, see Table V. Another suitable configuration, where the Kroupa and Price analysis was used is at 1 in the set of pictures (Figs. 30-31). The variation of Peierls stress with the size of the dislocation loop is shown in Fig. 33. The reported values of Peierls stress are after temperature correction in shear modulus of elasticity (μ). From Fig. 33 the Peierls stress decreases as loop size increases. This can be explained in view of greater difficulty in the nucleation and migration of a pair of kinks[27] in a smaller size loop. The nucleation might be difficult because the segments free from charged jogs, which are suitable for nucleation, are smaller in a smaller size loop. The migration might be difficult because the pair of kinks has to encounter greater number of charged jogs during motion in a smaller size loop.

Glide due to surface image interaction and dislocation loop of opposite b-vector

The big loops near 2 and 3 (Figs. 24-28) and near 1 (Figs. 29-31) are lost to the surfaces of the foil by gliding along [101] glide cylinders because of surface image forces. For these cases systematic quantitative measurements of displacements from the surface have been made but due to difficulty in the formulation of surface interaction energy, the Peierls stress could not be calculated. Direct electron microscopic evidence of the dependence of Peierls stress on loop size is shown in Fig. 34. Loop at 1 is situated at a depth 220 Å more than loop 2. This was found by measurements of a stereo pair (see Fig. 34B). The dirt particle, on the surface served as a reference. Both were gliding along the glide cylinder [101] due to the surface image forces, but loop 1 reached the surface of the foil first (Fig. 34D). Finally, both were lost to surface (Fig. 34E). There are many other examples in every set of pictures of loss of dislocation loops to the surfaces of the foil by glide (prismatic slip). From these results of the dependence of the Peierls stress on the size of the dislocation loop, one would expect, the Peierls stress for straight dislocations to be very low. This is indeed the case. Screw dislocations, running from the top to the bottom of the foil have been observed to move even while under observation due to electron beam heating. Dislocation loops remain unaffected unless they are very large.

Glide of dislocation loops of opposite b-vectors are shown in Fig. 35 at 1 and Fig. 36 at 1. These are examples where a vacancy and an interstitial dislocation loop glide along common glide cylinders and eventually annihilate each other.

In the previous literature there has been no equally direct evidence for the fact that both vacancy and interstitial loops are present in plastically deformed and subsequently annealed magnesium oxide. Groves and Kelly[25] found all the loops to be of vacancy type by contrast experiments in the electron microscope. Cass[3] using a similar technique concluded that both kinds were present. The configurations shown in Fig. 35 at 1 and Fig. 36 at 1 provide direct evidence for the presence of both kinds of defects in plastically deformed and subsequently annealed magnesium oxide. However occurrences such as the above were rather rarely observed and the same type of contrast for a given diffraction vector (outside or inside the extra half plane of an edge dislocation) was usually seen for all loops in the field of view. The same type of contrast would only be expected for mixed vacancy and interstitial loops if all the vacancy loops were on planes at 90° to the planes of all the interstitial loops. In the sodium chloride structure this is possible but highly unlikely. Also, stereo-pairs showed that most of the loops in a given field of view were generally on the same plane sloping to one side. It was concluded that the majority of the loops are vacancy type.

More examples of glide

One side of the big loop at 1 (Fig. 37), being close to the surface, has glided out of the foil along [101]. The dislocation loop has $b = \frac{1}{2}[101]$ and lies on the (101) plane. Part of the dislocation at 2 (Fig. 37) has glided out resulting in a narrow dipole and a dislocation. The resulting dipole and dislocation loops are of mixed character (partly edge and partly screw) as they are not along the [010] direction.

The big loops at 1 (Fig. 38) and at 5 (Figs. 25-27) were annihilated partly by climb and partly by glide when screw dislocations of the same b-vectors hit them.

Annealing of dislocation loops that intersect foil surfaces

The set of pictures in Fig. 39, shows the annealing behavior of a big loop $b = \frac{1}{2}[101]$, which was intersected by the foil surface. The stereo-pair (Fig. 39 B) showed that the loop was sloping downward from the upper surface of the foil. In Fig. 39C, one of the ends (end b) had started slipping along the glide cylinder. Due to surface image forces and line tension it was trying to be at 90° to the foil surface. In Fig. 39D, it has already passed the equilibrium position and one of its sides has slipped out. In Fig. 39E, the remaining part has also slipped out of the foil.

The amount of glide in loop at 1 (Fig. 40) is relatively smaller than at 1 in Fig. 39. This can be understood in view of a higher Peierls stress of loop at 1 in Fig. 40 than that at 1 in Fig. 39. Half loops at 2, 3 and 4 in Fig. 40 anneal out both by glide and surface diffusion. Pipe diffusion in these loops is negligible because of very little driving force for pipe diffusion and the relative ease of prismatic slip.

Glide of dislocation loops due to mutual interaction

Figure 14, at 6 shows an example where two dislocation loops are gliding under mutual interaction along glide cylinders that are at 90° to each other. Since both have outside plane contrast (image is outside the extra half plane), they must have opposite b-vectors (one of them interstitial and the other vacancy). These two loops came closer together along their glide cylinders and finally annihilated each other. Here

annhilation takes place primarily by pipe diffusion. As soon as two loops touch each other atoms from interstitial dislocation loop diffuse along the edge of extra half plane in vacancy loop and fill it, leaving the region of the crystal free from defects.

Some comments on annealing out the damage

When a moving screw dislocation hits the dislocation loop of the same b-vector it may promote pure glide [at 1, Fig. 38, at 5, Figs. 25-27] or pure climb (Fig. 6 at 2) or may do both. An example for the last case is at A in Figs. 25 and 26. It is interesting to note how the screw dislocation (at 6) of the same b-vector as the dislocation loop, (at A, Fig. 25) (both have b-vector $\frac{1}{2}$ [101]) enters inside the loop. There is appreciable glide at the end "a" because it is closer to the surface than end "b". Pipe diffusion along the screw dislocation is taking place simultaneously and the dislocation loop is annealed out rapidly (see the screw dislocations at 6, Fig. 26H). On further annealing it hits another dislocation loop at 7 and this loop is annealed out quickly by pipe diffusion along the screw dislocation (see Fig. 27I). One of the most interesting examples of annealing out by pipe diffusion at 8 is shown in Fig. 27J. The screw dislocation at 8 (Fig. 27J) enters inside the dislocation loop at 9 (Fig. 28K). Then the dislocation loop at 9 anneals out by rapid diffusion along the screw dislocation (see Fig. 28 K-L). It is to be noted that there is no opening up of this dislocation loop [as at 6 (Fig. 25)] perhaps because of higher Peierls stress of the smaller loop.

V. CONCLUSIONS AND REMARKS

Up to about 1300°C, the primary mechanism of annealing out the damage introduced by plastic deformation in MgO is pipe diffusion along edge dislocation (self climb) as well as along screw dislocations which connect dislocation loops inside the foil to the surfaces of the foil. Above that as most of the loops have coalesced to form single loops, bulk diffusion becomes predominant. Prismatic slip occurs whenever sources of interaction are close. Quantitative measurements were made in each case to find the activation energy and decide diffusion mechanism for the process. Results are as follows:

Pipe Diffusion

1. The activation energy for pipe diffusion along edge dislocations in MgO is 60,300 cal/mole and the value of the pre-exponential term $D_o^P a^P$ is $(7.5 \pm 4.3) \times 10^{-10}$ cm^4/sec.
2. Self climb is the primary mechanism of loop coarsening below 1300°C; above that temperature bulk diffusion predominates because most of the configurations appropriate for self climb have collapsed to form single loops.

Bulk Diffusion

1. The loop shrinkage rate in MgO is controlled by diffusion of vacancies rather than emission of vacancies from the dislocation.
2. The value of the activation energy for bulk diffusion (intrinsic) is 110,000 ± 4,200 cal/mole and that of D_o is $(1.37 \pm 0.26) \times 10^{-2}$ cm^2/sec.
3. The values of the activation energy for bulk diffusion in the extrinsic range above 1300°C is 63,600 ± 1,500 cal/mole (B-MgO).

4. This change from extrinsic to intrinsic diffusion at 1300°C in B-MgO has been attributed to precipitation of impurities and/or $Cu^{++} \rightarrow Cu^{+} + \frac{1}{2}\square^{--}$ transitions at this temperature.

5. Diffusion is controlled by oxygen ion mobility. The enthalpy of formation of the complete Schottky defect and the enthalpy of motion of oxygen ion are 3.6 ± 0.22 eV and 2.76 ± 0.11 eV, respectively.

Dislocation Glide

1. The Peierls stress in MgO depends strongly on the size of the dislocation loop. It decreases as the size of the loop increases.

The technique of annealing thin foils at high temperature, outside the electron microscope and photographing the same area repeatedly can be further useful in studying the mechanisms of annealing out the damage, introduced by irradiation, other modes of plastic deformation (abrasion, creep, fatigue etc.).

ACKNOWLEDGMENTS

I wish to express my sincere gratitude to Professor Jack Washburn for guidance and encouragement throughout this investigation. I am indebted to the late Prof. J. E. Dorn for his interest in this work and various stimulating discussions on theory of diffusion. Thanks are also due to Professors J. W. Morris, R. Hultgren and J. A. Pask for discussions on the subject. Professor F. H. Moffitt's help in stereo-microscopy is thankfully acknowledged.

Mention should be made of Prof. M. F. Merriam and his family and Dr. K. L. Murty whose association and friendship made my stay at Berkeley a pleasant memory.

Acknowledgments are also made to Mrs. Shirley Ashley, D. P. Kreitz and the IMRD Support staff for typing the thesis, photography and general help respectively.

This work was done under the auspices of the U. S. Atomic Energy Commission through the Inorganic Materials Research Division of the Lawrence Berkeley Laboratory.

REFERENCES

1. J. Washburn, Electron Microscopy and Strengths of Crystals, edited by G. Thomas and J. Washburn (Interscience, New York, 1963) Ch. 6.
2. J. Narayan and J. Washburn, LBL-436.
3. T. R. Cass, Ph. D. thesis, University of California, Berkeley, UCRL-11996, 1965.

4a. J. Narayan, M. S. Thesis, UCRL-20305, 1970.

4. G. W. Groves and A. Kelly, J. Appl. Phys. 33, Supplement, 456 (1962).
5. G. W. Groves and A. Kelly, J. Appl. Phys. 34, 3104 (1963).

5b. L. A. Girafalco, Atomic Migration in Crystals (Blaisdell Publishing Co., 1965).

6. C. A. Johnson, Phil. Mag. 5, 1255 (1960).
7. P. B. Price, Phil. Mag. 5, 873 (1960).
8. F. Kroupa and P. B. Price, Phil. Mag. 8, 243 (1961).
9. K. H. Westmacott, A. C. Roberts and R. S. Barnes, Phil. Mag., 7, 2035 (1962).
10. R. S. Barnes, J. Phys. Soc. (Japan) 18, Supp. III, 305 (1963).
11. J. A. Turnbull, Phil. Mag. 21, 83 (1970).
12. R. S. Barnes and D. J. Mazey, AERE, 4126 (1962).
13. A. J. E. Foreman and J. D. Eshelby, AERE R 4170.

13a. A. J. E. Foreman, AERE-R 4654.

14. J. Washburn, G. W. Groves, A. Kelly and G. K. Williamson, Phil. Mag. 5, 991 (1960).
15. P. S. Dobson, P. J. Goodhew and R. E. Smallman, Phil. Mag. 16, 9 (1967).

16. D. N. Seidman and R. W. Balluffi, Phil. Mag. 13, 649 (1966).

17. D. J. Bacon and A. G. Crocker, Phil. Mag. 12, 195 (1966).

18. P. P. Groves and D. J. Bacon, Phil. Mag. 22, 83 (1970).

19. M. O. Davies, J. Chem. Phys. 38 (9), 2047 (1963).

19a. D. W. James and G. M. Leak, Phil. Mag. 12, 491 (1965).

19b. M. J. Whelan, Phil. Mag. 14, 195 (1966).

20. Y. Oishi and W. D. Kingery, J. Chem. Phys. 33 (3), 905 (1960).

20a. L. W. Barr, et al., Trans. Faraday Soc. 56, 697 (1960).

21. B. C. Harding, D. M. Price, and A. J. Mortlock, Phil. Mag. 21, 399 (1970).

22. A. B. Lidiard, 1957, Handbuch der Physik, 20th edition edited by S. Flugee (Berlin).

23. L. W. Barr and A. B. Lidiard, Physical Chemistry-An Advanced Treatise 10, 151 (Academic Press, 1970).

24. B. J. Wuensch and T. Vasilos, J. Amer. Cream. Soc. 49, 433 (1966).

25. G. W. Groves and A. Kelly, Phil. Mag. 6, 1527 (1961); Phil. Mag. 7, 892 (1962).

26. W. M. Latimer, Oxidation Potentials (Prentice Hall, 1964) Ch. 11.

27. P. Guyot and J. E. Dorn, Cana. J. Phys. 45, 983 (1967).

28. B. S. Hickman and D. G. Walker, Phil. Mag. 11, 1101 (1965).

Table I.

Group of Loops	$\bar{X}$	Time in Sec	Temp. °K	Activation Energy
1 in Fig. 1 A	2.78			
		5402	1373	
B	2.68			60,300 ± 4000 cal/mole
		3257	1473	
C	2.44			
		2925	1510	
D	1.588			
E	Collapse			
2 in Fig. 1 A	3.42			
		5402	1373.5	
B	3.35			60,700 ± 3000 cal/mole
		3257	1473	
C	3.14			
		2925	1510	
D	Collapse			

Table II.

Group of Loops	$\bar{X}$	Time in Sec	Temp. °K	Activation Energy
1 in Fig. 14 A	3.19	2438	1359	
B	3.17	2392	1523	59,200 ± 3000 cal/mole
C	3.04	1570	1523	
D	2.98	1202	1523	
E	2.845			
F	Collapse			
2 in Fig. 14 A	3.99	2438	1539	59,500 ± 4000 cal/mole
B	3.96	2392	1523	
C	3.57	1570	1523	
D	2.80	1202	1523	
E	Collapse			

Table III.

Group of Loop	$\bar{X}$	Time in Sec	Temp. °K	Activation Energy
1 in Fig. 3 A	4.91	4565	1468	
B	4.81	2305	1468	60,100 ± 3000 cal/mole
C	4.74	1810	1512	
D	Collapse			
4 in Fig. 4 A	4.49	4565	1468	
B	4.30	2305	1468	59,500 ± 3000 cal/mole
C	4.16			
D	Collapse			
5 in Fig. 11 A	4.37	4565	1468	
B	4.15	2305	1468	60,500 ± 4000 cal/mole
C	3.97			
D	Collapse			

Table IV.

Group of Loops	$\bar{X}$	Time in Sec	Temp. °K	Activation Energy
7 in Fig. 9 A	3.90	2690	1373	
9 B	3.83	3257	1473	Eact 59,500 ± 2500 cal/mole
10 B	3.34			
11 A	Collapse			

Table V. Prismatic slip.

	Diameter of The Loop	Displacement Along The Glide Cylinder	Temp.	Peierls Stress After Temp. Correction of U
Fig. 24 B-C at 1	300 A°	78.5 A°	1250°C	7.25×10^{8} dynes/cm^2 (Foreman)
				1.1×10^{10} dynes/cm^2 (Foreman and Eshelby)
Figs. 24-26 at 2	506 A°	440 A°	1250°C	1.94×10^{8} dynes/cm^2
Figs. 30-31 at 1	442 A°	180 A°	1200°C	3.3×10^{8} dynes/cm^2

FIGURE CAPTIONS

Fig. 1 Illustration of the center of gravity movement when a vacancy is formed at the point P.

Fig. 2 Variation of interaction energy with Z for two circular edge dislocation loops, $X/r = 2$ when they touch each other.

Fig. 3 Interaction of a circular edge dislocation loop with a infinite straight edge dislocation (shown schematically).

Fig. 4 A. Plot of interaction energy (E_{int}) vs $\bar{X}$ (X/r_1) for Coplanar pairs ($r_2 = r_1$).

B. Plot of $d\bar{X}/dE_{int}$ vs $\bar{X}$ for pairs in Fig. 4A.

C. Plot of interaction energy (E_{int}) vs $\bar{X}$ (X/r_1) for Coplanar pairs ($r_2 = r_1/2$).

D. Plot of $d\bar{X}/dE_{int}$ vs $\bar{X}$ for pairs in Fig. 4C.

E. Plot of interaction energy (E_{int}) vs $\bar{X}$ (X/r_1) for Coplanar pairs ($r_2 = r_1/10$).

F. Plot $d\bar{X}/dE_{int}$ vs $\bar{X}$ for pairs in Fig. 4E.

Fig. 5 [r/ln (1.7 r/b)] vs r graph for dislocation loops (used in bulk diffusion calculations).

Fig. 6 6A → 6B, annealing time 20 mts at 1126°C. At 1 and 3, there is self climb of prismatic disslocation loops, b = 1/2[101]. At 2, pipe diffusion along screw dislocation of same b-vector as the dislocation loop (b = 1/2[101]).

Fig. 7 7A → 7B, annealing time 27 min 5 sec at 1194.5°C. At 1 and 2, there is self climb of prismatic edge dislocation loops, b = 1/2[101]. There is opening up of dipoles at 3 and 4, and the big loop at 5 has slipped out by prismatic slip; all have b-vector 1/2[101].

Fig. 8 A → B, 31 min 40 sec at 1194.5°C.

B → C, 40 min at 1194.5°C.

C → D, 45 min 5 secs at 1194.5°C.

Self climb at 1, 2 and 3 dislocation loop, (b = 1/2[101] near the center of the foil at 5 is shrinking purely by bulk diffusion; loops (b = 1/2 [101]) at 6 and 7, being close to sinks are shrinking rapidly. Dislocation loop at 8, b = 1/2 [101] has slipped out of the foil.

Fig. 9,10,11 These are from the same area after different annealing treatments;

9A → 9B,44 min 50 secs at 110°C;

9B → 10A, 20 min 42 secs at 1200°C;

10A → 10B, 33 min 35 secs at 1200°C;

10B → 11A, 38 min 45 secs at 1237°C;

11A → 11B, 64 min 40 secs at 1200°C;

Self climb at 1, 2, 3, 7, a, b, c and d of dislocation loops b = 1/2 [101], prismatic slip due to surface interaction of the foil at 5 and 9 of loops b = 1/2[101].

Fig. 12 A → B, 4502 secs at 1373°K;

B → C, 3257 secs at 1473°K;

Fig. 12 C → D, 2925 secs at 1510°K;

D → E, 3880 secs at 1473°K;

E → F, 2720 secs at 1473°K.

The set of pictures shows self climb at 1, 2, 3 and 6, loops at 4 and 5 have slipped out of the foil.

Fig. 13 A → B, 2438 secs at 1359°K;

B → C, 2392 secs at 1523°K;

C → D, 1570 secs at 1523°K;

D → E, 1202 secs at 1523°K;

E → F, 2369 secs a5 1523°K.

The set of pictures shows self climb at 1 and 2, also same of the loops have slipped of the foil.

Fig. 14 A → B, 4565 secs at 1468°K;

B → C, 2305 secs at 1468°K;

C → D, 1810 secs at 1512°K.

Shows self climb at 1, 2, 3, 4 and 5, climb due to bulk diffusion at 7 (just above 4). At 6 there is mutual annihilation of vacancy and interstitial loops on glide cylinders at 90° to each other.

Fig. 15 A → B, 2115 secs at 1446.66°K;

B → C, 1230 secs at 1508°K.

Shows self climb at 1.

Fig. 16 A → B, 42 min 5 secs at 1368°C;

B → C, 45 min 52 secs at 1291°C;

C → D, 150 min 8 secs at 1202°C;

D → E, 46 min 10 secs at 1243°C.

Shows climb due to bulk diffusion at 1, 2, 3 and 4.

Fig. 17 A → B, 42 min 5 secs at 1368°C;

B → C, 45 min 52 secs at 1291°C;

C → D, 60 min 0 secs at 1202°C;

D → E, 90 min 8 secs at 1202°C + 46 min 10 secs at 1243°C.

Shows climb of dislocation loops ,b = 1/2[101] at 1 and 2, which are near the center of the foil, due to bulk diffusion.

Fig. 18 A → B, 64 min 0 secs at 1260°C;

B → C, 80 min 0 secs at 1260°C;

C → D, 20 min 10 secs at 1400°C;

D → E, 20 min 5 secs at 1400°C.

The set of pictures shows climb due to bulk diffusion at 1 and 2 for loops b = 1/2[101] which are near the center of the foil.

Fig. 19 A → B, 11 min 0 secs at 1427°C

B → C, 16 min 0 secs at 1427°C

C → D, 24 min 35 secs at 1400°C;

D → E, 9 min 1 sec at 1400°C.

Shows climb due to bulk diffusion at 1, 2 and 3.

Fig. 20 A,B,C r^2 vs t plots for dislocation loops in Figs. 16-19.

Fig. 21 A → B, 42 min 5 secs at 1368°C;

B → C, 45 min 52 secs at 1291°C;

C → D, 150 min 8 secs at 1202°C;

D → E, 46 min 10 secs at 1243°C.

Shows climb due to bulk diffusion at 1, 2, 3, and 5 for B-MgO.

Fig. 22 r^2 vs t plots for loops in Fig. 21

Fig. 23 D vs 1/T plot for both A-MgO and B-MgO in the temperature range 1080-1427°C.

Fig. 24-28 This set represents the same area at five temperatures.

A → B, 20 min 2 secs at 1250°C;

B → C, 20 min 0 secs at 1250°C;

C → D, 19 min 29 secs at 1250°C;

D → E, 49 min 15 secs at 1100°C;

E → F, 45 min 12 secs at 1100°C;

F → G, 44 min 50 secs at 1100°C;

G → H, 20 min 42 secs at 1200°C;

H → I, 33 min 35 secs at 1200°C;

I → J, 38 min 45 secs at 1237°C;

J → K, 64 min 40 secs at 1200°C;

K → L, 45 min 20 secs at 1200°C.

Prismatic slip at 1, 2 and 3; self climb at 4; pipe diffusion and glide at 5, 6, 7 and 9 and numerous examples of self climb and prismatic slip.

Fig. 29-32 This is another set at five temperatures.

A → B, 45 min 12 secs at 1100°C;

B → C, 44 min 50 secs at 1100°C;

C → D, 20 min 42 secs at 1200°C;

D → E, 33 min 35 secs at 1200°C;

E → F, 38 min 45 secs at 1237°C;

F → G, 64 min 40 secs at 1200°C;

G → H, 45 min 20 secs at 1200°C.

Prismatic slip at 1 and 4, self climb at 2 and numerous examples of self climb and prismatic slip due to surfaces of the foil.

Fig. 33 Plot of Peierls stress vs diameter of the loop b = 1/2[101]. The values of Peierls stress have been plotted after temperature correction in shear modulus of elasticity.

Fig. 34 The set of pictures shows the effect of size of the loop on Peierls stress. Both loops 1 and 2 are near the surface of the foil but 1 is situated at 220A° below the same b-vector 1/2[101].

A → B, 44 min 50 secs at 1100°C;

B → C, 54 min 17 secs at 1200°C;

C → D, 38 min 45 secs at 1237°C;

D → E, 64 min 40 secs at 1200°C.

Stereo pair of B is also given.

Fig. 35 This is an example of prismatic slip of dislocation loops (at 1) of opposite b-vectors (one interstitial and other vacancy type).

A → B, 26 min 55 secs at 1050°C;

B → C, 34 min 2 secs at 1050°C.

Fig. 36 At 1, there is an example similar to 35.

A → B, 59 min 31 secs at 1250°C.

Fig. 37 Shows prismatic slip at 1 and 2.

A → B, 10 min 0 secs at 1086°C;

B → C, 19 min 5 secs a5 1086°C.

Fig. 38 Shows dislocation glide at 1; self climb at 2, 3 and 4; prismatic slip due to surface at 5 and 6.

A → B, 26 min 10 secs at 1250°C;

B → C, 40 min 2 secs at 1250°C.

Fig. 39 Shows prismatic slip at 1. Stereo pair (B) is given.

A → B, 19 min 5 secs at 1086°C;

B → C, 16 min 55 secs at 1086°C;

C → D, 23 min 2 secs at 1086°C;

D → E, 40 min 38 secs at 1086°C;

Fig. 40 Shows annealing of dislocation loops b = 1/2[101], cut by the surface of the foil.

A → B, 19 min 5 secs at 1086°C;

B → C, 39 min 57 secs at 1086°C;

C → D, 40 min 38 secs at 1086°C.

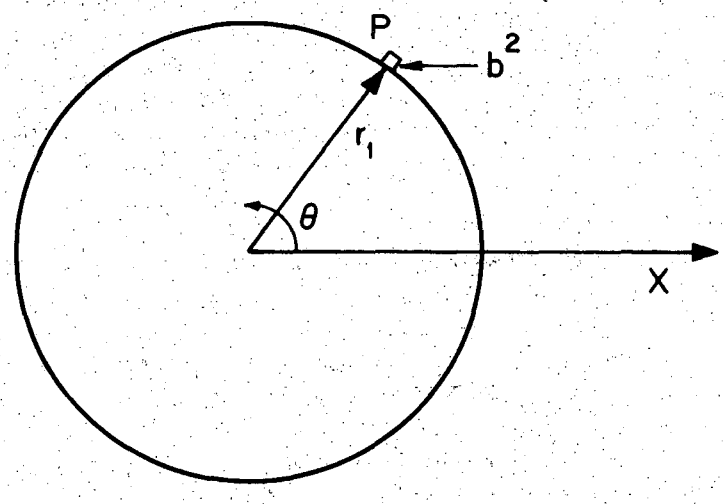

XBL 7111-4698

Fig. 1

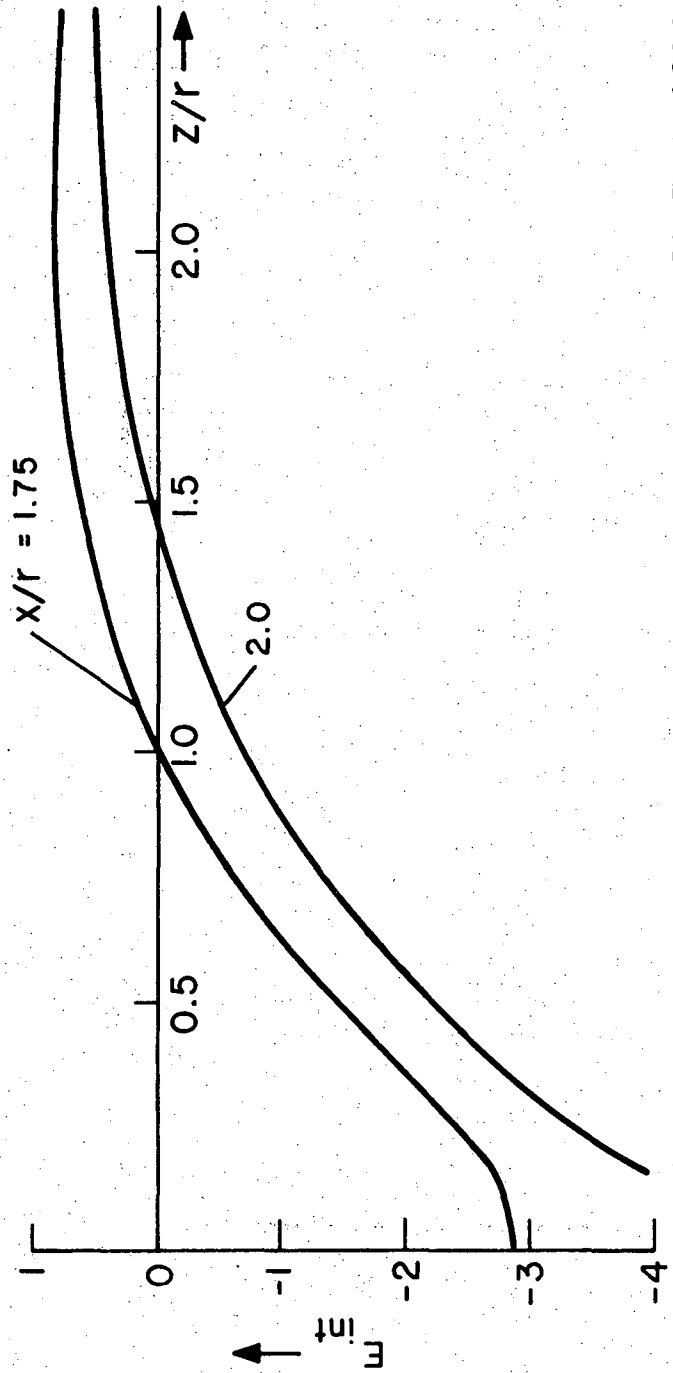

XBL 7111-4699

Fig. 2

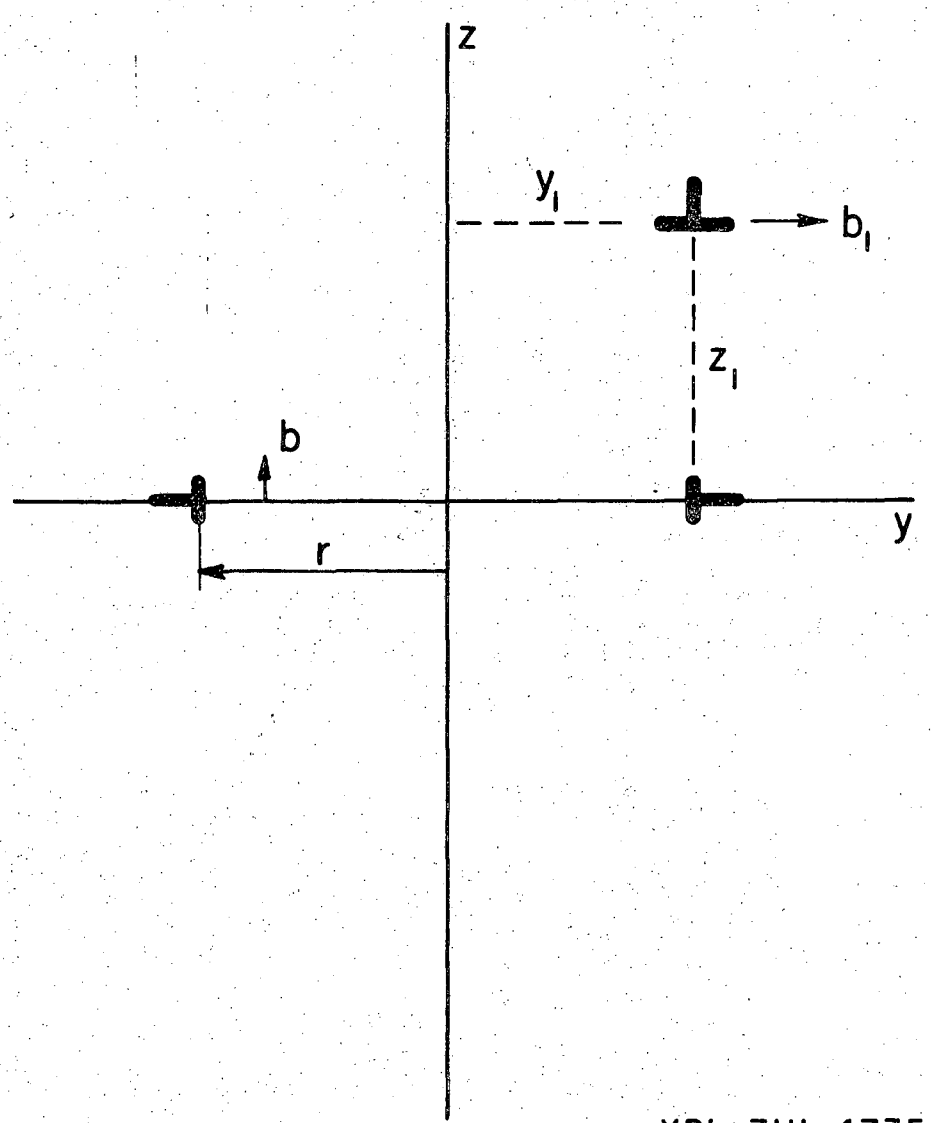

Fig. 3

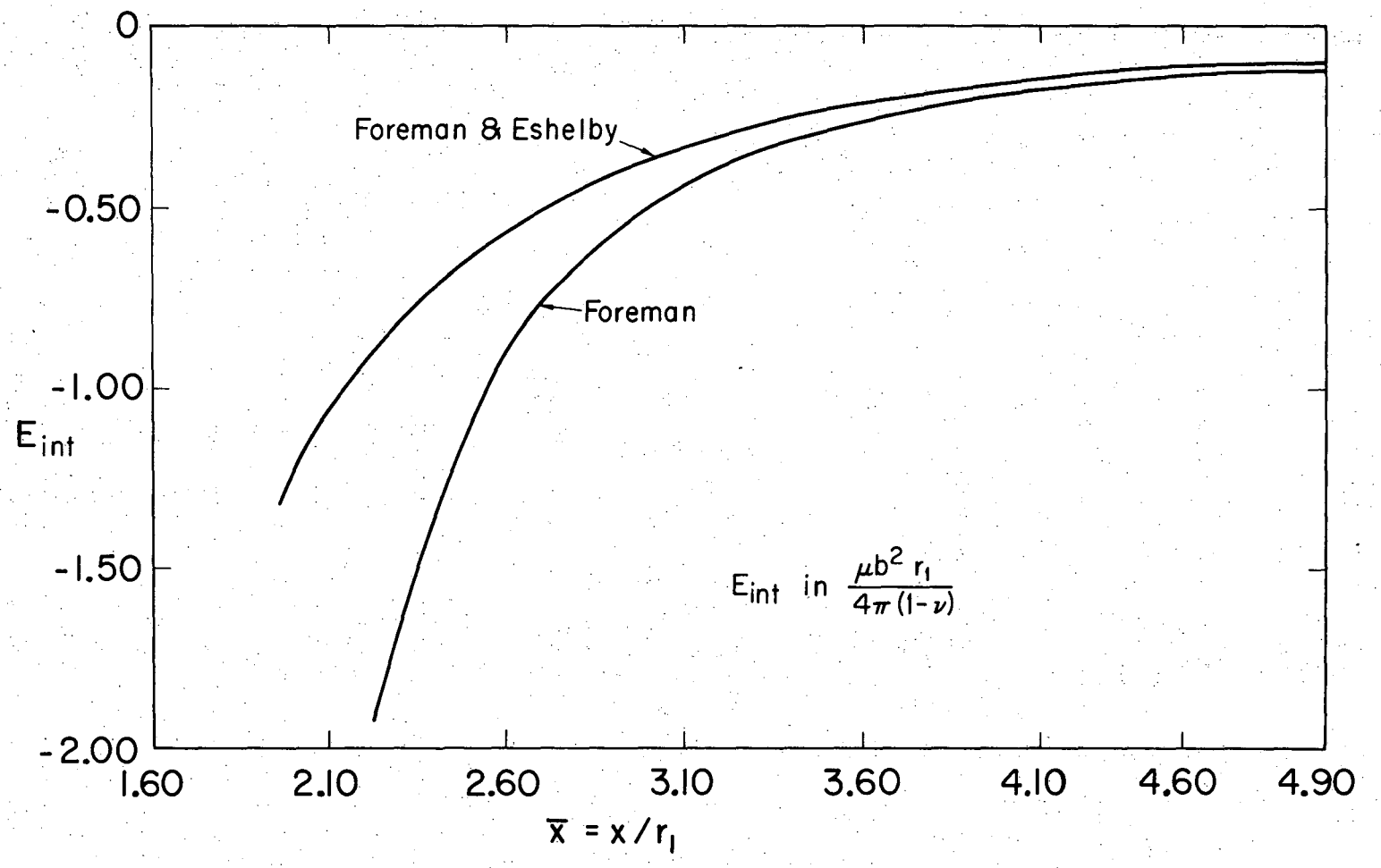
0
-0.50
-1.00
-1.50
-2.00
E_{int}
Foreman & Eshelby
Foreman
E_{int} in $\frac{\mu b^2 r_1}{4\pi(1-\nu)}$
1.60
2.10
2.60
3.10
3.60
4.10
4.60
4.90
$\bar{x} = x/r_1$
XBL7111-4697

Fig. 4A

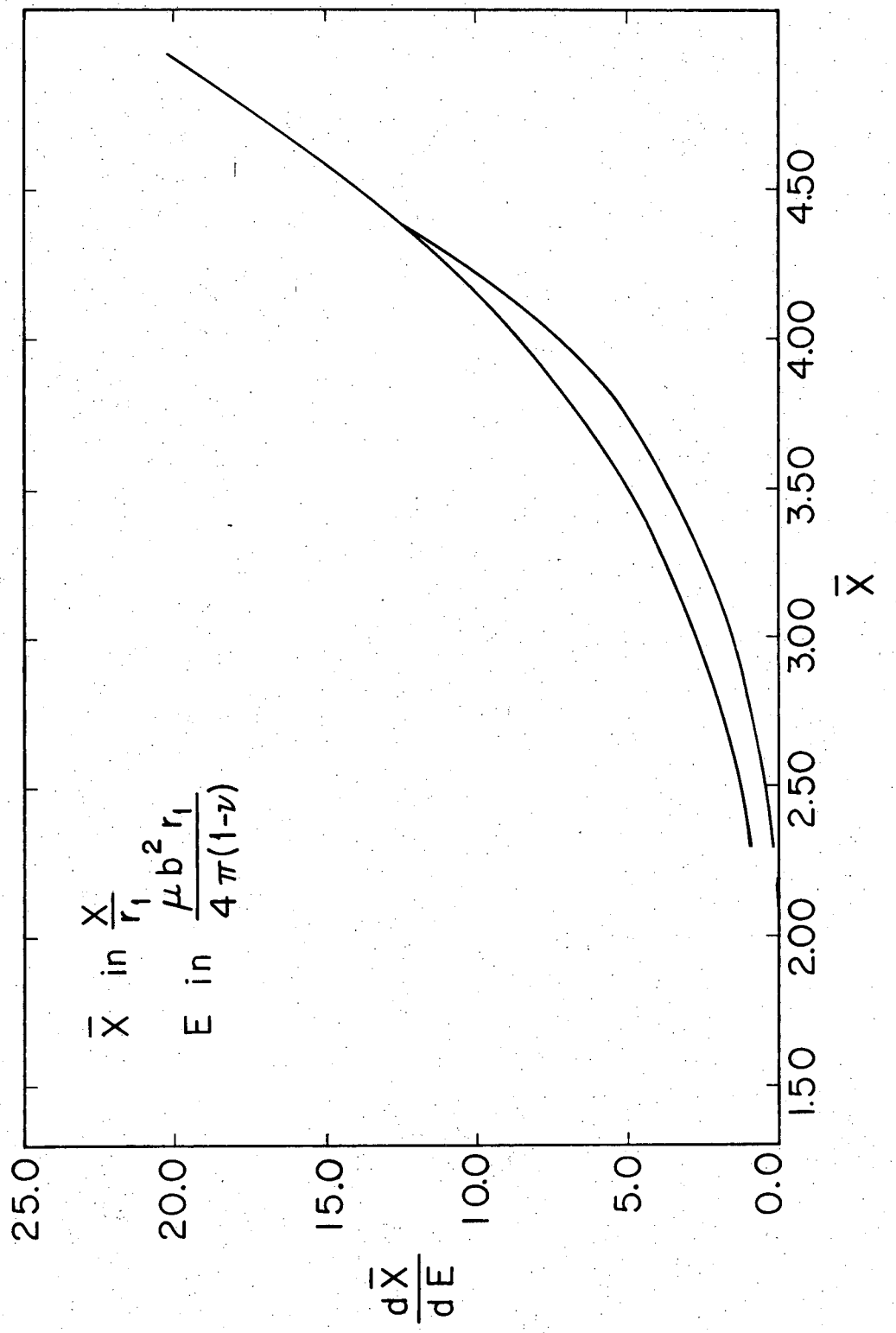

XBL716-3637

Fig. 4B

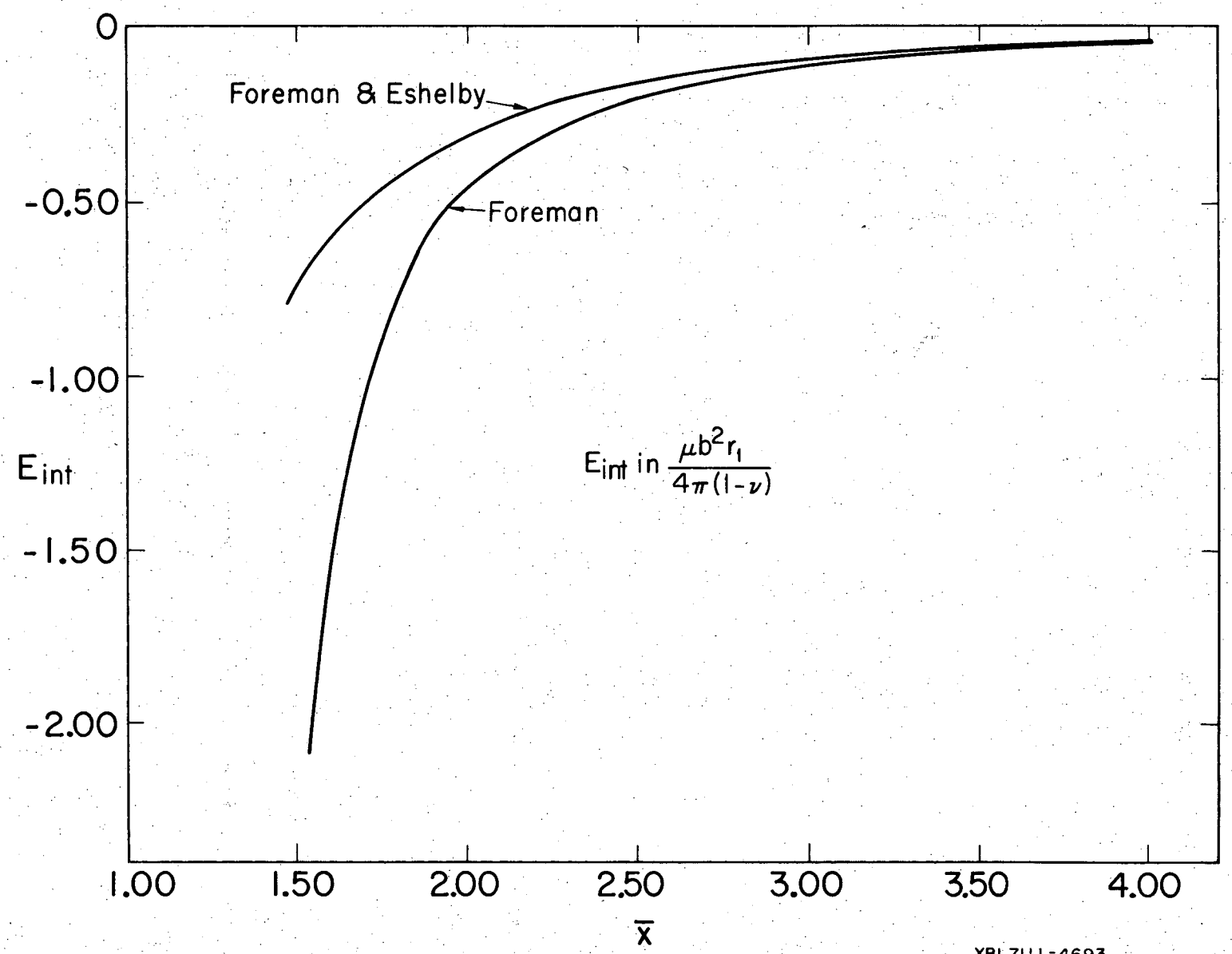
0
-0.50
-1.00
-1.50
-2.00
Eint
Foreman & Eshelby
Foreman
Eint in $\frac{\mu b^2 r_1}{4\pi(1-\nu)}$
1.00
1.50
2.00
2.50
3.00
3.50
4.00
$\bar{x}$
XBL7111-4693

Fig. 4C

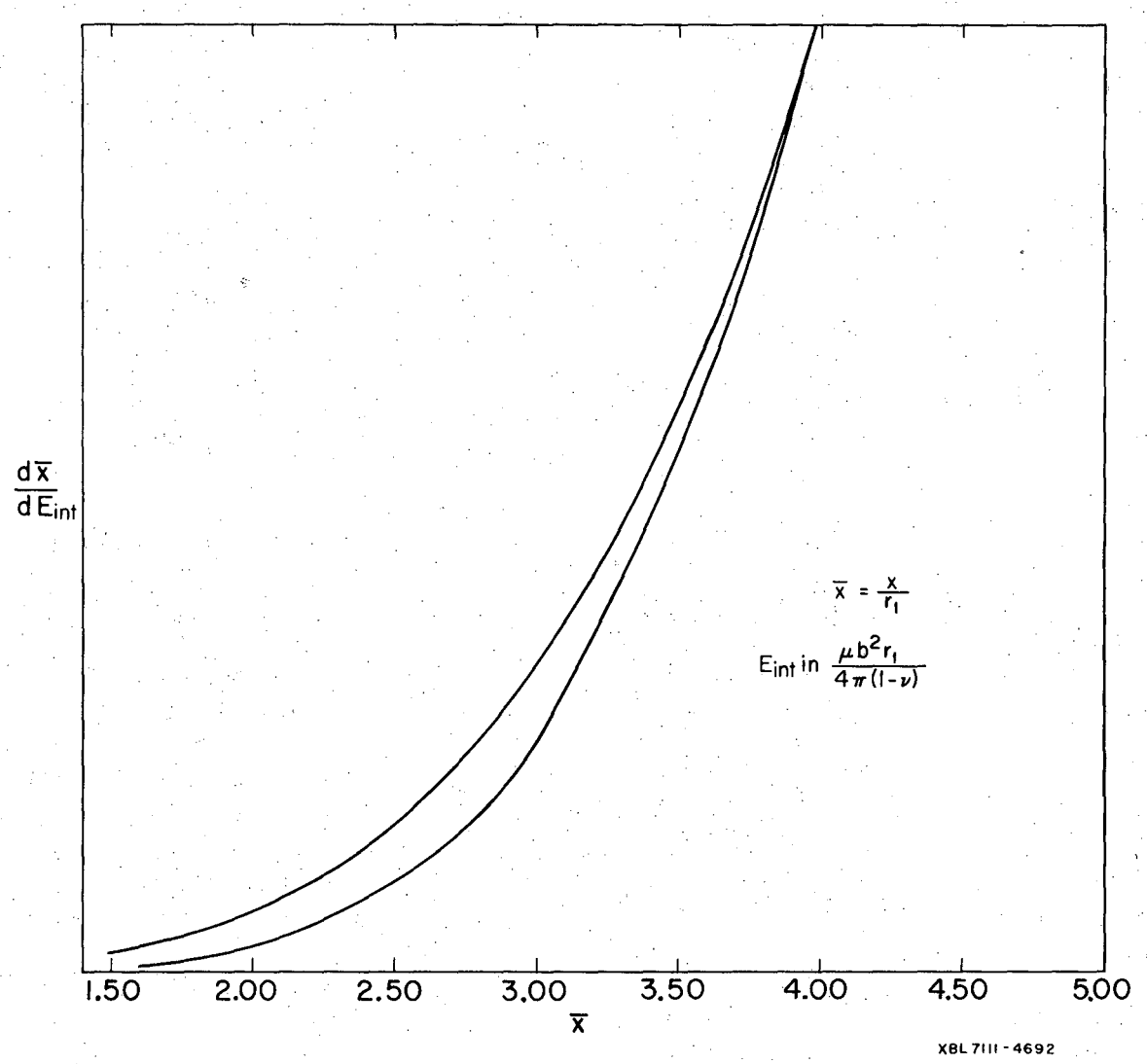

Fig. 4D

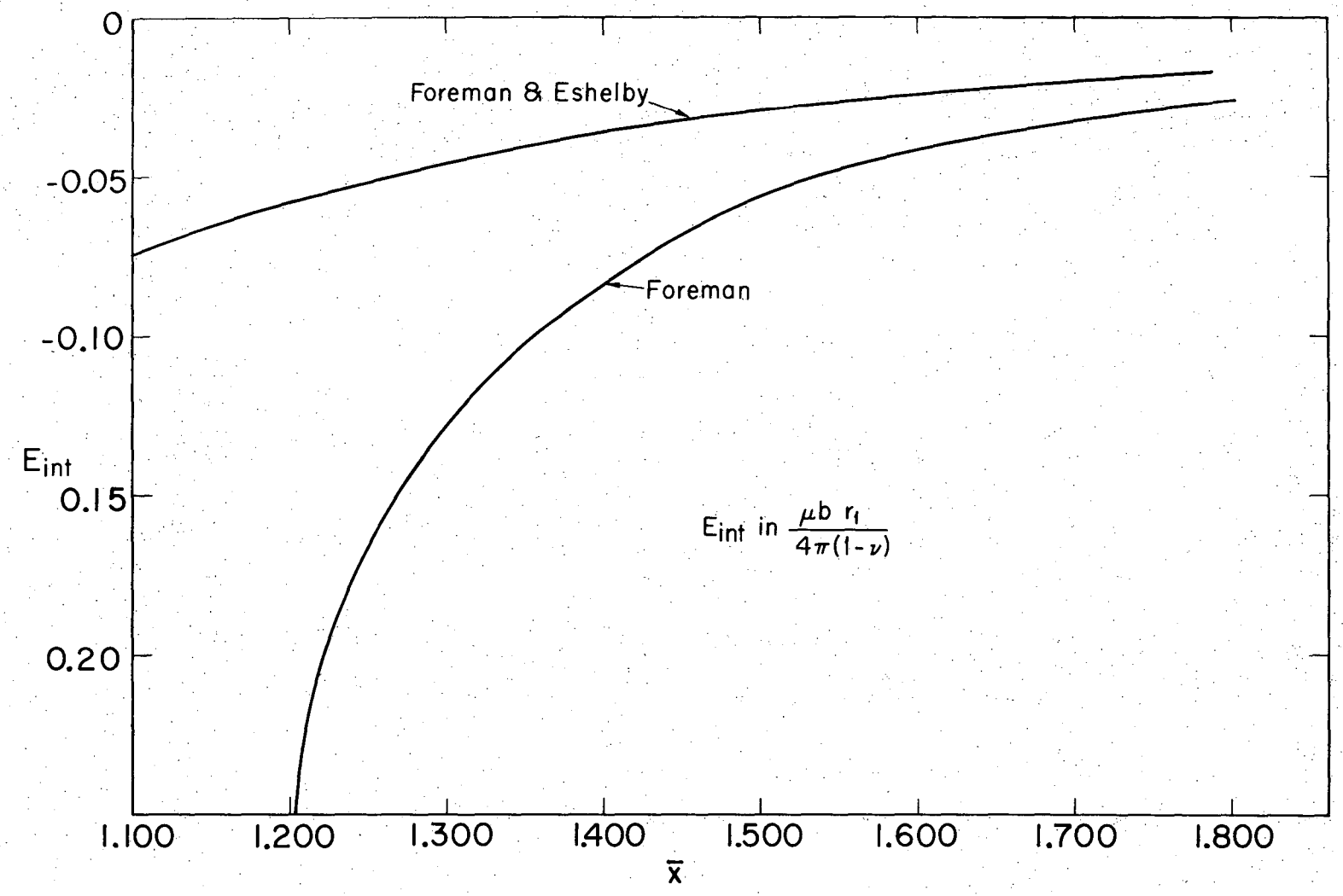

XBL7111-4696

Fig. 4E

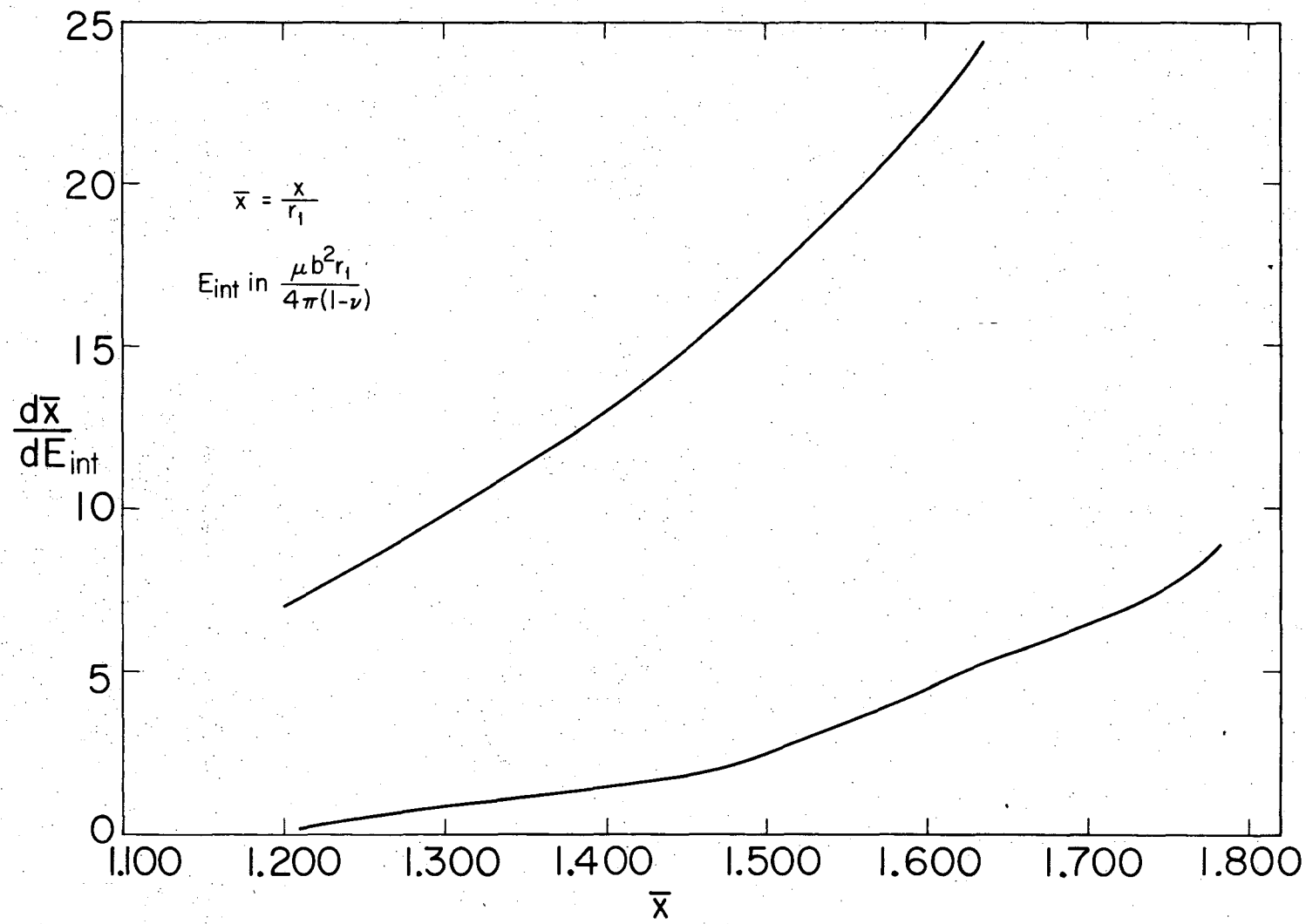

XBL 7111 - 4694

Fig. 4F

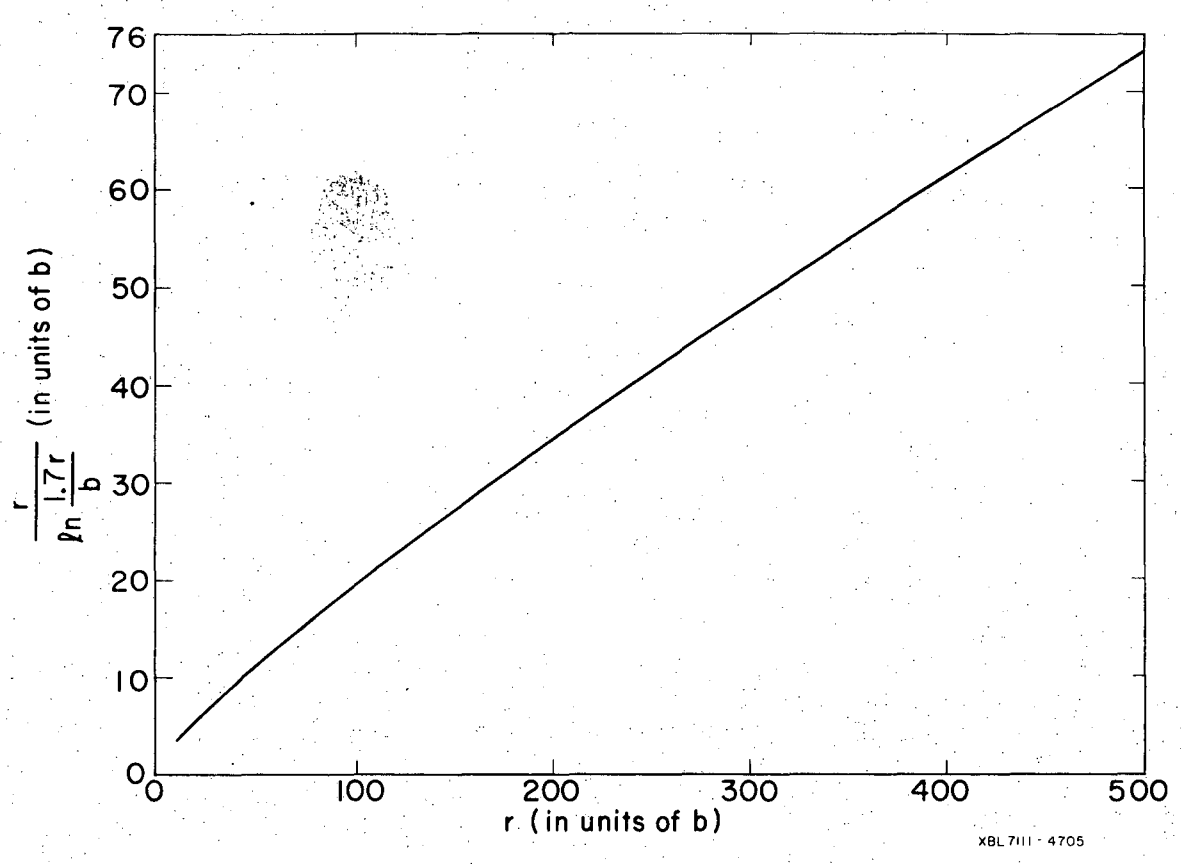
76
70
60
50
40
30
20
10
0
0
100
200
300
400
500
r (in units of b)
$\frac{r}{\ln \frac{1.7r}{b}}$ (in units of b)
XBL 7111 - 4705

Fig. 5

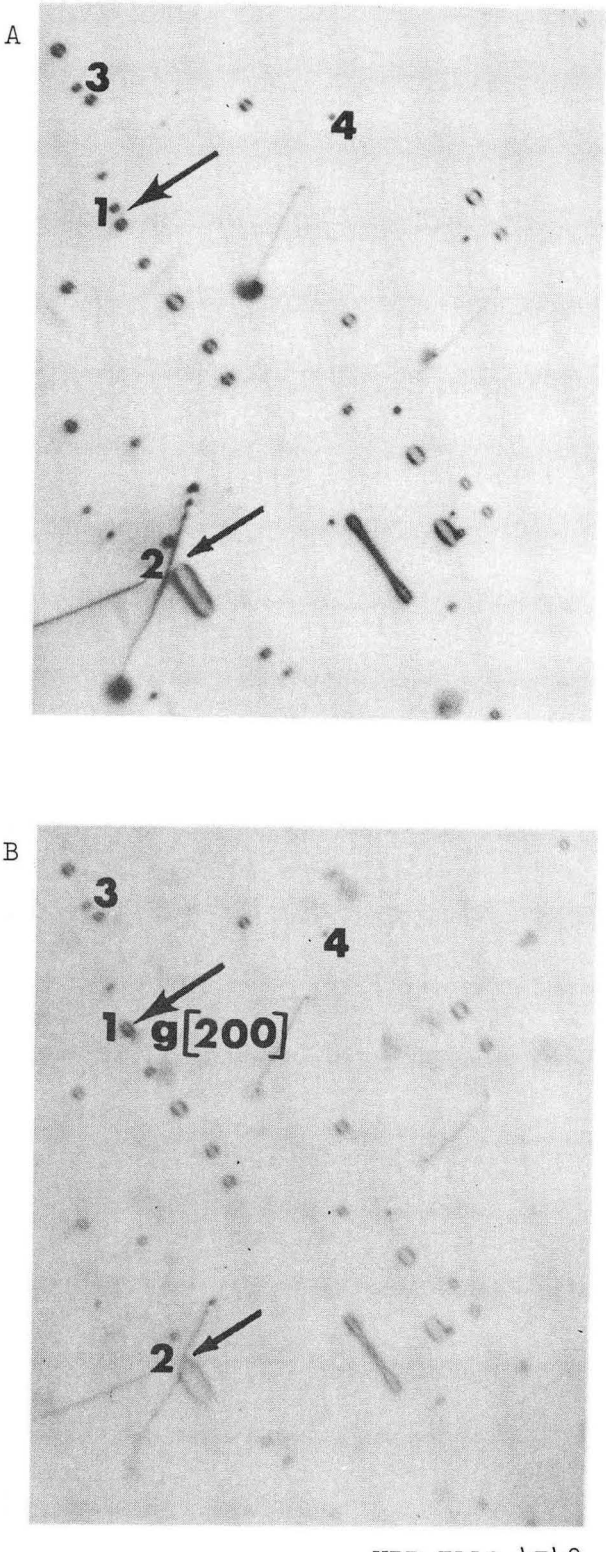

XBB 7110-4748

Fig. 6 Magnification 48400×.

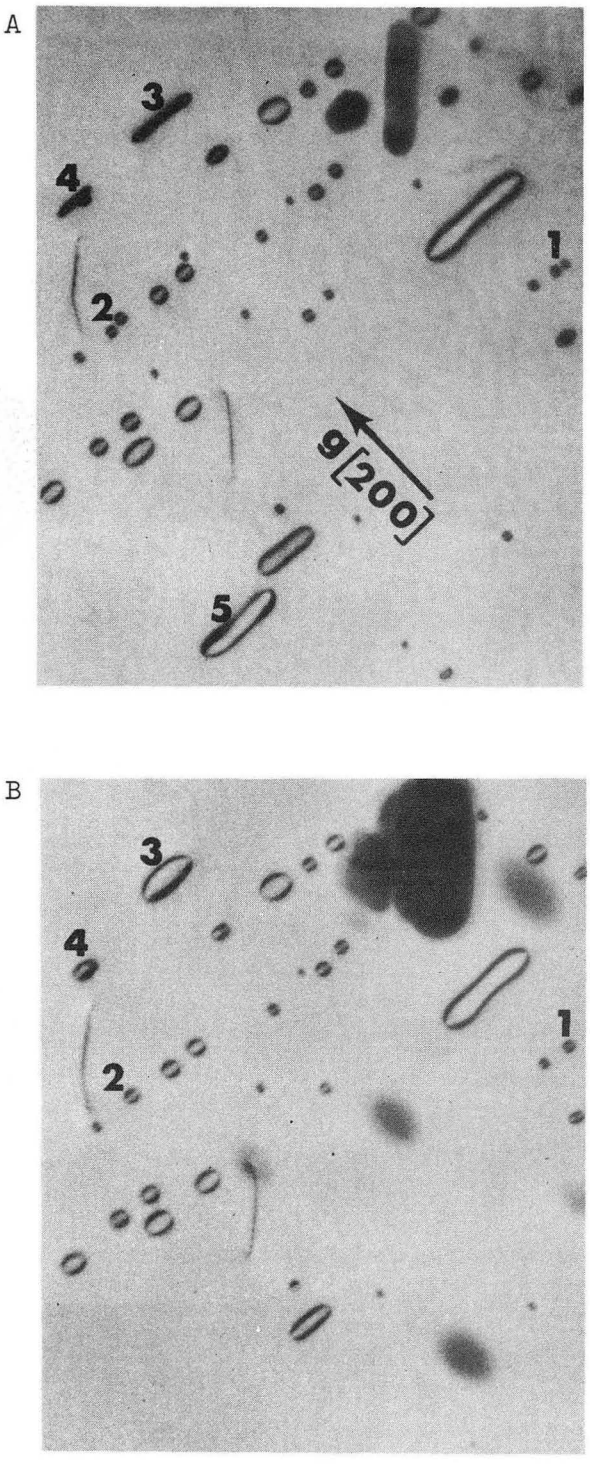

XBB 7110-4746

Fig. 7 Magnification 47400×.

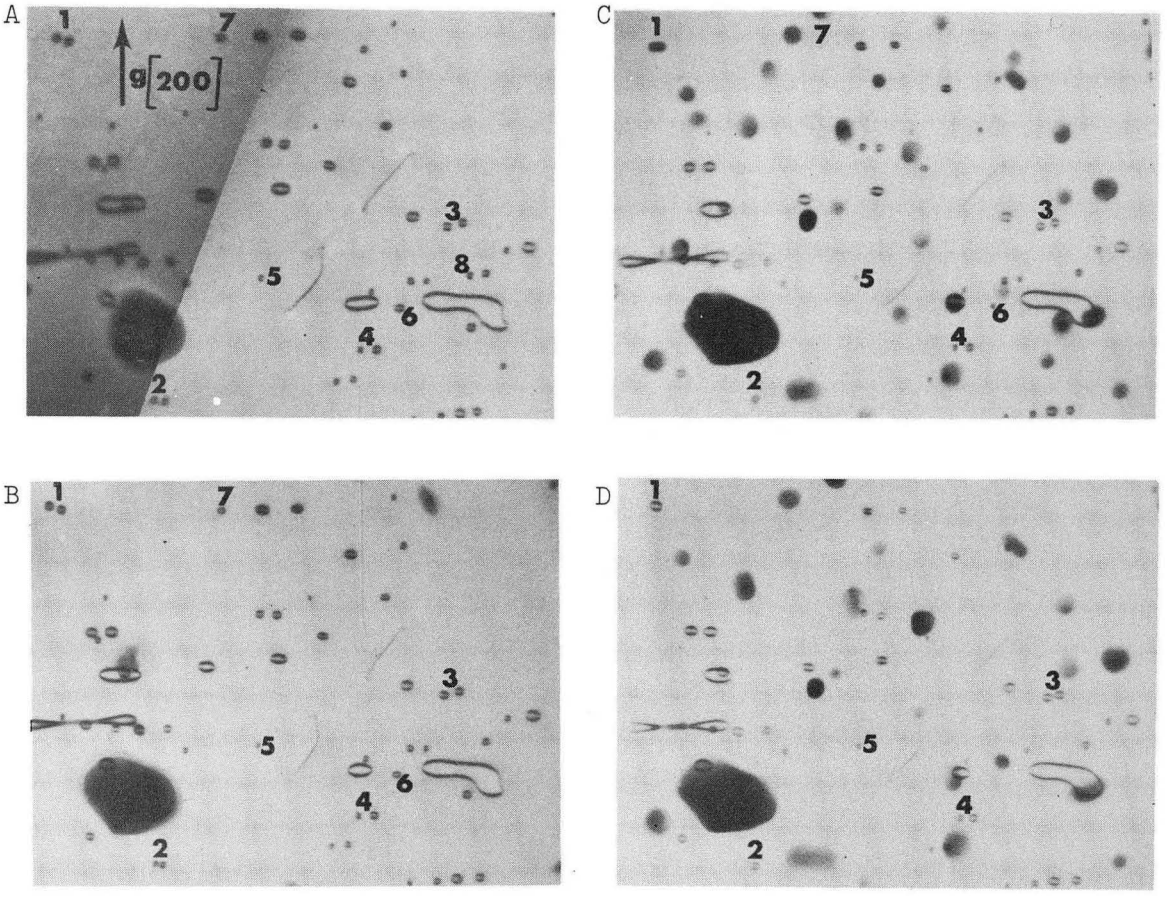

XBB 7110-4751

Fig. 8 Magnification 35600×.

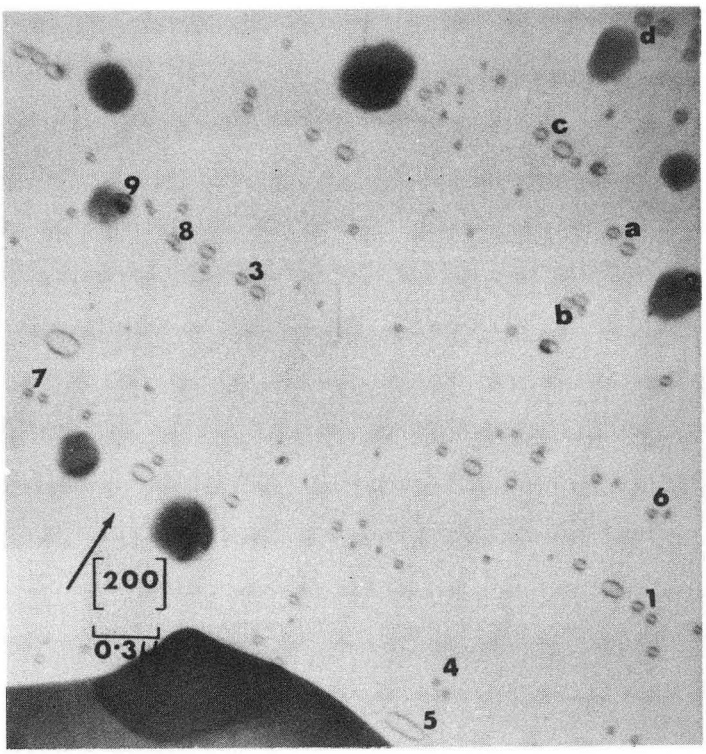

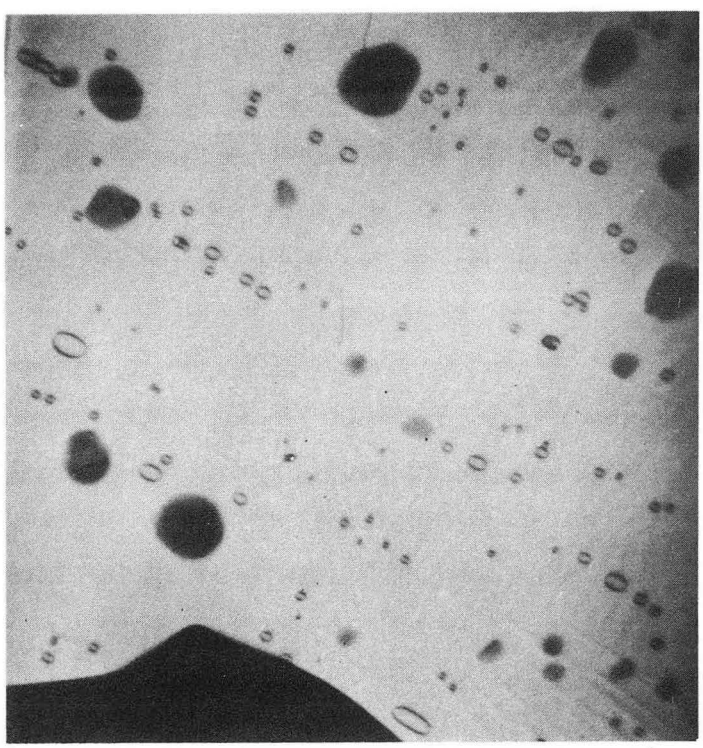

XBB 7111-5427

Fig. 9

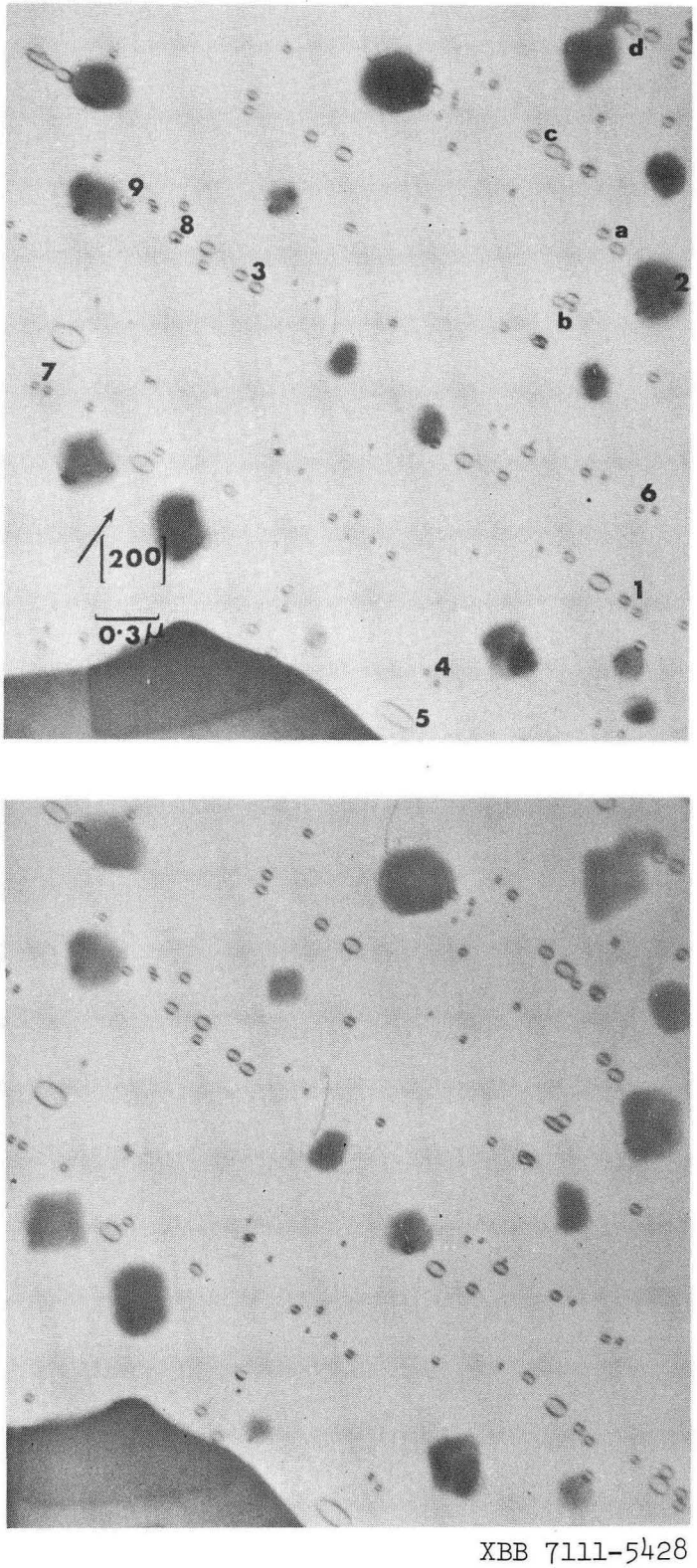

XBB 7111-5428

Fig. 10

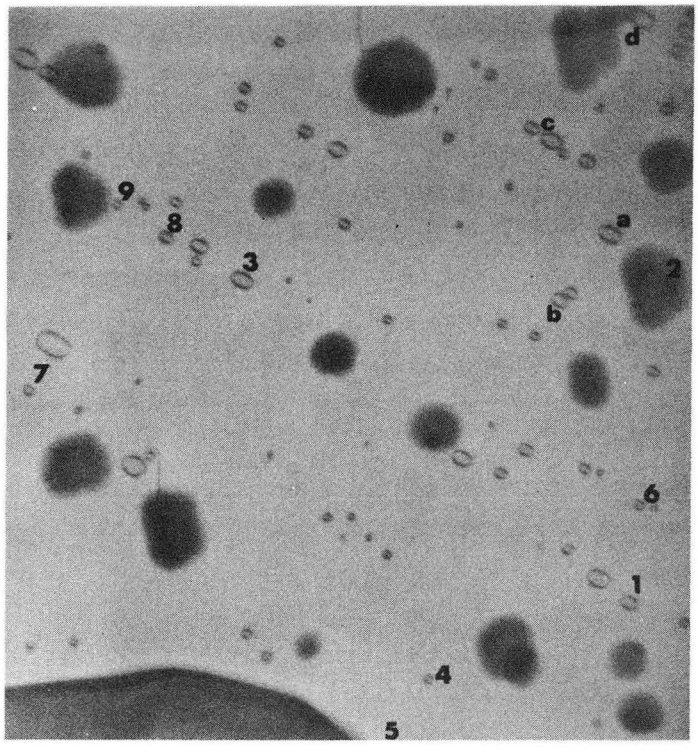

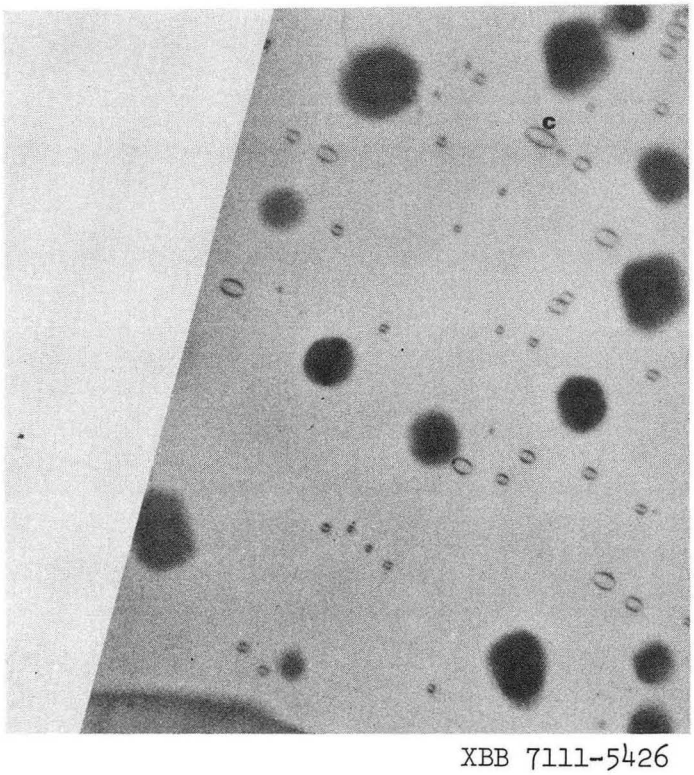

XBB 7111-5426

Fig. 11

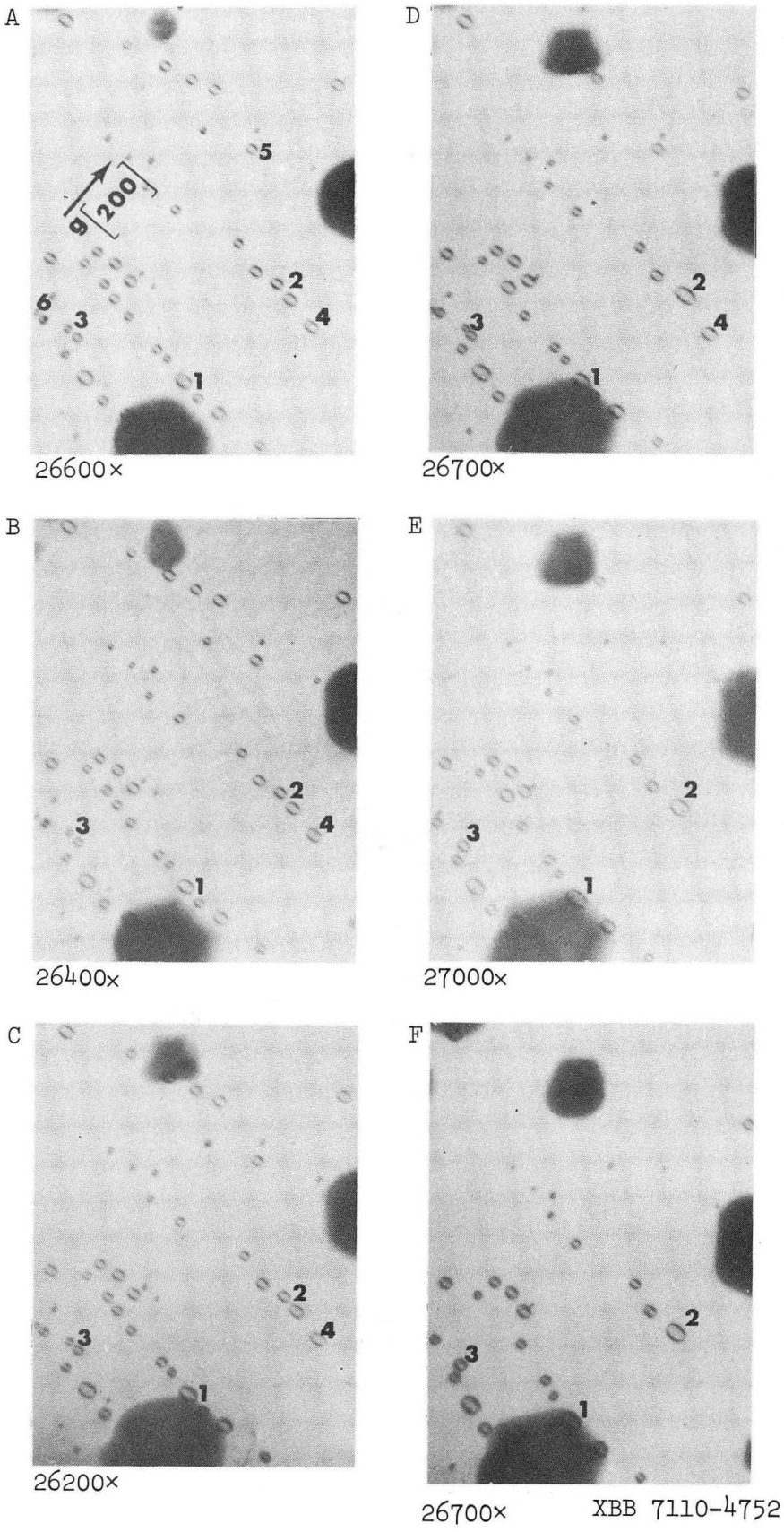

Fig. 12

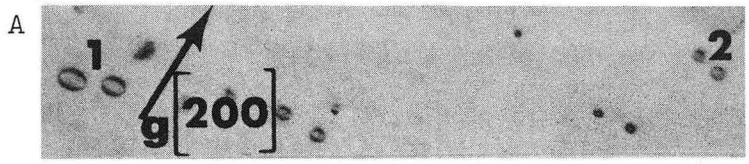

46800×

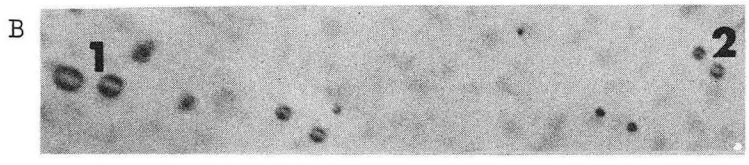

46800×

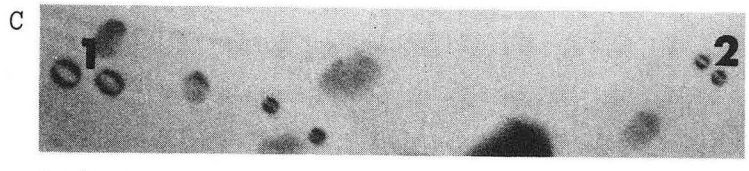

47800×

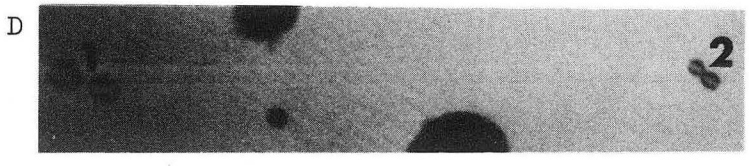

47200×

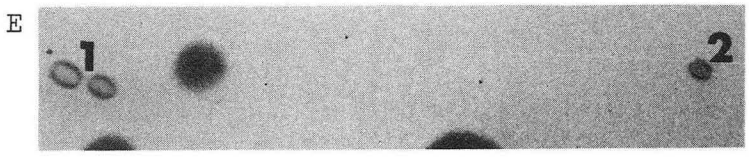

46400×

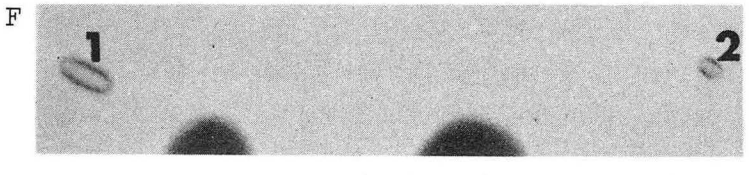

46500×

XBB 7110-4744

Fig. 13

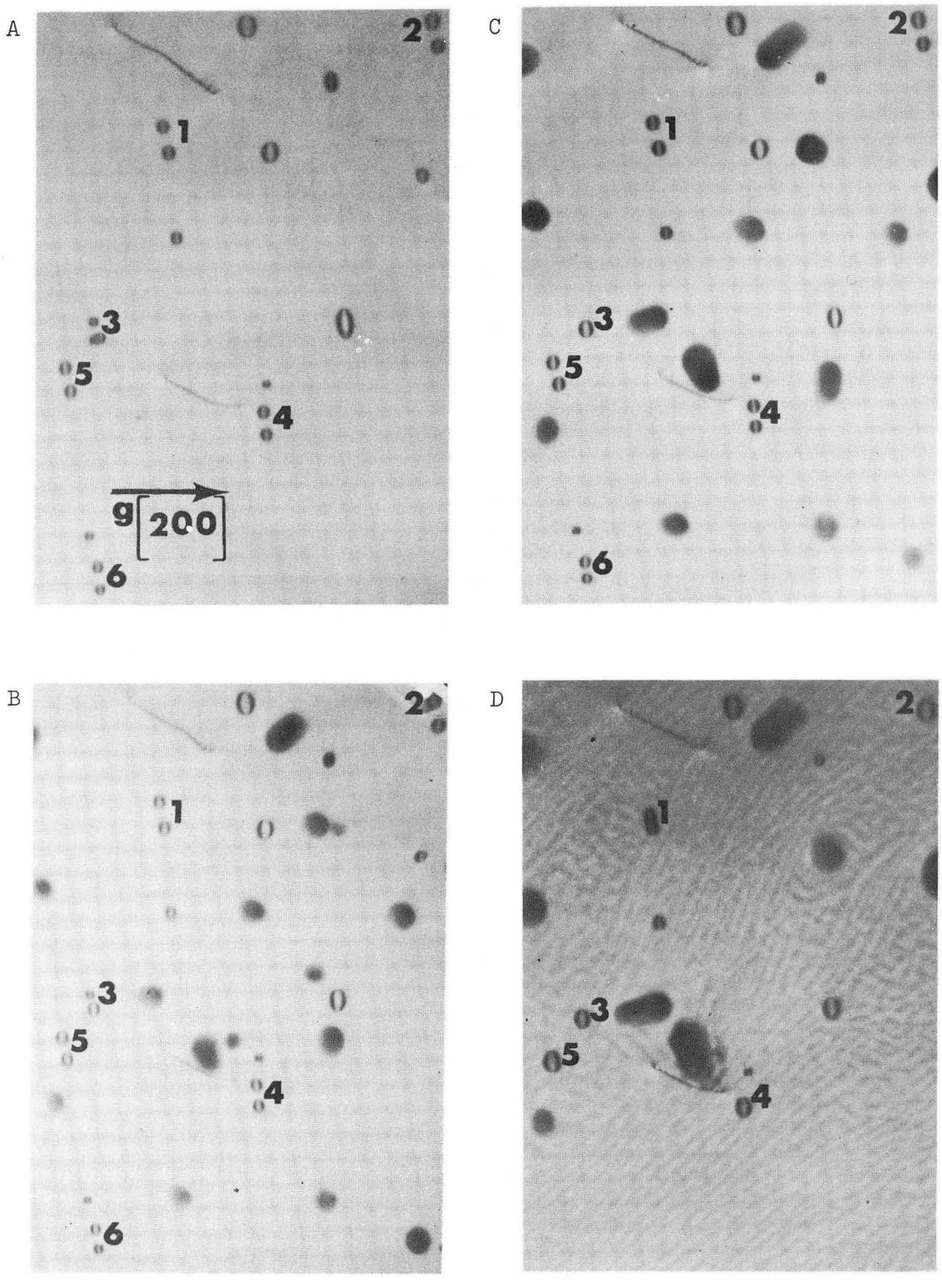

XBB 7110-4747

Fig. 14 Magnification 41900×.

A

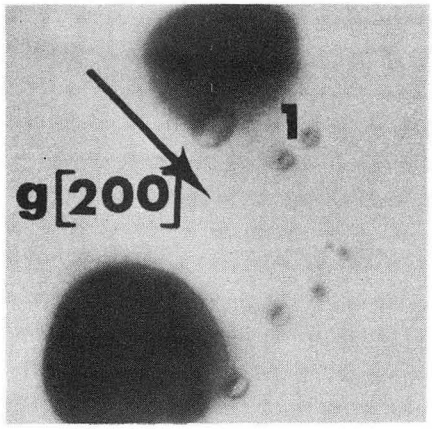

58500×

B

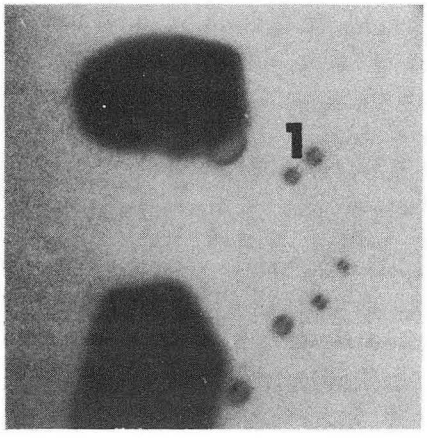

58500×

C

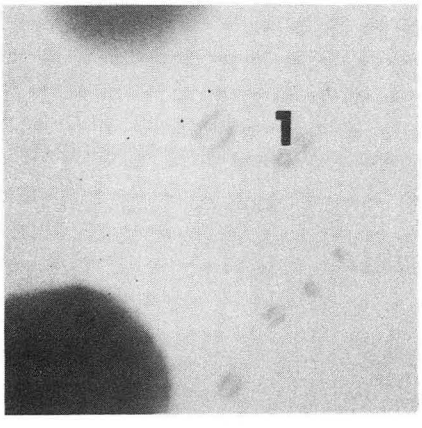

XBB 7110-4750

59800×

Fig. 15

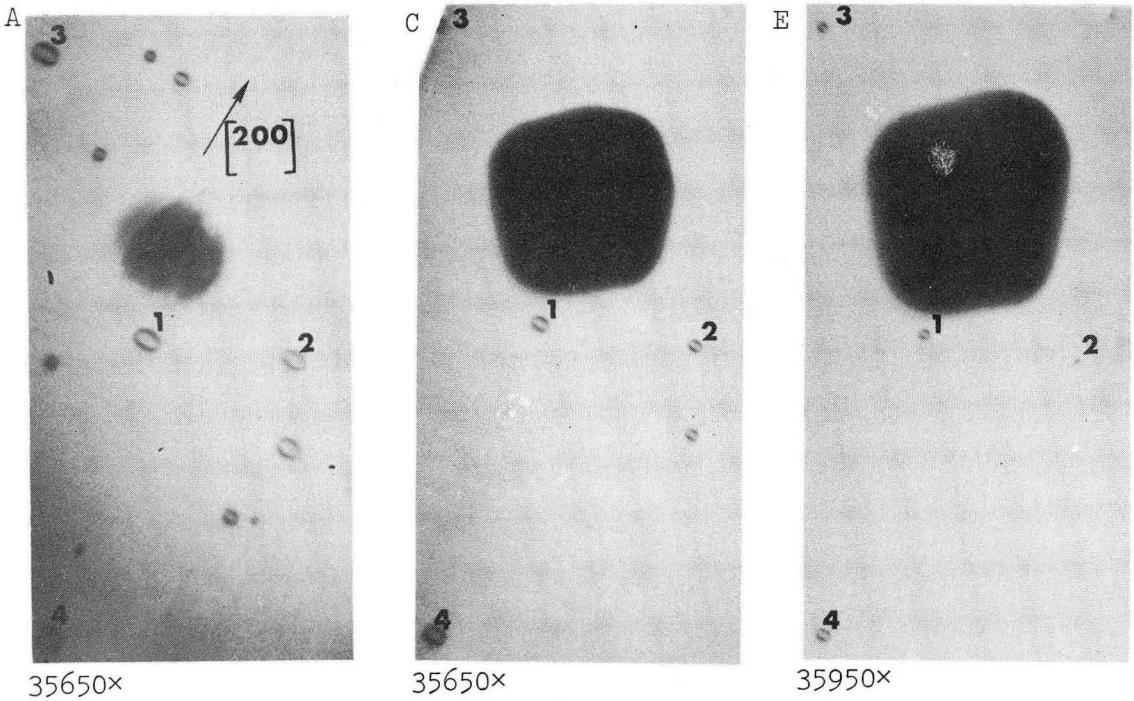

35650× 35650× 35950×

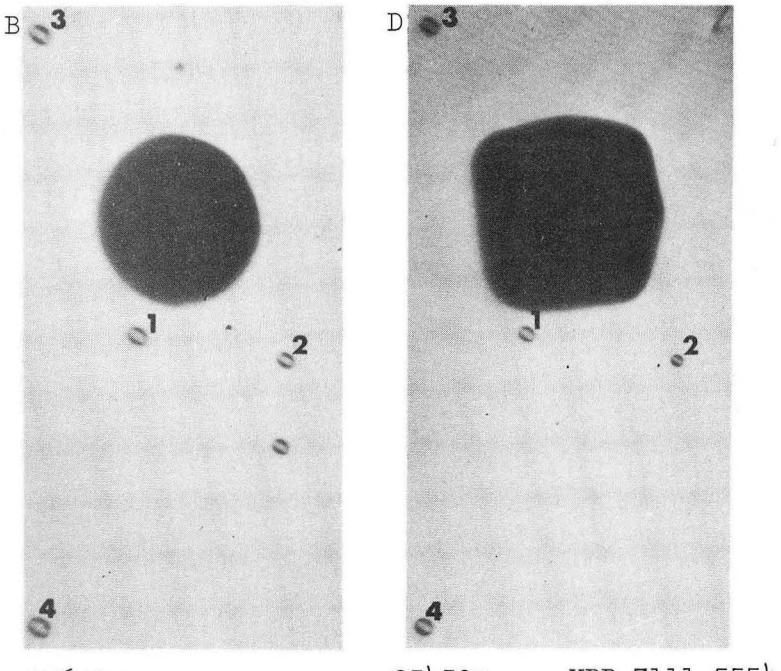

35650× 35450× XBB 7111-5554

Fig. 16

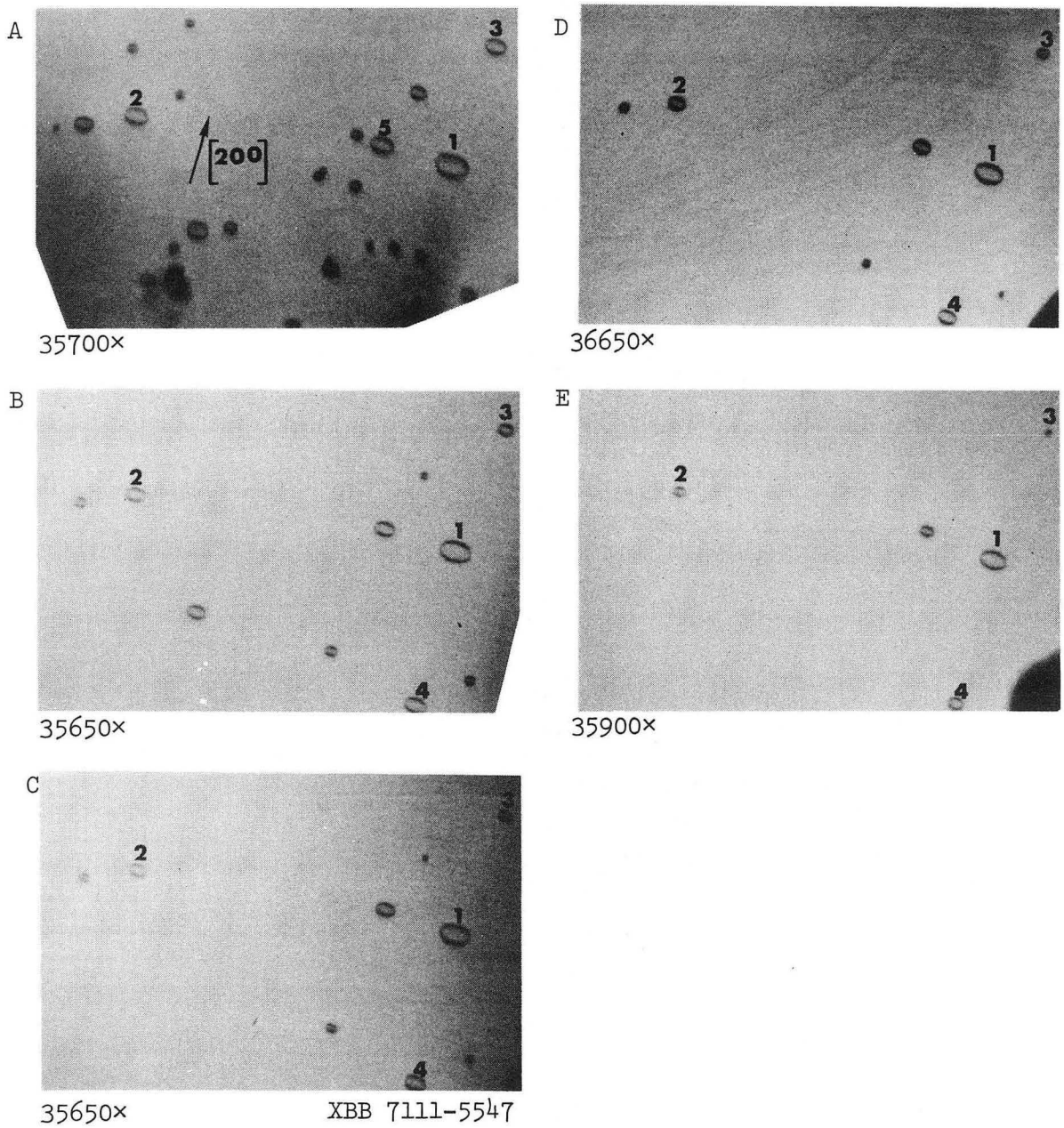
A
3
2
[200]
5
1
35700×
D
3
2
1
4
36650×
B
3
2
1
4
35650×
E
3
2
1
4
35900×
C
2
1
4
35650×
XBB 7111-5547

Fig. 17

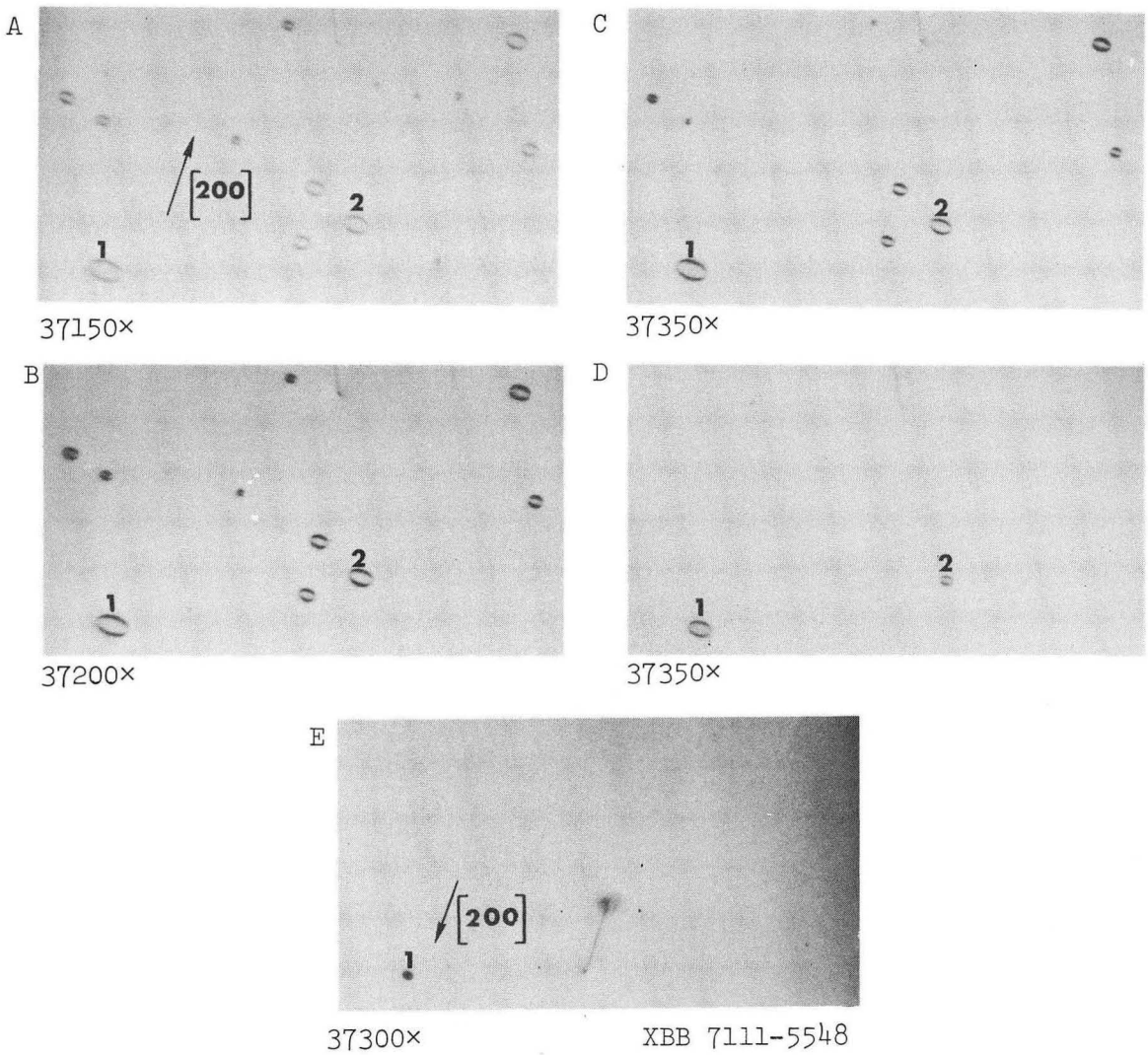

Fig. 18

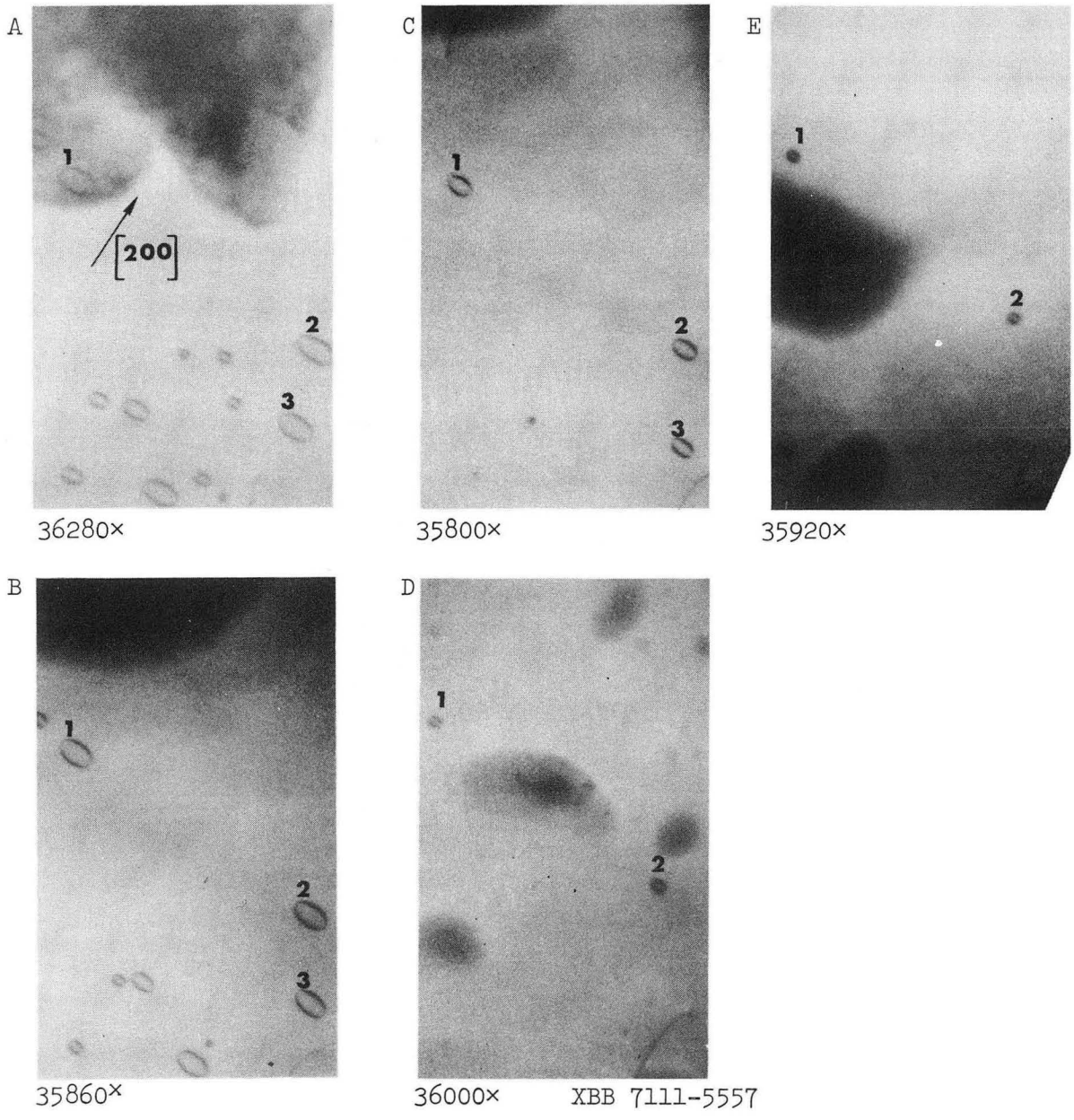
A
1
[200]
2
3
36280×
C
1
2
3
35800×
E
1
2
35920×
B
1
2
3
35860×
D
1
2
36000×
XBB 7111-5557

Fig. 19

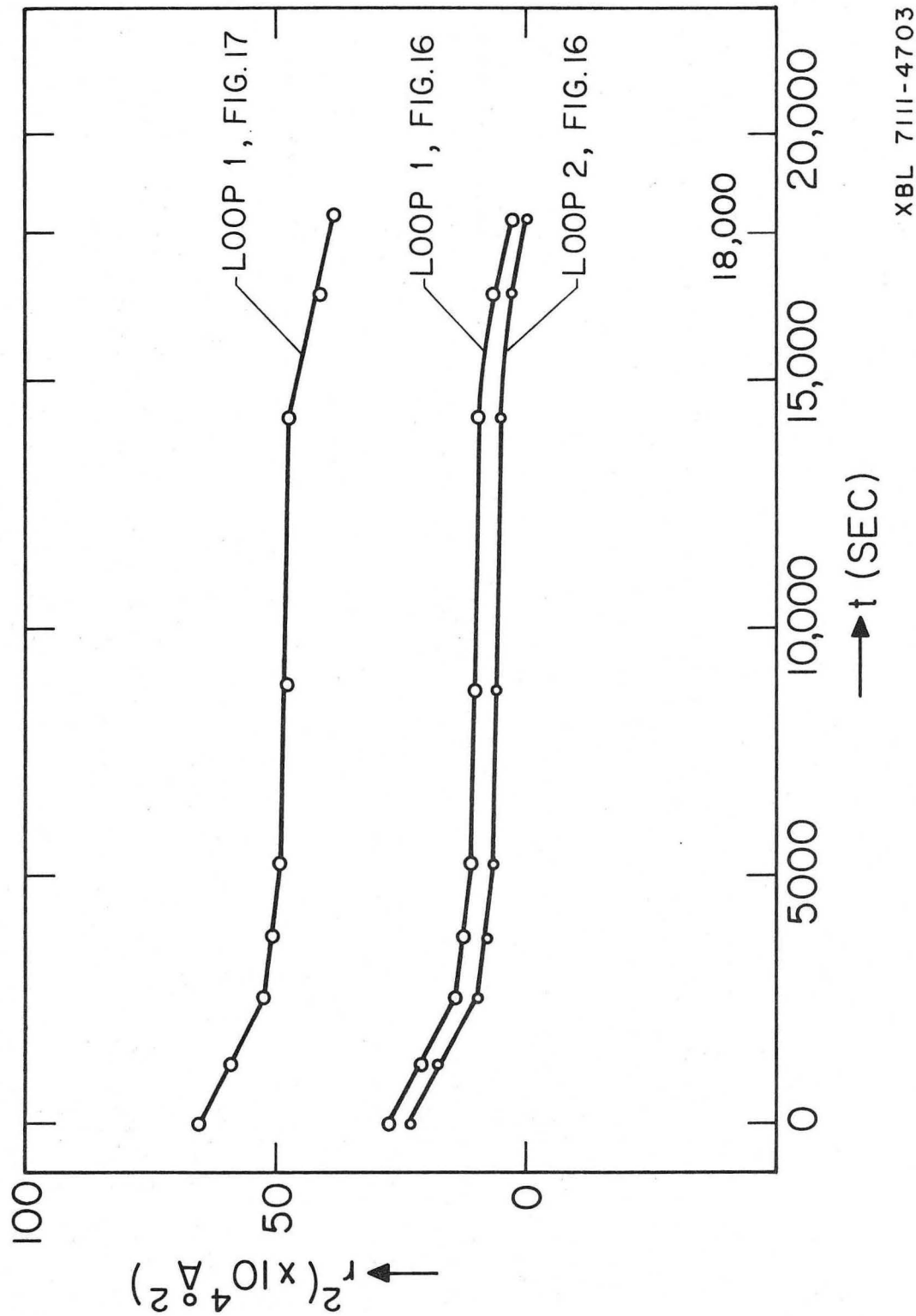

XBL 7111-4703

Fig. 20A

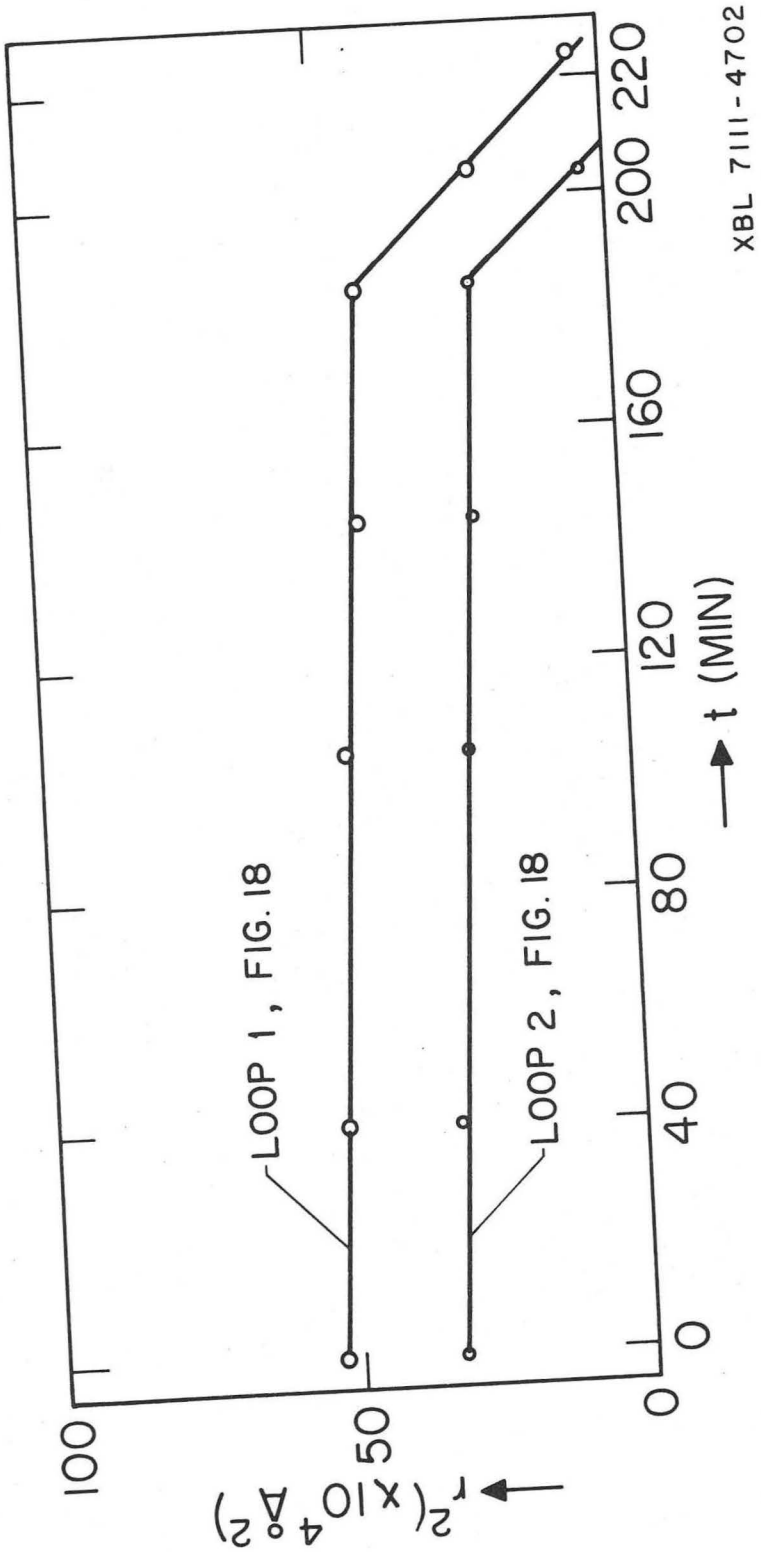
100
50
0
r^2 ($\times 10^4$ Å^2)
0
40
80
120
160
200 220
t (MIN)
LOOP 1, FIG. 18
LOOP 2, FIG. 18
XBL 7111-4702

Fig. 20B

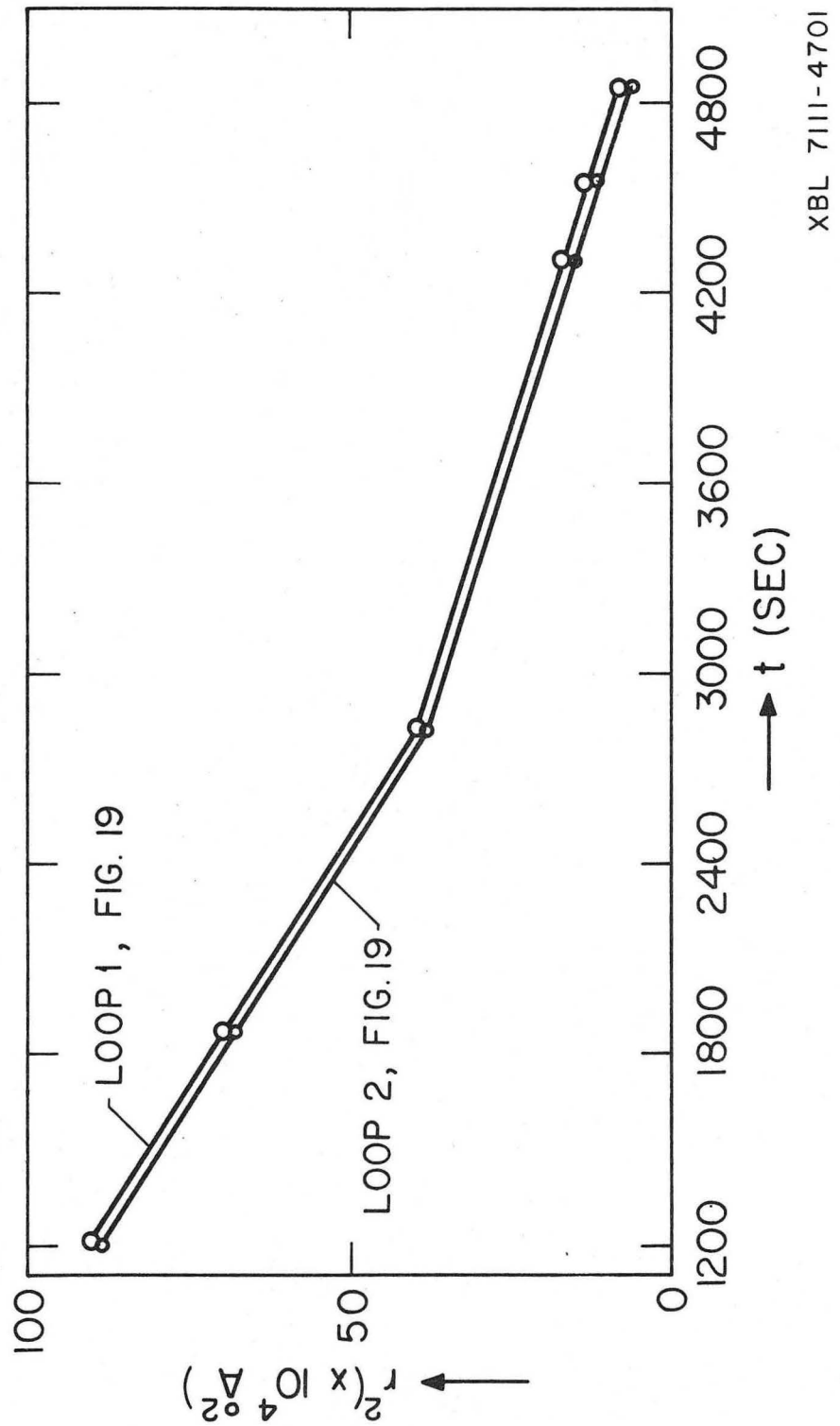

XBL 7111-4701

Fig. 20C

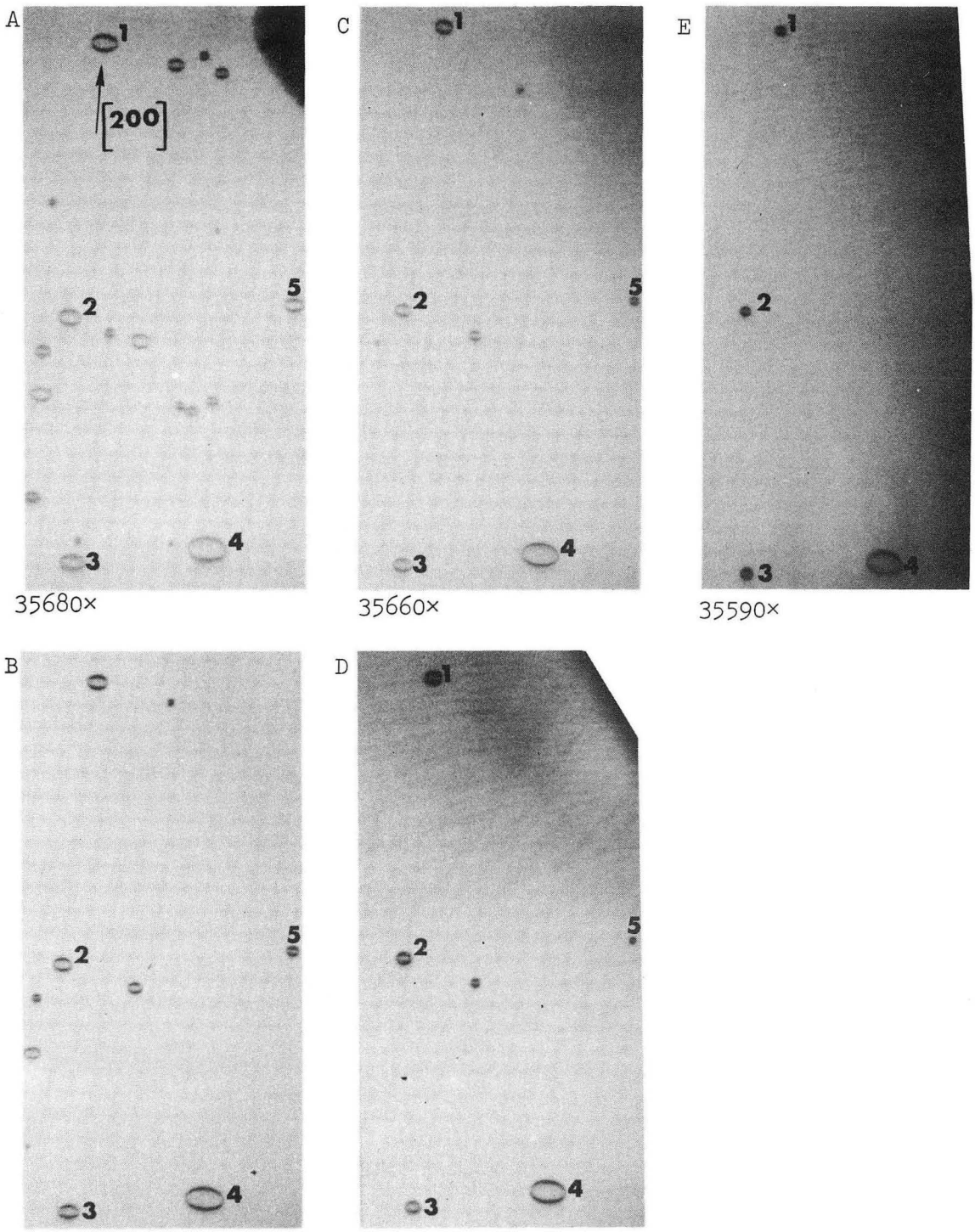
A
1
[200]
2
3
4
5
35680×
C
1
2
3
4
5
35660×
E
1
2
3
4
35590×
B
2
3
4
5
35630×
D
1
2
3
4
5
35660×
XBB 7111-5556

Fig. 21

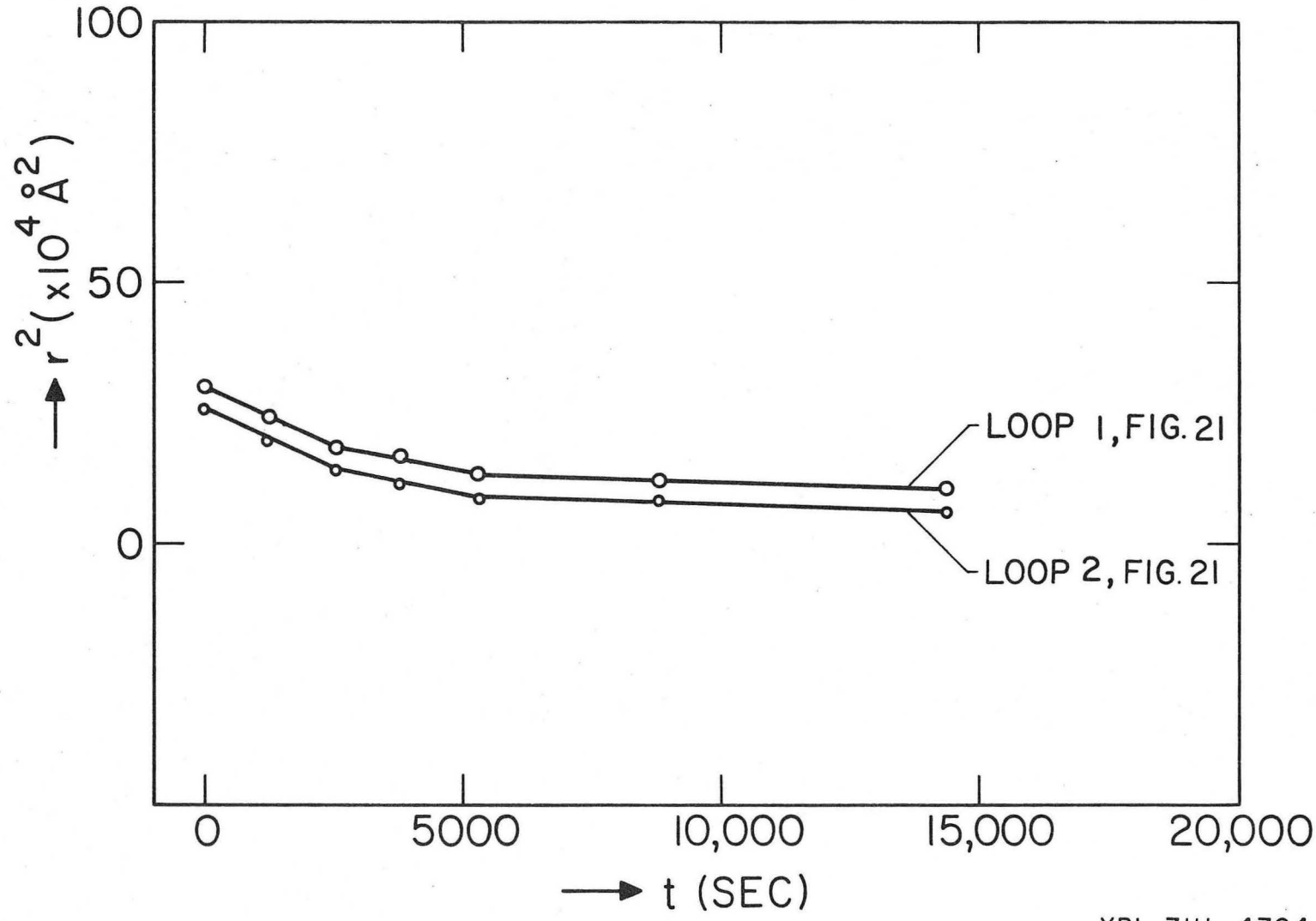
100
50
0
r^2 (x10^4 Å^2)
LOOP 1, FIG. 21
LOOP 2, FIG. 21
0
5000
10,000
15,000
20,000
t (SEC)
XBL 7111-4704

Fig. 22

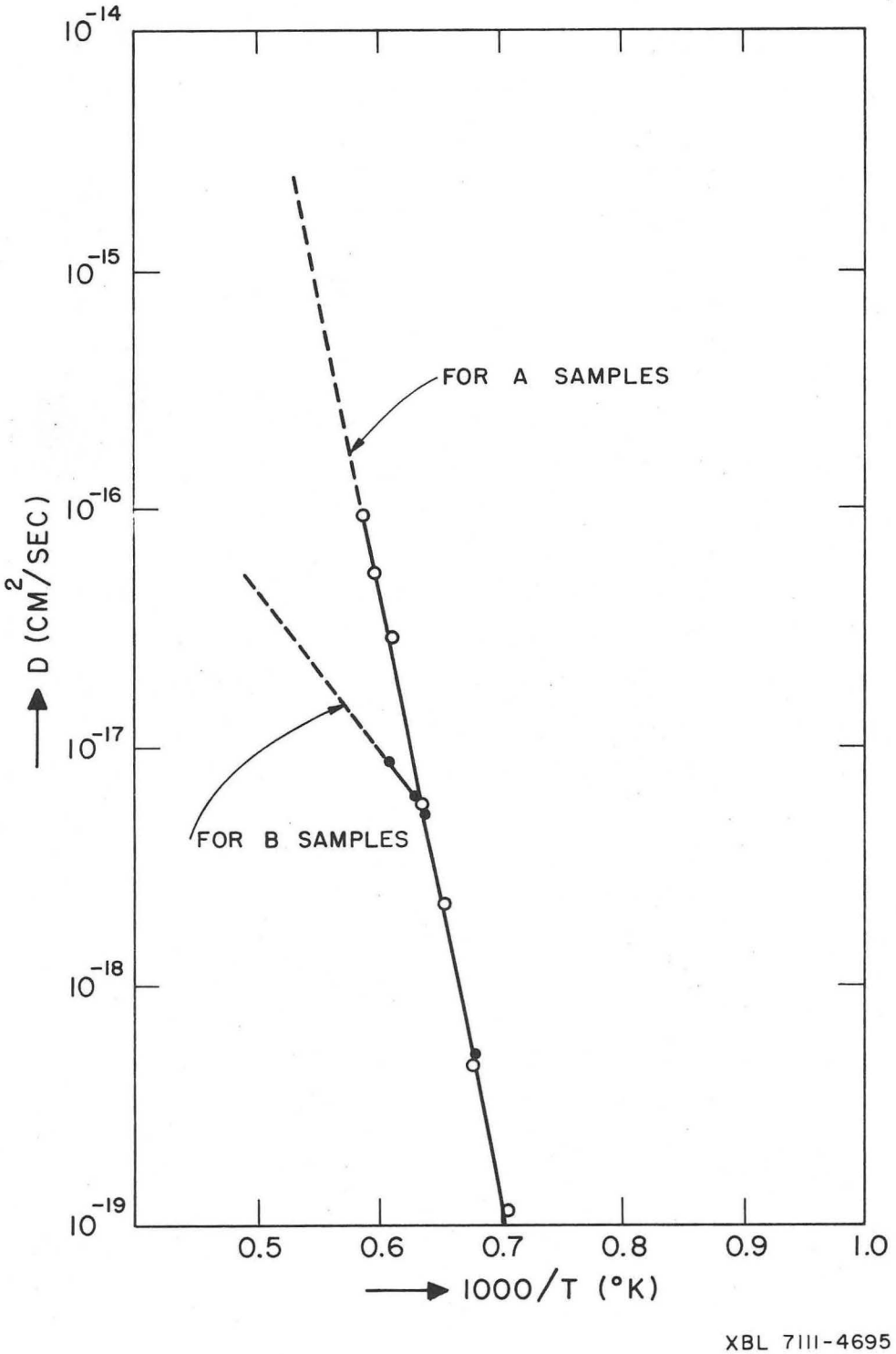
10^{-14}
10^{-15}
10^{-16}
10^{-17}
10^{-18}
10^{-19}
D (CM^2/SEC)
FOR A SAMPLES
FOR B SAMPLES
0.5
0.6
0.7
0.8
0.9
1.0
1000/T (°K)
XBL 7111-4695

Fig. 23

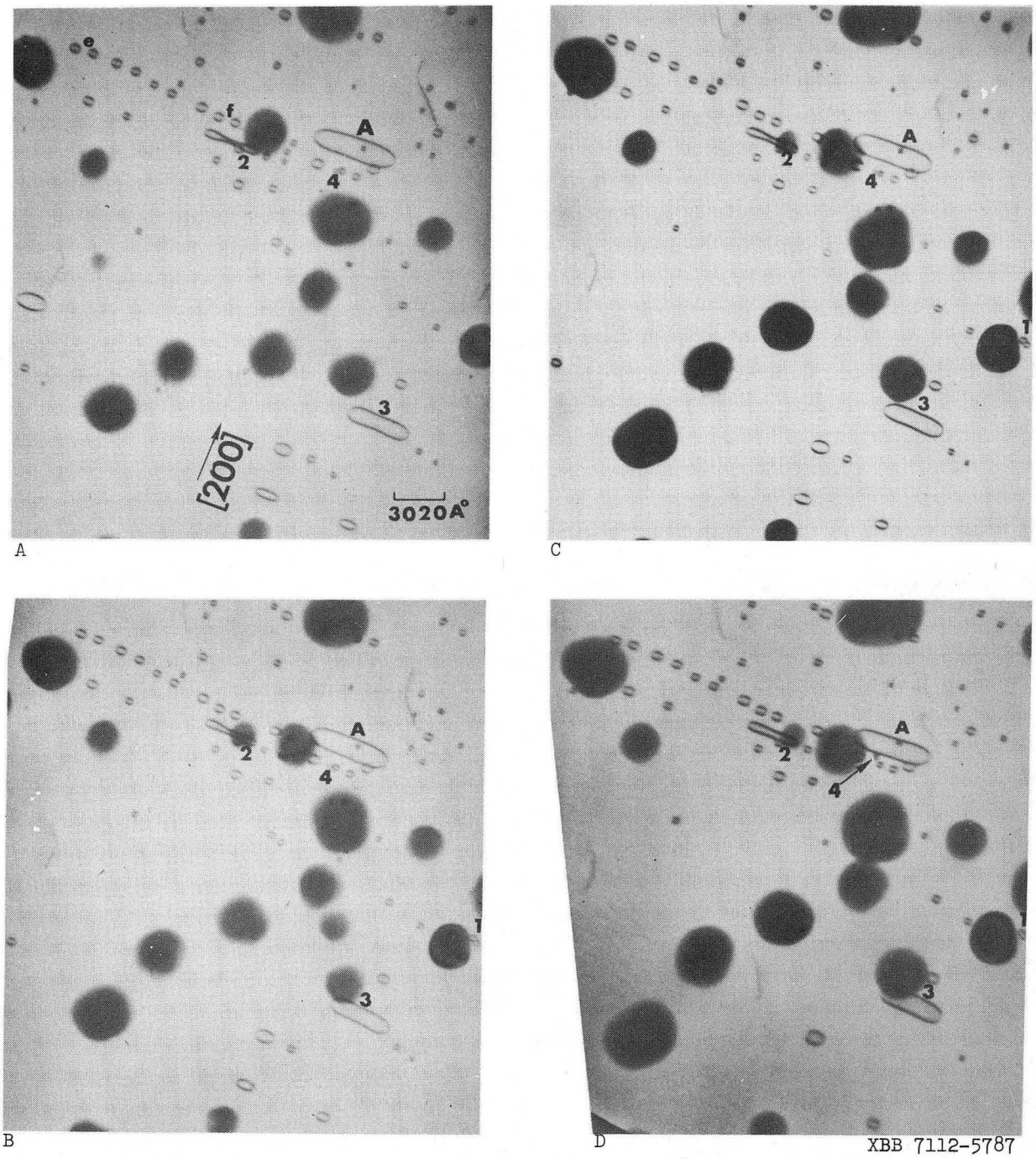

Fig. 24

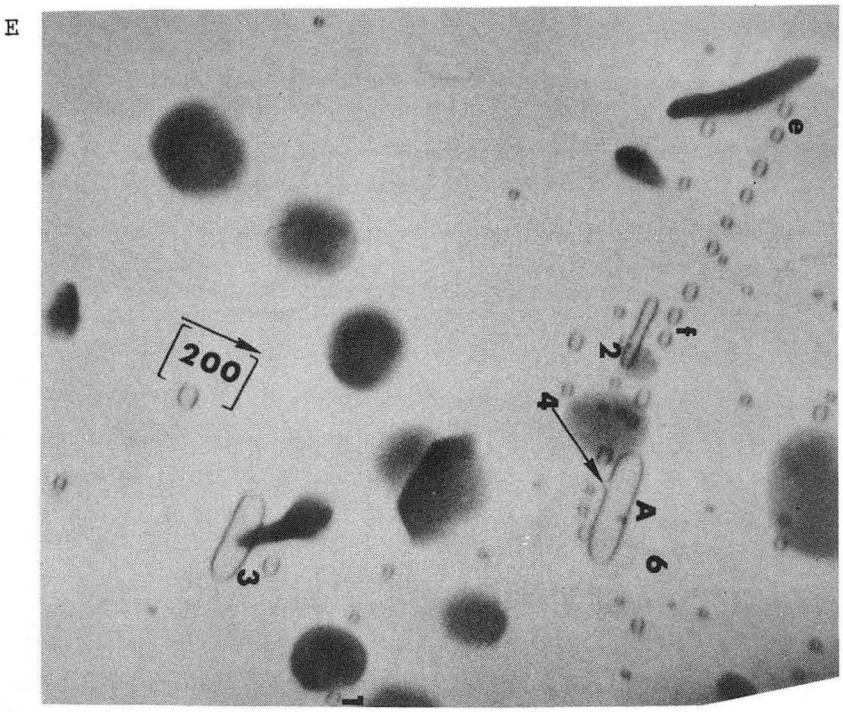

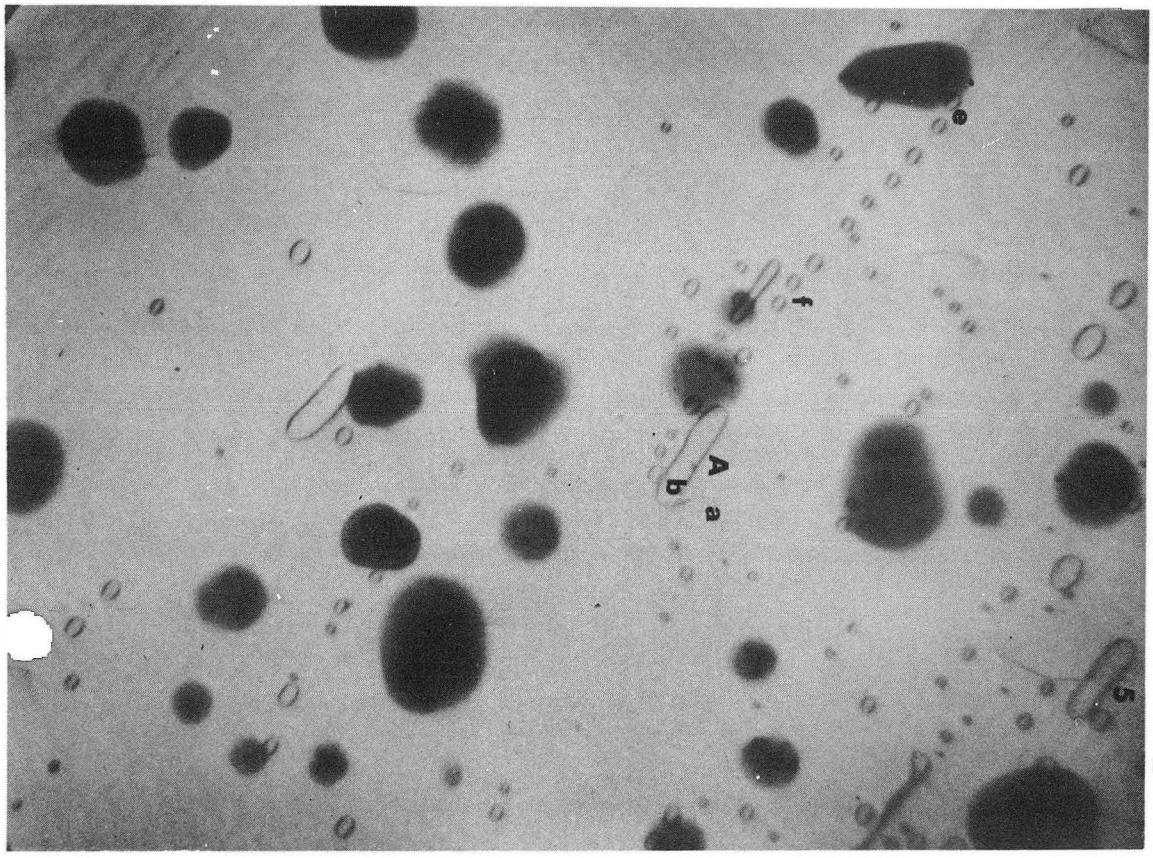

XBB 7112-5788

Fig. 25

G

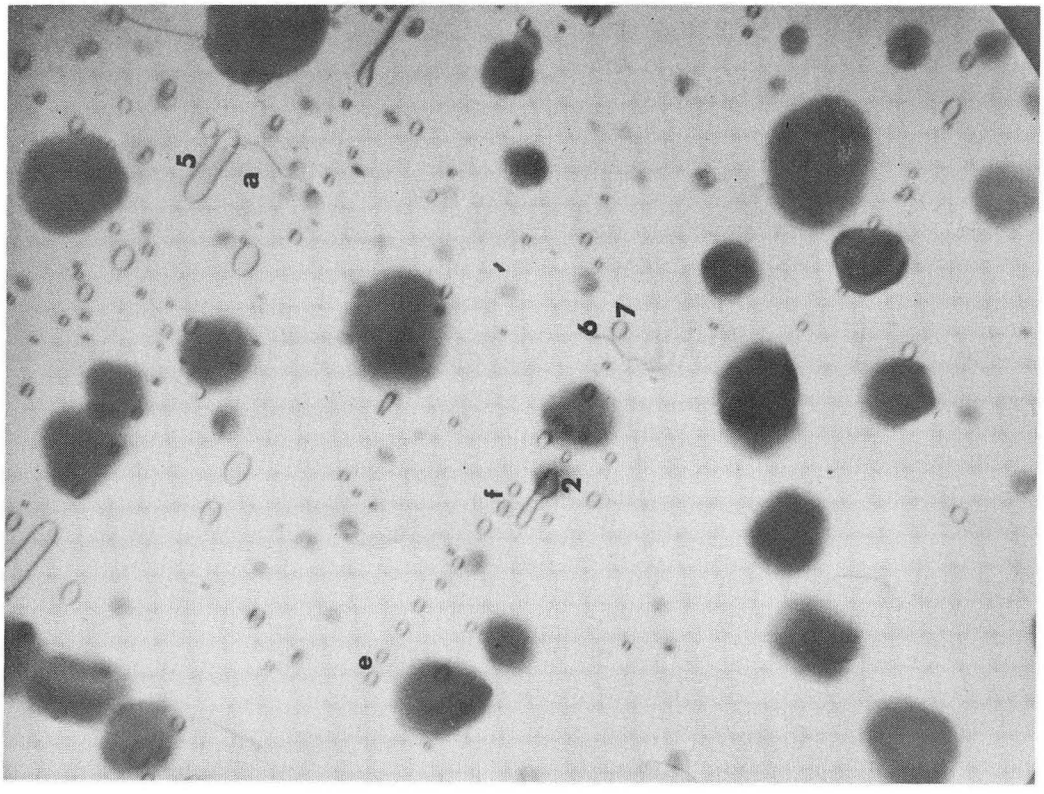

H

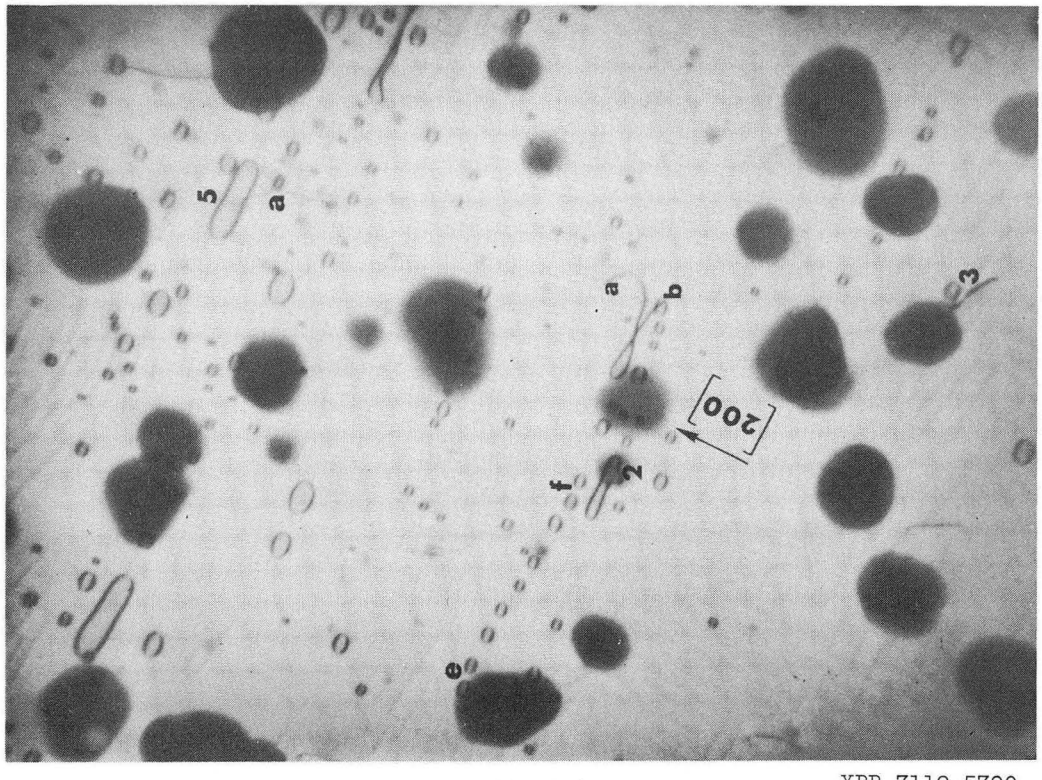

Fig. 26

XBB 7112-5790

I

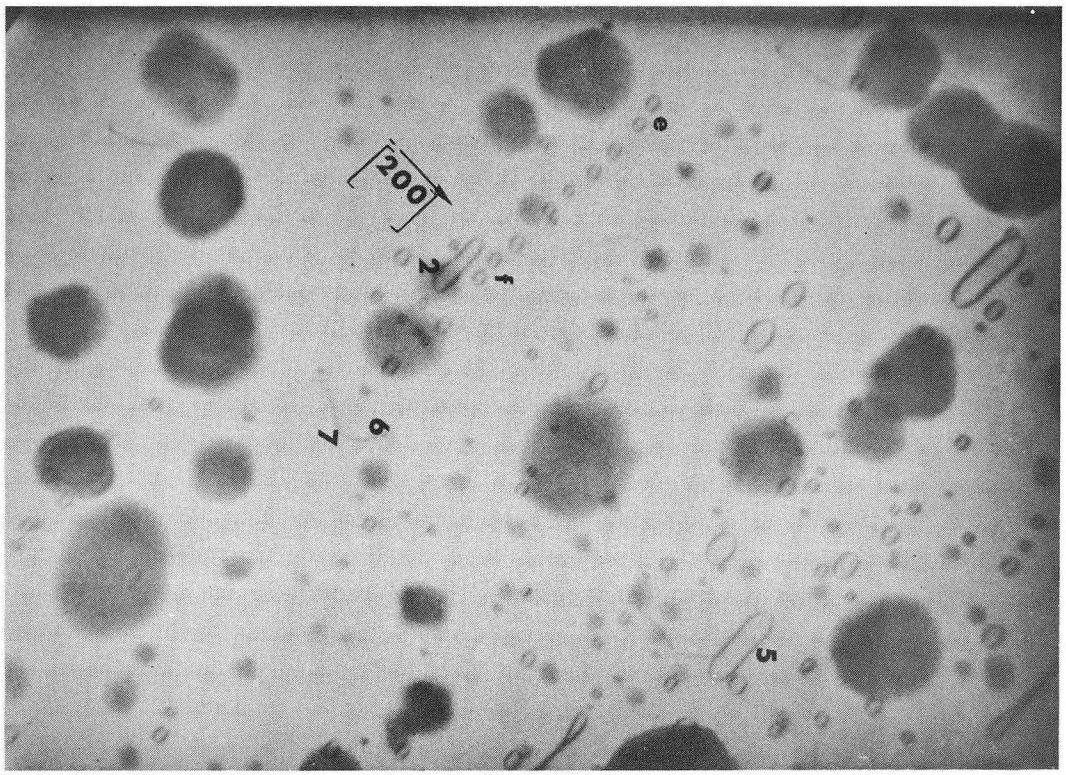

J

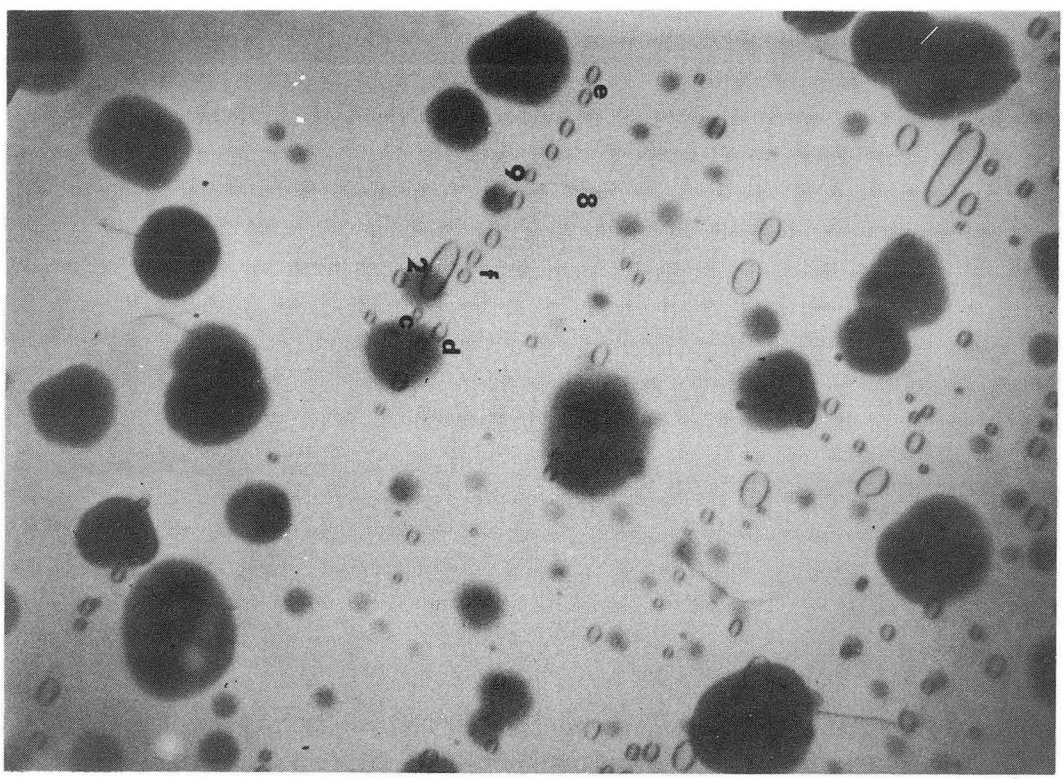

Fig. 27

XBB 7112-5789

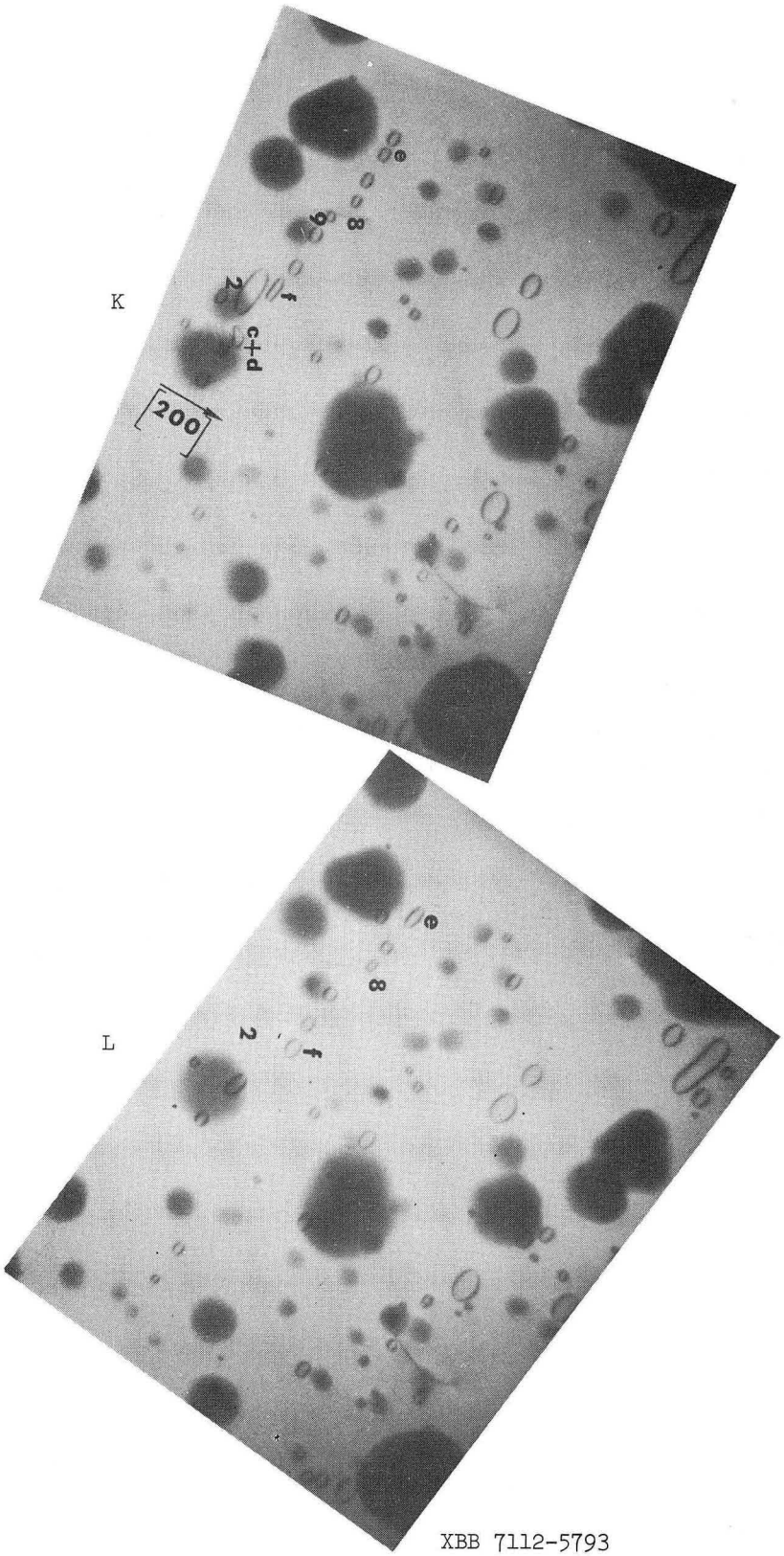

XBB 7112-5793

Fig. 28

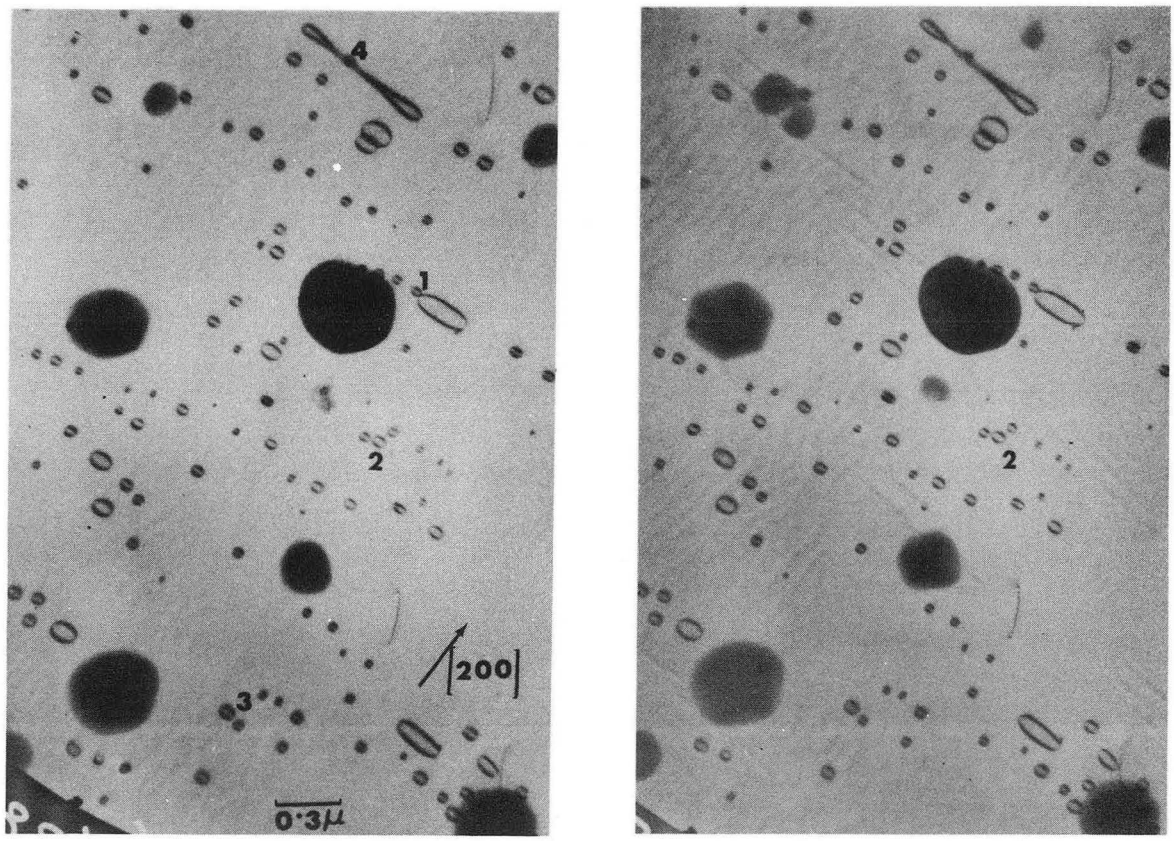

XBB 7111-5434

Fig. 29

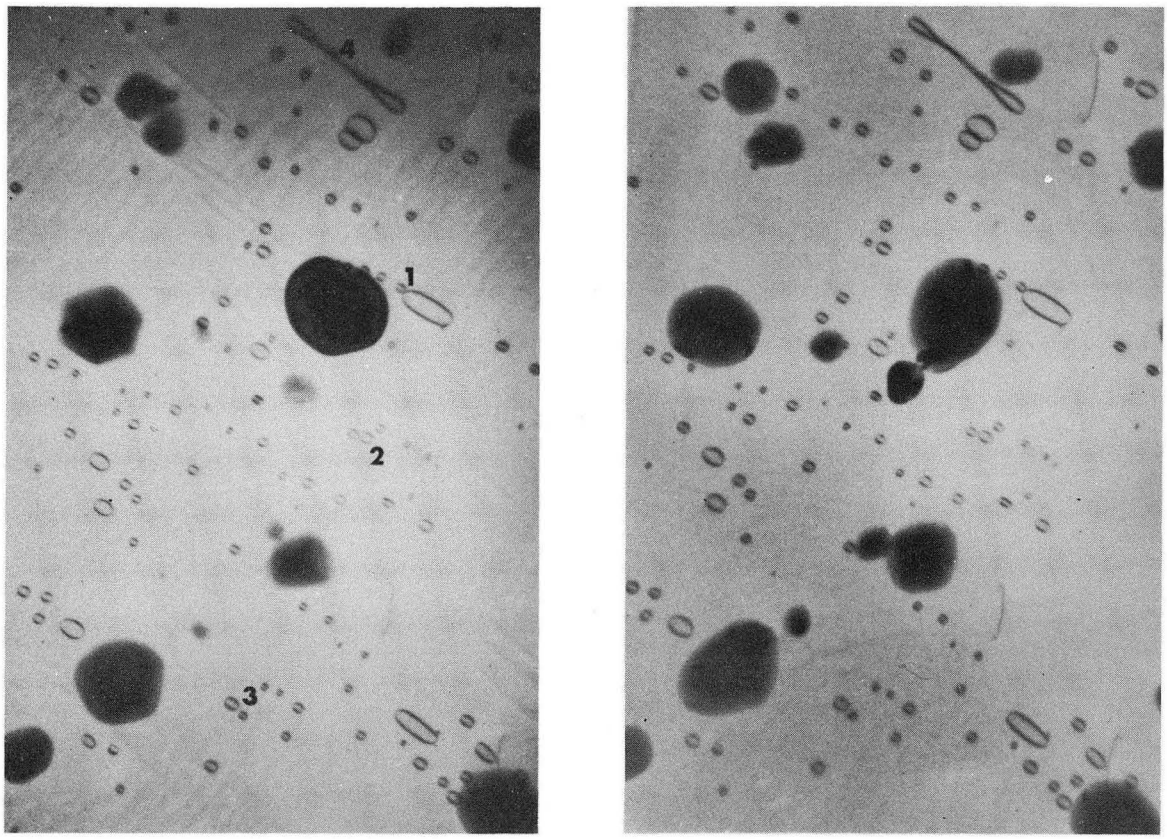

XBB 7111-5425

Fig. 30

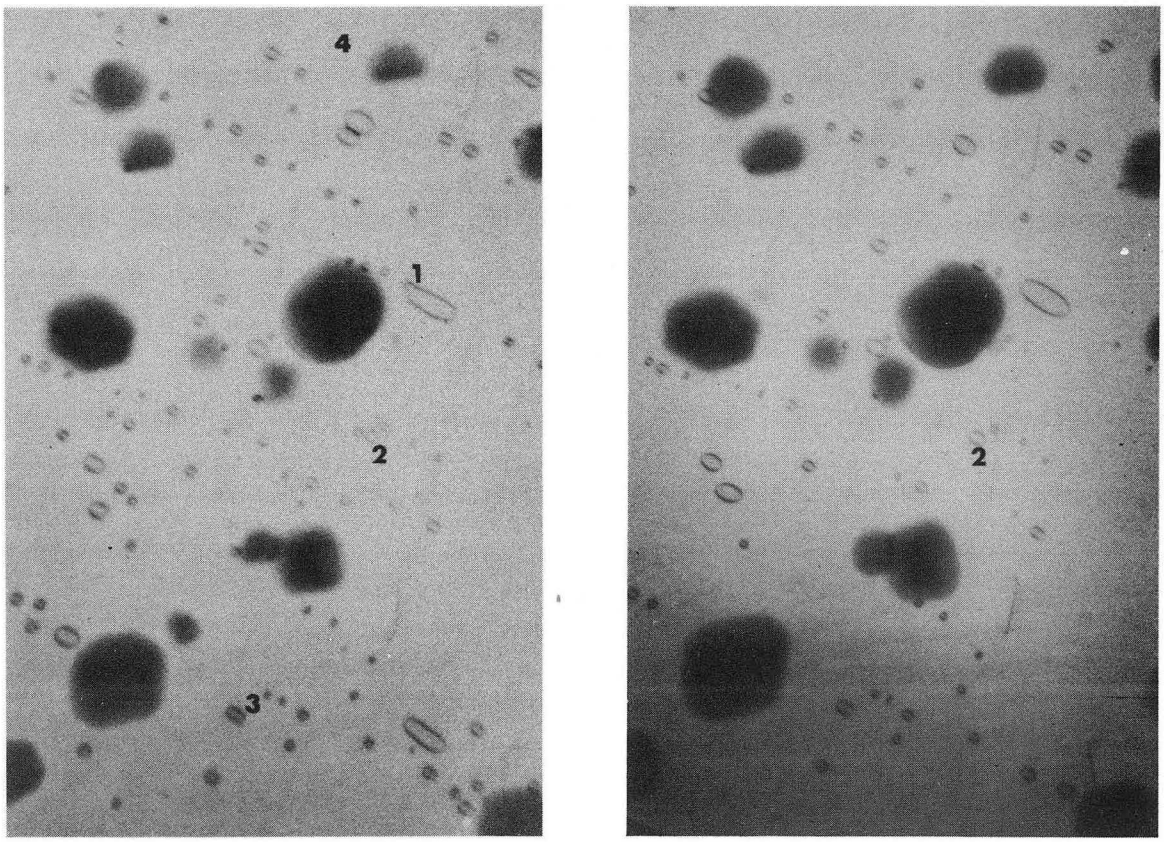

XBB 7111-5424

Fig. 31

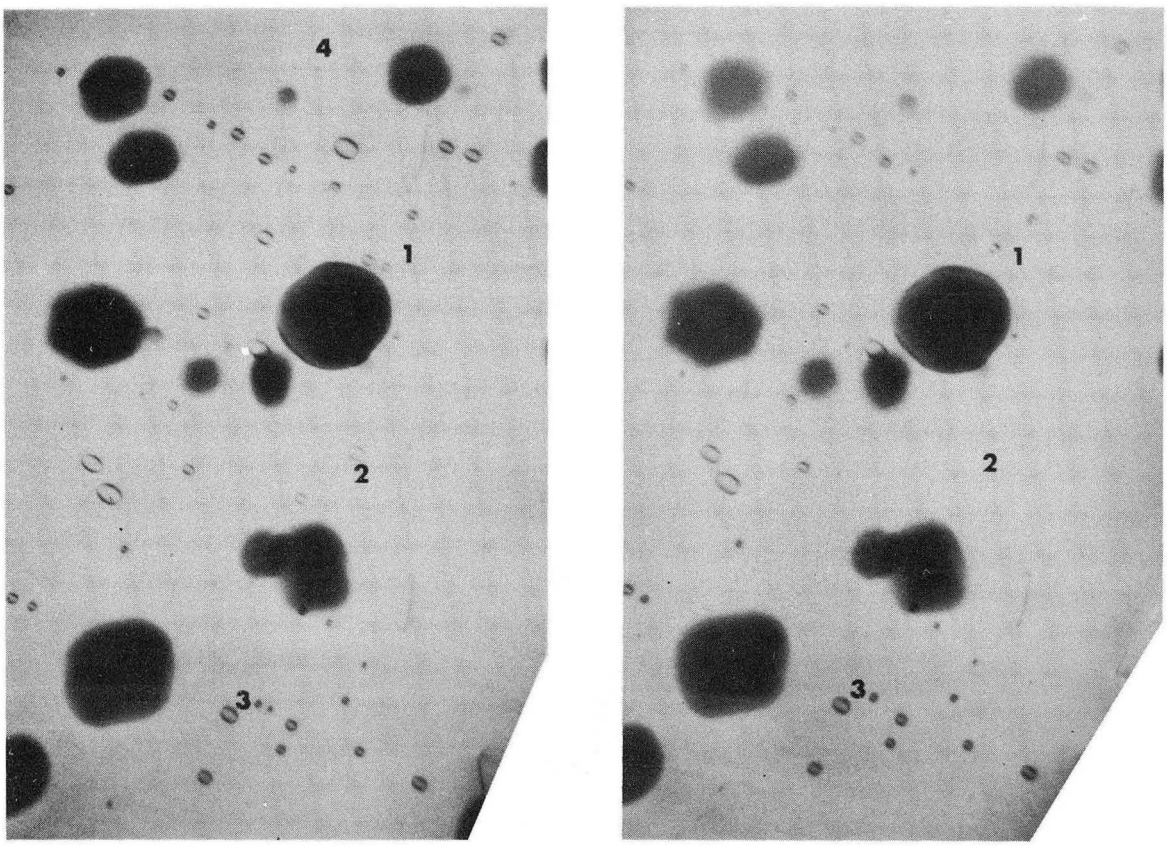

XBB 7111-5423

Fig. 32

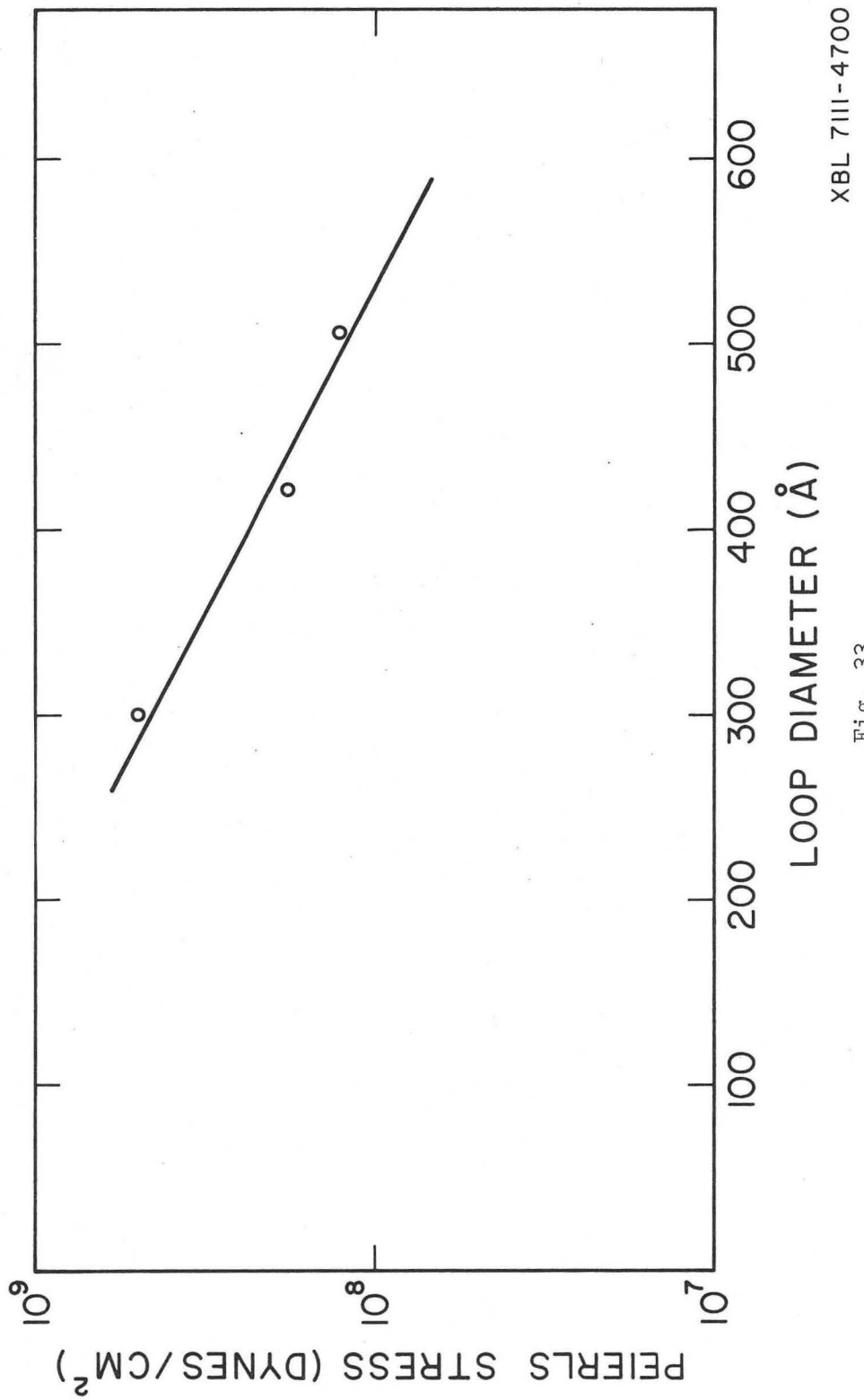

XBL 7111-4700

Fig. 33

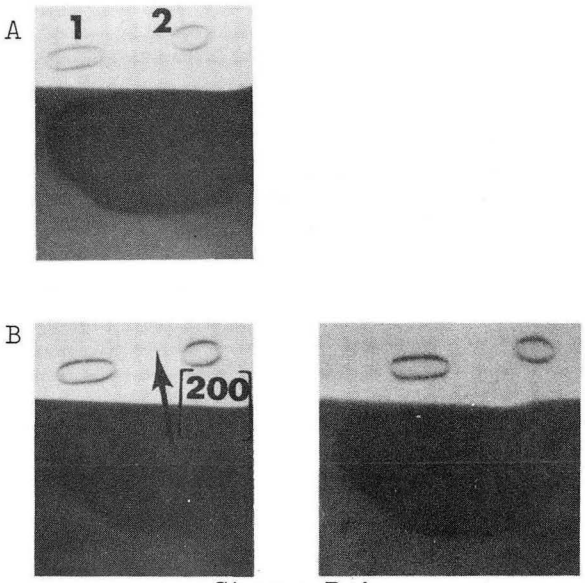

XBB 7111-5551

Fig. 34

A

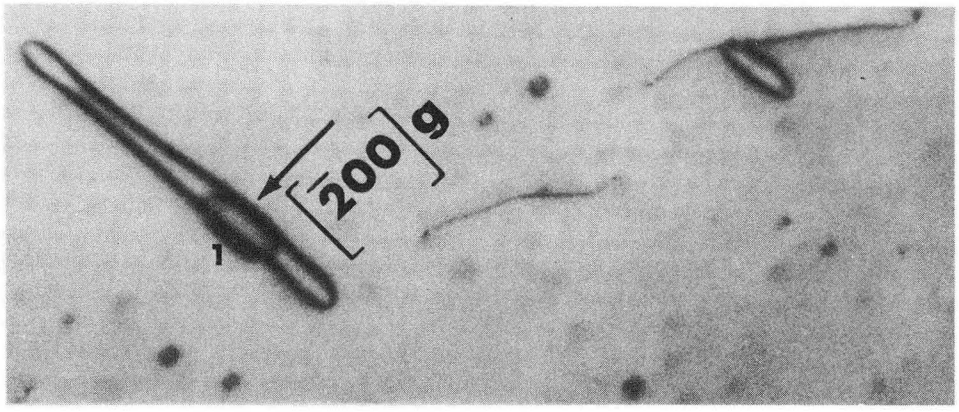

89400×

B

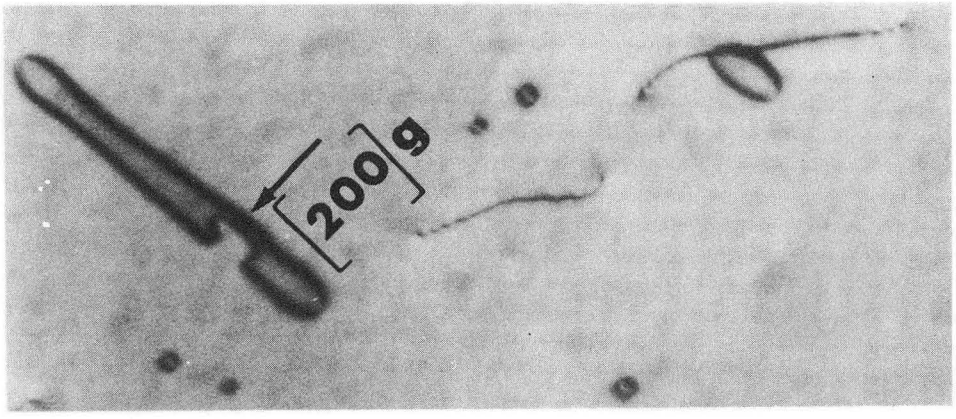

90500×

C

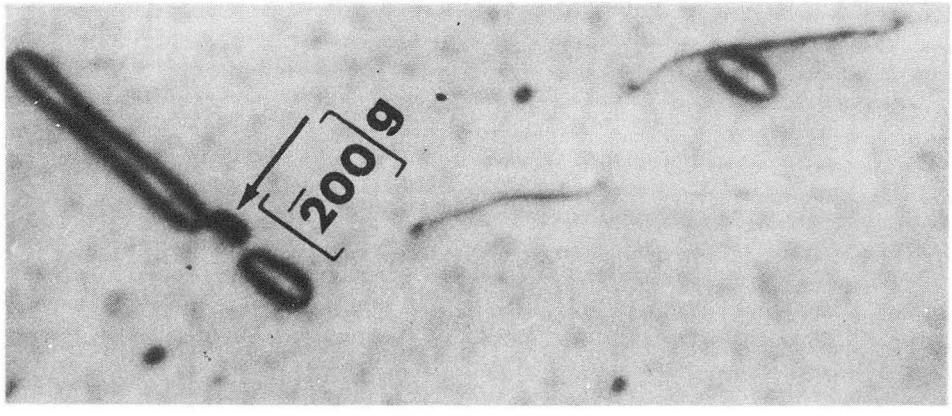

91100×

XBB 7110-4745

Fig. 35

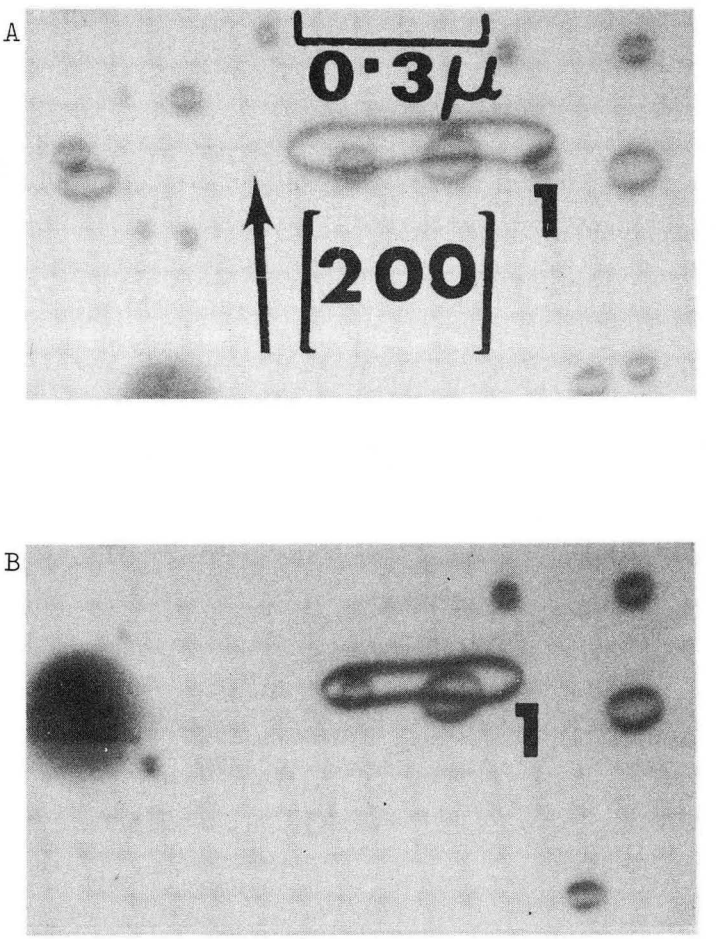

XBB 7111-5549

Fig. 36

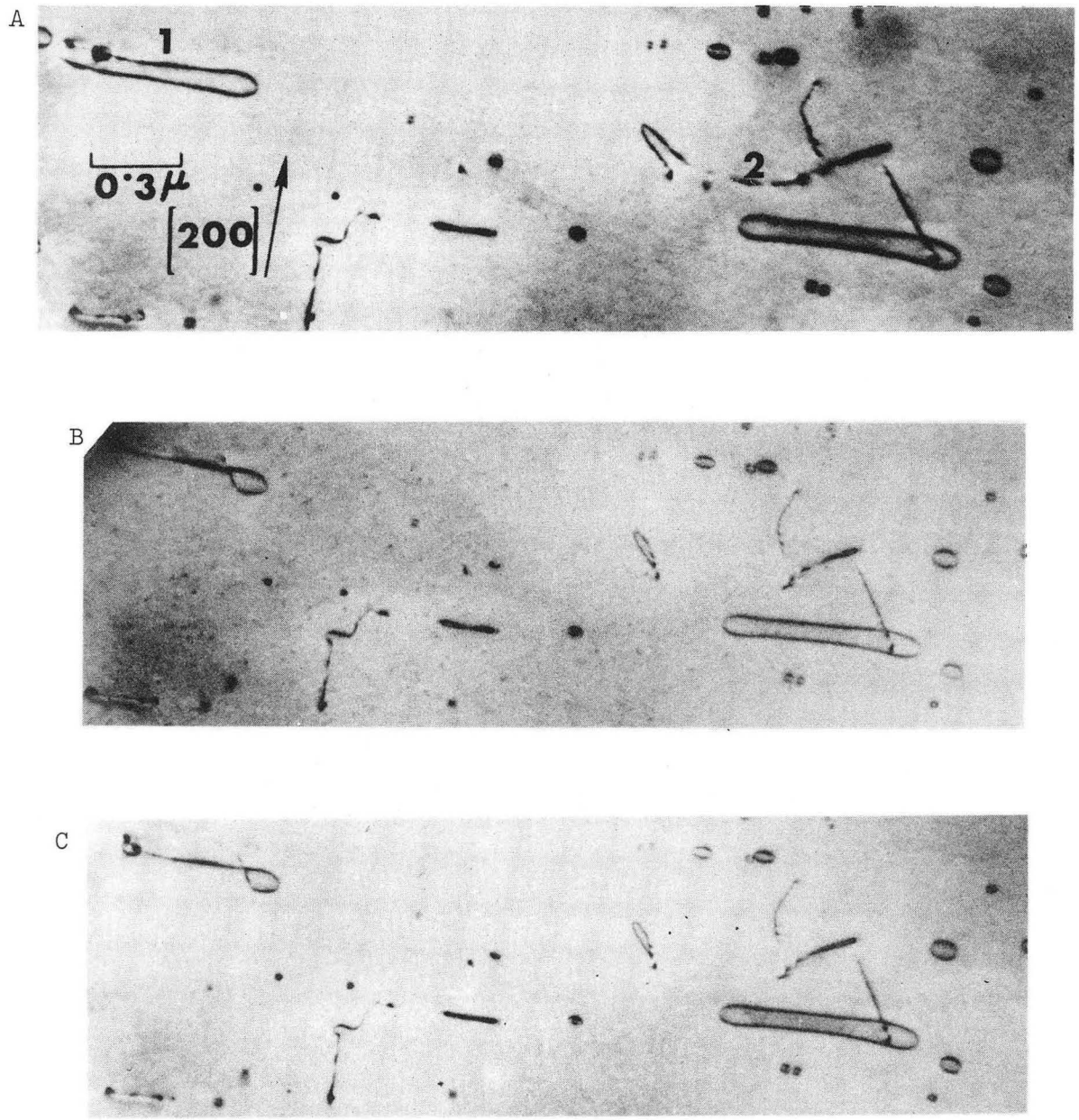

XBB 7111-5553

Fig. 37

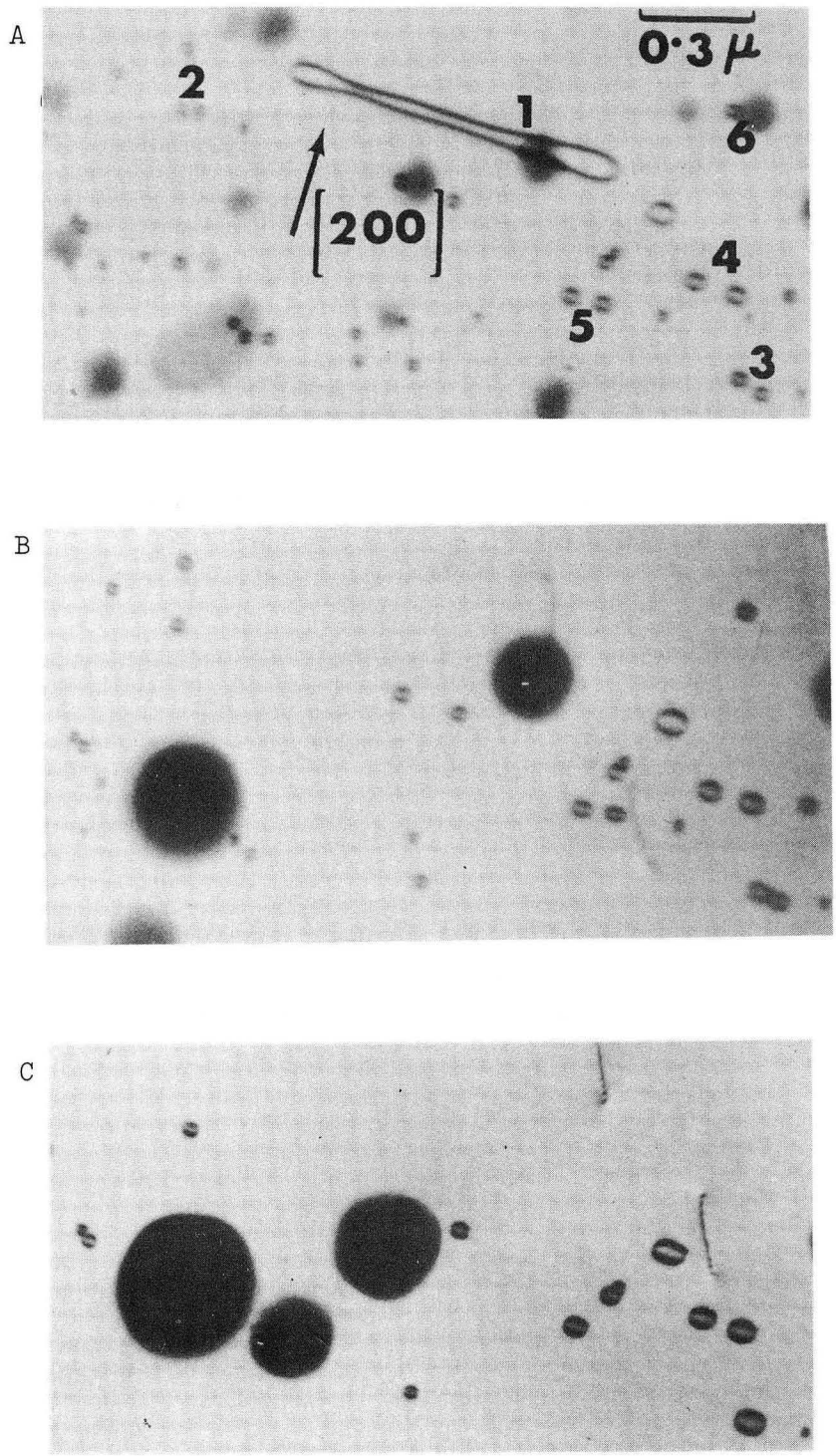

XBB 7111-5552

Fig. 38

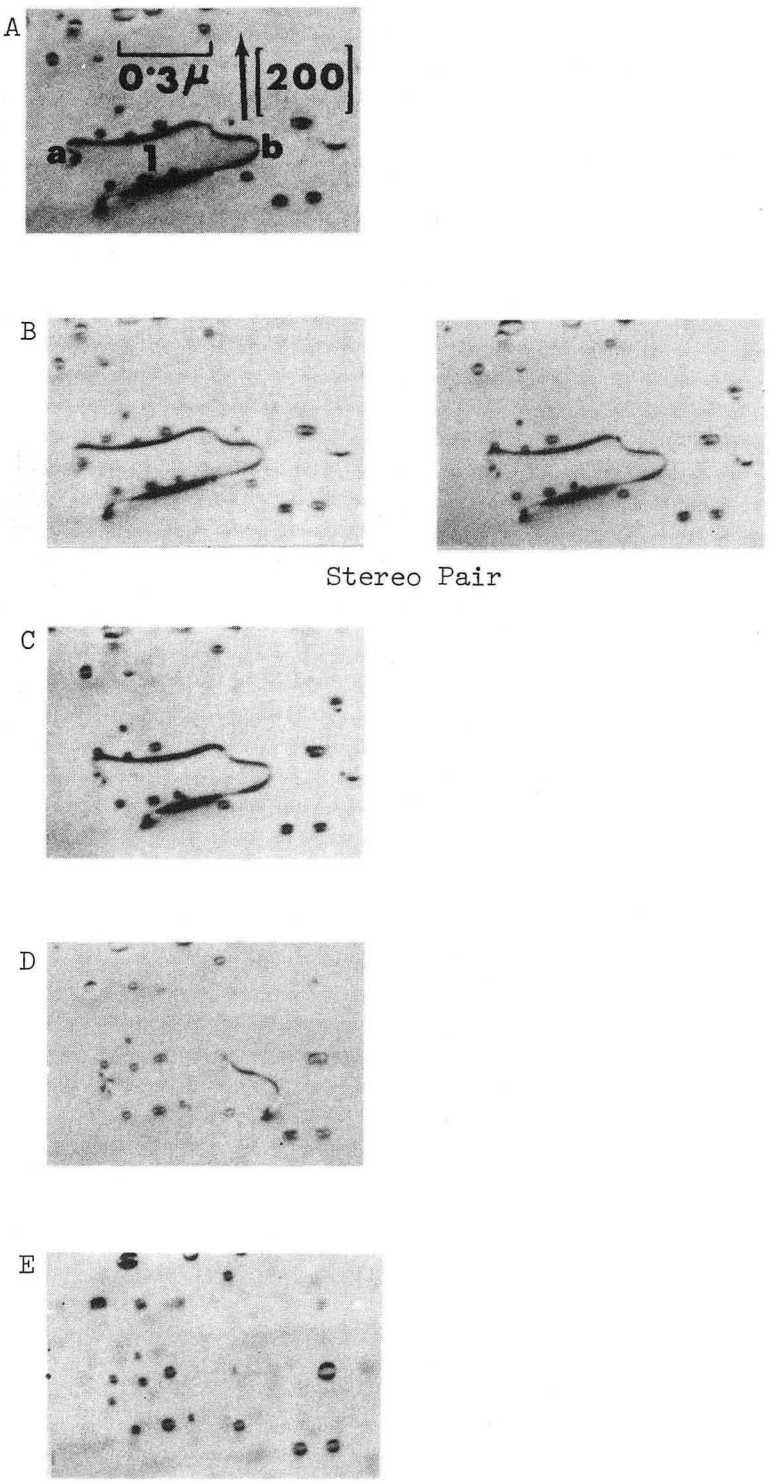

XBB 7111-5550

Fig. 39

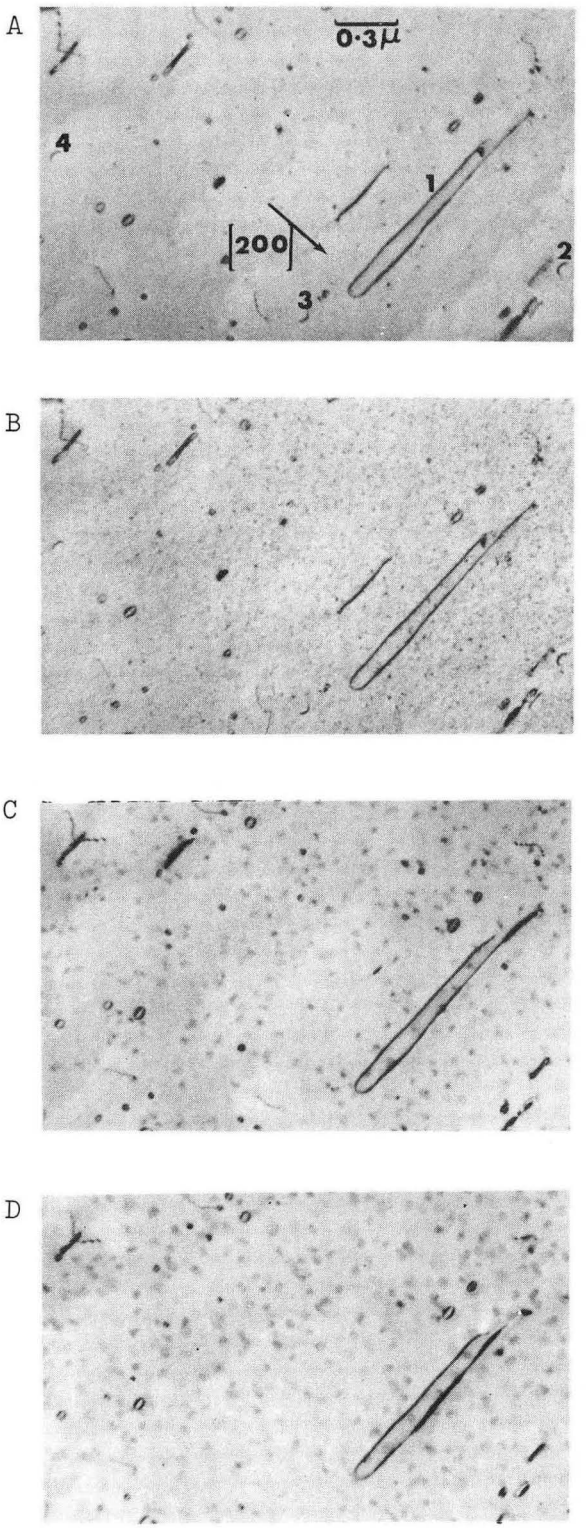

XBB 7111-5555

Fig. 40

TECHNICAL INFORMATION DIVISION
LAWRENCE BERKELEY LABORATORY
UNIVERSITY OF CALIFORNIA
BERKELEY, CALIFORNIA 94720